2-11-2016

Modeling Neurodevelopmental Disorders Involving Genomic Imprinting at Human Chromosome 15q11-q13 Using iPSC and CRISPR/Cas9 Technology

Pin-Fang Chen
University of Connecticut Health Center, pchen@uchc.edu

Modeling Neurodevelopmental Disorders Involving Genomic Imprinting at Human Chromosome 15q11-q13 Using iPSC and CRISPR/Cas9 Technology

Ivy Pin-Fang Chen, Ph.D.

University of Connecticut, 2016

Abstract

Human chromosome 15q11-q13.1 is associated with three distinct neurodevelopmental disorders—Angelman (AS), Prader-Willi (PWS), and 15q duplication (Dup 15q) syndromes. While symptomatic treatments are prescribed, no cure is currently available. Using iPSC technology, we established *in vitro* model systems from AS, PWS, and Dup 15q patient samples to study chromosome 15q11-q13.1 gene regulation. We demonstrated that iPSCs maintain correct imprinting status at the PWS imprinting center after reprogramming and that *UBE3A* imprinting occurs in iPSC-derived neurons. Using CRISPR/Cas9 genome editing technology, we tagged UBE3A protein with GFP to create a reporter cell line. We also created RBFOX1 and RBFOX2 single and double knockouts and found that these alternative splicing factors are not required for neuron-specific processing or expression of *SNURF/SNRPN* lncRNA. Using these disease-specific iPSC models and the powerful CRISPR/Cas9 genome editing tool, we hope to elucidate underlying disease mechanisms and contribute to developing effective treatments for AS, PWS, and Dup 15q syndrome.

Modeling Neurodevelopmental Disorders Involving Genomic Imprinting at Human Chromosome 15q11-q13 Using iPSC and CRISPR/Cas9 Technology

Ivy Pin-Fang Chen

B.A., Wesleyan University, 2009

A Dissertation

Submitted in Partial Fulfillment of the

Requirements for the Degree of

Doctor of Philosophy

at the

University of Connecticut

2016

APPROVAL PAGE

Doctor of Philosophy Dissertation

Modeling Neurodevelopmental Disorders Involving Genomic Imprinting at Human Chromosome 15q11-q13 Using iPSC and CRISPR/Cas9 Technology

Presented by

Ivy Pin-Fang Chen, B.A.

Major Advisor_____
Stormy J. Chamberlain

Associate Advisor_____
Marc E. Lalande

Associate Advisor_____
Yuanhao (James) Li

Associate Advisor_____
Xue-Jun (June) Li

Associate Advisor_____
Blanka Rogina

University of Connecticut
2016

To my friends and family,

who supported me unconditionally and made me who I am.

Acknowledgments

I am eternally grateful to everyone in my life that shaped me, challenged me, and supported me. It has been an incredible journey, and I attribute my personal achievements to you all.

I am unbelievably lucky to have met my thesis advisor, Dr. Stormy Chamberlain, who has been a great mentor and a dear friend. She taught me patience and persistence in conducting science and her positive attitude cheered me on. She gave me guidance and great advice in career development as well as personal life. Stormy made me a better scientist and a better person.

Dr. Marc Lalande took me under his wing when I first started my graduate career. He has been the paternal figure who watches over everyone in the lab and helped us young scientists navigate through this unpredictable and challenging phase of life. He also provided guidance to my thesis project. Drs. James Li and June Li have been immensely helpful by providing useful scientific critiques and generously sharing laboratory reagents with me. They cared for me like their own students. I would like to acknowledge Dr. Blanka Rogina, who was instrumental in my advancement through the program and kept me on track.

My labmates, Jack Hsiao, Carissa Sirois, Alexandra Goetjen, and Dr. Noelle Germain, as well as members in the Lalande lab, made my everyday life fun and enjoyable. They are the balance in the lab and I am extremely thankful for their camaraderie. Leann Crandall and Christopher Stoddard of the UConn Stem Cell Core provided excellent technical supports and were a pleasure to work with. Heather Glatt-

Deeley and Erin Banda made lab work easy by keeping the space organized and staying on top of purchase orders. Staff in the Genetics and Genome Sciences Office have been extremely helpful and made the working environment comfortable. I would also like to thank my friends here at the UConn Heath Center for keeping me grounded and reminding me to enjoy life.

I would like to acknowledge my college mentor, Jason Wolf, who is no longer here to see my accomplishments. He taught me how to conduct experiments from the ground up. Without him, I would not have become a research scientist. My college friends have been my surrogate family and kept me sane through graduate school. I would like to thank the Freeman Foundation for financially supporting my undergraduate study and providing the opportunity to meet these wonderful individuals.

I thank my family for their unwavering supports and trust in me. Even though they are half the globe away, I know that they are very proud of me and that they love me for who I am. Last but not least, I would like to thank Jared Woods, who was my ultimate support system in the past few years. His love and support helped me through some of the darkest days of my life.

This work was funded by the National Institutes of Health [R01HD068730 to S.J.C]; the Raymond and Beverly Sackler foundation [S.J.C]; and the state of Connecticut under the Connecticut Stem Cell Research Grants Program [Grant 09SCAUCHC14 to S.J.C]. Perseverance and supports from families with AS, PWS, and Dup 15q patients made this work possible.

Modeling Neurodevelopmental Disorders Involving Genomic Imprinting at Human Chromosome 15q11-q13 Using iPSC and CRISPR/Cas9 Technology

Ivy Pin-Fang Chen

TABLE OF CONTENTS

Chapter 4: RBFOX1 and RBFOX2 are dispensable in iPSCs and iPSC-derived neurons and do not contribute to neural-specific paternal *UBE3A* silencing

List of Figures

Chapter 1

Chapter 2

Chapter 3

Chapter 4

List of Tables

Chapter 4

Chapter 1

Chromosome 15q11-q13.1 and Genomic Imprinting Disorders

1.1 General Introduction

Human chromosome 15q11-q13.1 is associated with three distinct neurodevelopmental disorders—Angelman (AS), Prader-Willi (PWS), and 15q duplication (Dup 15q) syndromes. Human chromosome 15q11-q13.1 harbors several common breakpoints composed of low-copy repeats or repetitive sequences that bracket imprinted as well as non-imprinted genes (**Figure 1**) (Amos-Landgraf et al., 1999; Wang et al., 2004). When aligned inappropriately during meiosis, these breakpoints could lead to large *de novo* deletions or duplications, which are transmitted through the germ line. Paternal deletions cause PWS, maternal deletions result in AS, and duplications, often of maternal origin or epigenotype, lead to Dup 15q syndrome (Christian et al., 2008; Cook et al., 1997). Other than large deletions, AS and PWS can be caused by other genetic anomalies at chromosome 15q11-q13.1, which are discussed below. Overall, the incidence of each of these three disorders is approximately 1/15,000~1/30,000 live births (Battaglia, 2005; Cassidy and Driscoll, 2009; Chamberlain and Lalande, 2010b). While symptomatic treatments are prescribed for AS, PWS, and Dup 15q patients, no cure is currently available. Similar to many other developmental disorders, early intervention is highly desirable for improved quality of life for these patients.

1.2 Angelman, Prader-Willi, and 15q Duplication Syndromes

AS patients have disproportionally small heads, known as microcephaly, and suffer from developmental delay, severe mental retardation, and frequent and intense seizures. Owing to absence of speech, motor dysfunction, and frequent smiling, AS

patients have been characterized as having a “happy puppet” affect (Lossie et al., 2001). AS is caused by the loss of maternal *UBE3A*, a gene residing in the imprinted domain of chromosome 15q11-q13.1 (Kishino et al., 1997). This results in the neuronal loss of an encoded ubiquitin protein ligase E3A (also known as E6-AP). In neurons, ubiquitin protein ligase E3A plays an important role in the regulation of synaptic proteolysis and has been implicated in synaptic plasticity as well as postsynaptic function (Greer et al., 2010; Jiang et al., 1998; Weeber et al., 2003). In addition to maternal deletions (70%), maternally-transmitted loss-of-function mutations (10%), maternal imprinting defects (5%), and paternal uniparental disomy (5%) all lead to a loss of the ubiquitin protein ligase in brain and result in AS (Lalande and Calciano, 2007; Lossie et al., 2001).

PWS patients suffer from mild to moderate cognitive deficits and display infantile hypotonia and failure to thrive. Soon after the first year of life, PWS patients develop obesity, followed by insatiable appetite, known as hyperphagia, in later childhood. PWS patients exhibit hypogonadism, have small hands and feet, and are short in stature if not subjected to growth hormone therapy. A large proportion of affected individuals display mood and behavioral disorders, such as temper tantrums and obsessive-compulsive disorder (Cassidy and Driscoll, 2009). PWS is caused by the loss of paternal expression from the imprinted domain of chromosome 15q11-q13.1. By overlapping atypical microdeletions carried by rare PWS patients, the critical region has been narrowed down to a 91 kb stretch of DNA that encodes for *SNORD116* snoRNA cluster and a non-coding RNA, *Imprinted in Prader-Willi* (*IPW*) (Bieth et al., 2015). Functions of these RNA transcripts and the molecular pathway leading to PWS are still not well understood.

To date, there are only five reported cases of the aforementioned microdeletion patients (Anderlid et al., 2014; Bieth et al., 2015). Most PWS patients carry large deletions on the paternal allele of chromosome 15q11-q13.1 (70%). Maternal uniparental disomy (25%) and imprinting defects (5%) accounts for the rest of the PWS population (Cassidy and Driscoll, 2009).

Dup 15q patients are present with hypotonia, epilepsy, and delayed motor and language development. Dup 15q patients are cognitively impaired and have learning disabilities. Affected individuals are often diagnosed with autism, accounting for 1-3% of total autistic population. In fact, copy number variation of chromosome 15q11-q13.1 is the most common chromosomal anomaly linked to autism (Cook et al., 1998; Schroer et al., 1998). Dup 15q can be caused by either an interstitial duplication (int dup(15)) of chromosome 15q11-q13.1 or a supernumerary isodicentric chromosome (idic(15)) formed by inverted duplication of proximal chromosome 15 (Battaglia, 2005). Although a molecular mechanism leading to Dup 15q is yet to be discovered, many genes within the duplicated region have been proposed to contribute to the disease etiology. Due to the fact that affected individuals often carry duplications of maternal origin or epigenotype, excessive *UBE3A* was proposed to be the primary cause of Dup 15q (Chamberlain and Lalande, 2010b). *UBE3A*, the gene disrupted in AS, is the only gene in the imprinted domain that is expressed exclusively from the maternal allele in brain. Furthermore, copy number across chromosome 15q11-q13.1 positively correlates with phenotype severity for Dup 15q syndrome, suggesting that there is a gene dosage effect (Schinzel et al., 1994).

In summary, AS, PWS, and Dup 15q syndrome are three clinically distinct neurodevelopmental disorders that are caused by mutations at chromosome 15q11-q13.1. Due to genomic imprinting, the parental origin of mutation at chromosome 15q11-q13.1 dictates the phenotype. It is clear that proper gene regulation at chromosome 15q11-q13.1 on both maternal and paternal alleles is important for normal brain development. In Chapter 2, we developed modeling systems for AS, PWS, and Dup 15q syndrome by utilizing recently developed induced pluripotent stem cell (iPSC) technology. By studying all three disorders side by side, we hope to gain a holistic insight into the molecular mechanism of gene regulation at chromosome 15q11-q13.1. Our ultimate goal is to facilitate therapeutic development for these patients. In the following sections, I will discuss genomic imprinting at chromosome 15q11-q13.1 and the current view on how genes are regulated in this region during neural differentiation, including *UBE3A* and a long non-coding antisense transcript, *UBE3A-ATS*.

1.3 Genomic Imprinting

Humans possess two copies of each autosome, one from the mother and one from the father. Most autosomal genes are expressed bi-allelically, with equal contributions from the paternal and maternal allele. In the past few decades, scientists have identified a subset of genes that are expressed mono-allelically in a parent-of-origin-specific manner. Such mono-allelic expression is established by an epigenetic phenomenon, known as genomic imprinting.

Genomic imprinting is an evolutionarily conserved gene regulatory mechanism and plays a vital role during development. The effect of imprinting may be global, as

evidenced by the silencing of paternal chromosomes in all somatic cells in a group of male mealybugs (Khosla et al., 2006). It can also be tissue- or developmental stage-specific. For example, *UBE3A* is bi-allelically expressed in most human tissues except brain, where there is only maternal expression due to silencing of the paternal allele. Currently, more than one hundred mammalian genes are known to be regulated by genomic imprinting. With the use of detailed tissue-specific analysis, many more may be discovered (Gregg et al., 2010).

Genomic Imprinting is established in the germ line and is traditionally associated with DNA methylation and chromatin modifications (Vu et al., 2004; Yamasaki et al., 2005). However, the parent-of-origin-specific epigenetic marks acquired during gametogenesis do not explain how tissue-specific imprinting is achieved, as these marks are present in all somatic cells to distinguish the two parental alleles from one another. This indicates that tissue-specific imprinted expression requires secondary imprinting regulators during cell differentiation to establish tissue-specificity, and these regulators depend on the existing parent-of-origin-specific marks to achieve allele-specificity (Kishino, 2006). In addition to secondary DNA methylation and chromatin modifications, previous studies have implicated transcription and long non-coding antisense transcripts in regulating imprinting acquisition (Chotalia et al., 2009; Yamasaki et al., 2003). Given that the known genomic imprinting mechanisms cannot explain all incidences of imprinting-related disorders, there are likely other pathways yet to be identified (Buiting et al., 2003).

1.4 Regulation of Imprinted Genes at Chromosome 15q11-q13.1

At human chromosome 15q11-q13.1, genomic imprinting regulates several genes that cluster in an imprinted domain (**Figure 1**). We focus on a small stretch of genes in the imprinted domain, from *SNURF/SNRPN* to *UBE3A*, which is important for gene regulation at this locus. Most genes in this region, including *SNURF/SNRPN*, *SNORD116*, *IPW*, *SNORD115*, and *UBE3A-ATS*, are expressed exclusively from the paternal allele. The coding portion of *SNURF/SNRPN*, *SNORD116*, and *IPW* are ubiquitously expressed, while the downstream *SNORD115* and *UBE3A-ATS* exhibit neuron-specific expression. *UBE3A* and *ATP10A* are the only two maternally expressed genes in this region in brain. However, *ATP10A* may not be imprinted in all individuals (Hogart et al., 2008). *UBE3A* is biallelically expressed in most human tissues, while the paternal allele shuts down in brain, resulting in maternal-specific *UBE3A* expression. The imprinted gene expressions mentioned above are controlled by two factors—a bipartite imprinting center (Reis et al., 1994; Saitoh et al., 1996) and a long non-coding antisense RNA (Landers et al., 2004; Rougeulle et al., 1998)—as described below.

1.4.1 *Bipartite Imprinting Center*

Genes residing in the imprinted domain of chromosome 15q11-q13.1 are regulated by a bipartite imprinting center, which includes a Prader-Willi syndrome imprinting center (PWS-IC) and an Angelman syndrome imprinting center (AS-IC) (Saitoh et al., 1996). PWS-IC encompasses the first exon of *SNURF/SNRPN* and a differentially methylated region (DMR). AS-IC represses the activity of PWS-IC

when establishing parent-of-origin-specific epigenetic marks in the maternal germ line. This repression results in DNA methylation on the maternal DMR and silencing of paternal-specific genes on the maternal allele in daughter somatic cells. On the other hand, the paternal DMR remain unmethylated, which allows paternal-specific expression of *SNURF/SNRPN* and its downstream transcripts, including *SNORD116*, *IPW*, and *SNORD115*. For these transcripts, PWS-IC functions as a canonical promoter, but PWS-IC also acts as an enhancer element for the proximal paternally expressed genes (Rodriguez-Jato et al., 2005).

1.4.2 *Long Non-coding Antisense RNA—UBE3A-ATS*

Paternally expressed *SNURF/SNRPN* and its downstream transcripts are transcribed as a single long non-coding RNA, which goes through extensive and complicated splicing events to produce two protein-coding transcripts and a variety of long and short noncoding RNAs (Runte et al., 2001). In most human tissues, this long RNA transcript starts at *SNURF/SNRPN*, encompasses *SNORD116*, and stops at *IPW*. In neurons, transcription continues through *IPW*, produces downstream non-coding transcripts, including *SNORD115*, and encompasses almost the entire region antisense to *UBE3A*. This neuron-specific long non-coding antisense RNA, known as *UBE3A-ATS*, is thought to epigenetically control the imprinted expression of *UBE3A* in brain, although the precise mechanism is not known (Landers et al., 2004; Rougeulle et al., 1998). Its paternal-specific expression is controlled by the DMR in PWS-IC. When the AS-IC, a repressor of the PWS-IC, is perturbed, the maternal allele assumes a

paternal epigenotype and results in AS (Buiting et al., 1999; Saitoh et al., 1996). This is presumably due to the aberrant maternal *UBE3A-ATS* expression in neurons that silences *UBE3A* on the maternal allele. Furthermore, when active transcription of *UBE3A-ATS* is disrupted, the dormant paternal *UBE3A* allele becomes un-silenced in neurons (Huang et al., 2012; Meng et al., 2015).

It remains perplexing how the regulatory *UBE3A-ATS* is expressed in a tissue-specific fashion, since the same specificity does not apply to the upstream *SNURF/SNRPN* coding transcripts, *SNORD116*, and *IPW*. One possibility is that tissue-specific alternative promoters, instead of the canonical *SNURF/SNRPN* promoter at exon 1, may be utilized in neurons to produce neuron-specific transcripts that encompass *UBE3A-ATS*. Indeed, several alternative neuron-specific exons upstream of *SNURF/SNRPN* that are spliced to *UBE3A-ATS* have been characterized previously in a murine model (Landers et al., 2004). Another possibility is that tissue-specific alternative splicing regulators may alter the splicing pattern at this region and result in neuron-specific splicing products that include *UBE3A-ATS*. As discussed in Chapter 4, we identified splicing factors that were enriched in *SNURF/SNRPN* lncRNA binding but did not contribute to its regulation/expression.

The mechanism through which *UBE3A-ATS* silences *UBE3A* on the paternal allele is also largely unknown. It was proposed that *UBE3A-ATS* may alter *UBE3A* promoter activity *in cis* and, hence, lead to *UBE3A* repression (Landers et al., 2004). However, this is unlikely because paternal *UBE3A* promoter was found to be hypomethylated and lack allele-specific histone modifications in brain (Kishino, 2006;

Makedonski et al., 2005). One of the most widely accepted hypotheses is that active *UBE3A-ATS* transcription blocks *UBE3A* transcription through steric hindrance between colliding RNA polymerase complexes (Shibata and Lee, 2003). Other mechanisms involving extensive sense-antisense overlap, such as RNA-hybridization *in cis*, are not excluded (Shibata and Lee, 2003).

1.5 The Angelman Syndrome Gene—*UBE3A*

As mentioned previously, *UBE3A* is the only gene in the imprinted domain that is expressed exclusively from the maternal allele in brain. Loss of maternal *UBE3A* results in Angelman syndrome, while excessive *UBE3A* was proposed to be the primary cause of Dup 15q syndrome. In brain, *UBE3A* imprinting only occurs in mature neurons, as *UBE3A* is biallelically expressed in neural precursors and glial cells (Dindot et al., 2008; Judson et al., 2014; Yamasaki et al., 2003). Maternal UBE3A protein expression is upregulated in mature neurons, presumably to compensate for the loss of paternal expression due to genomic imprinting (Dindot et al., 2008). UBE3A protein level is also regulated in an activity dependent manner—neuronal depolarization and fear conditioning lead to an increase in UBE3A protein *in vitro* and *in vivo*, respectively (Filonova et al., 2014). As neurons mature, UBE3A protein subcellular localization changes from cytoplasmic to nuclear (Judson et al., 2014; Miao et al., 2013). Interestingly, UBE3A protein level decreases during normal aging in mammalian and human postmortem brains (Williams et al., 2010b). Changes in UBE3A protein expression and localization during neuronal maturation and aging suggest that UBE3A may play different roles in developing and adult brain (Sell and Margolis, 2015). Indeed, recent studies showed that *Ube3a* restoration in adulthood was not sufficient to rescue

all neurological phenotypes in murine AS models (Meng et al., 2015; Silva-Santos et al., 2015). Prenatal reinstatement of *Ube3a*, on the other hand, successfully reversed all AS-relevant phenotypes (Silva-Santos et al., 2015). Due to the fact that a prolonged period of time is required for human brain development, the critical window for therapeutic intervention is likely to be much longer in AS patients. To determine the timing of paternal *UBE3A* silencing in human, we attempted to create a UBE3A-GFP fusion reporter using AS iPSCs through CRISPR/Cas9-mediated gene editing, as described in Chapter 3. However, we were unable to detect abundant UBE3A-GFP fusion proteins in these cells, most likely caused by low expression or instability at the protein level. Nevertheless, a successful UBE3A-GFP reporter AS iPSC line would be informative on spatiotemporal regulation of UBE3A expression during human neurodevelopment as well as a useful tool for high throughput drug screening for AS treatments.

Like most genes, *UBE3A* is subjected to alternative splicing and/or polyadenylation. It gives rise to five different RNA transcripts and is predicted to encode three different UBE3A protein isoforms in human (Yamamoto et al., 1997). In mouse, three *Ube3a* transcripts have been identified. Of these three *Ube3a* transcripts, isoform 2 has the longest open reading frame, encoding for an 870 aa protein isoform. Compared to isoform 2, the protein product of isoform 3 lacks 21 aa on the N-terminus, while the protein product of isoform 1 lacks 21 aa on the N-terminus as well as 87 aa on the C-terminus (Miao et al., 2013). The shortened C-terminus encoded by isoform 1 renders its protein product catalytically inactive (Valluy et al., 2015). In human, the fifth

UBE3A RNA transcript undergoes alternative polyadenylation and corresponds to the murine *Ube3a* isoform 1 (Valluy et al., 2015). The unique 3'-UTR of *Ube3a* isoform 1 mRNA regulates dendrite complexity and spine morphogenesis by acting as a sponge and sequestering regulatory microRNAs in rats (Valluy et al., 2015). On the other hand, catalytically active Ube3a proteins from isoform 2/3 are important for polarized dendrite morphogenesis in mouse pyramidal neurons through dendritic Golgi deployment (Miao et al., 2013). In addition, when overexpressed in mouse brain, Ube3a isoform 1 and 2 are largely cytosolic, while isoform 3 mostly localizes to the nucleus (Miao et al., 2013). These findings in murine models suggest that each *UBE3A* isoforms may have its unique role in brain development.

UBE3A encodes for an ubiquitin protein ligase E3A, also known as E6-AP. E6-AP is one of the E3 ubiquitin ligases, which are important for protein degradation through proteasome by tagging poly-ubiquitin chains to its targets (Huang et al., 1999; Scheffner et al., 1993). Recently, it was reported that catalytically active E6-AP functions as an oligomer (Ronchi et al., 2014). Since mutations or short in-frame deletions that render E6-AP catalytic domain nonfunctional have been reported in AS patients, improper regulation and accumulation of E6-AP substrate(s) was proposed to be the major cause for AS (Cooper et al., 2004). On the other hand, excessive E6-AP is hypothesized to cause accelerated protein degradation and reduced substrate level in Dup 15q syndrome. In the past few years, identifying disease-relevant substrates for E6-AP has been one of the major focuses in the field, although few of them have been reported, including Pbl/ECT2 (Reiter et al., 2006), Ephexin5 (Margolis et al., 2010), Arc

(Greer et al., 2010), and GAT1 (Egawa et al., 2012). Whether Arc is a direct substrate of E6-AP is still debatable (Kuhnle et al., 2013; Mabb et al., 2014). In addition to protein ubiquitination, E6-AP has been reported as a transcriptional coactivator, although this function is not associated with central AS phenotypes (Nawaz et al., 1999; Smith et al., 2002). Other secondary changes in protein level or activity caused by the loss of E6-AP were also reported, such as Na^+/K^+-ATPase α1 subunit (Kaphzan et al., 2013) and hippocampal CaMKII phosphorylation (van Woerden et al., 2007; Weeber et al., 2003). By modulating downstream targets of E6-AP, some AS characteristic phenotypes can be rescued in murine models (Egawa et al., 2012; Kaphzan et al., 2013; Mandel-Brehm et al., 2015; van Woerden et al., 2007). However, not a single target alone can fully reverse the effect of E6-AP loss in AS neurons, indicating that AS is likely caused by alterations of a complicated gene and protein network (Sell and Margolis, 2015).

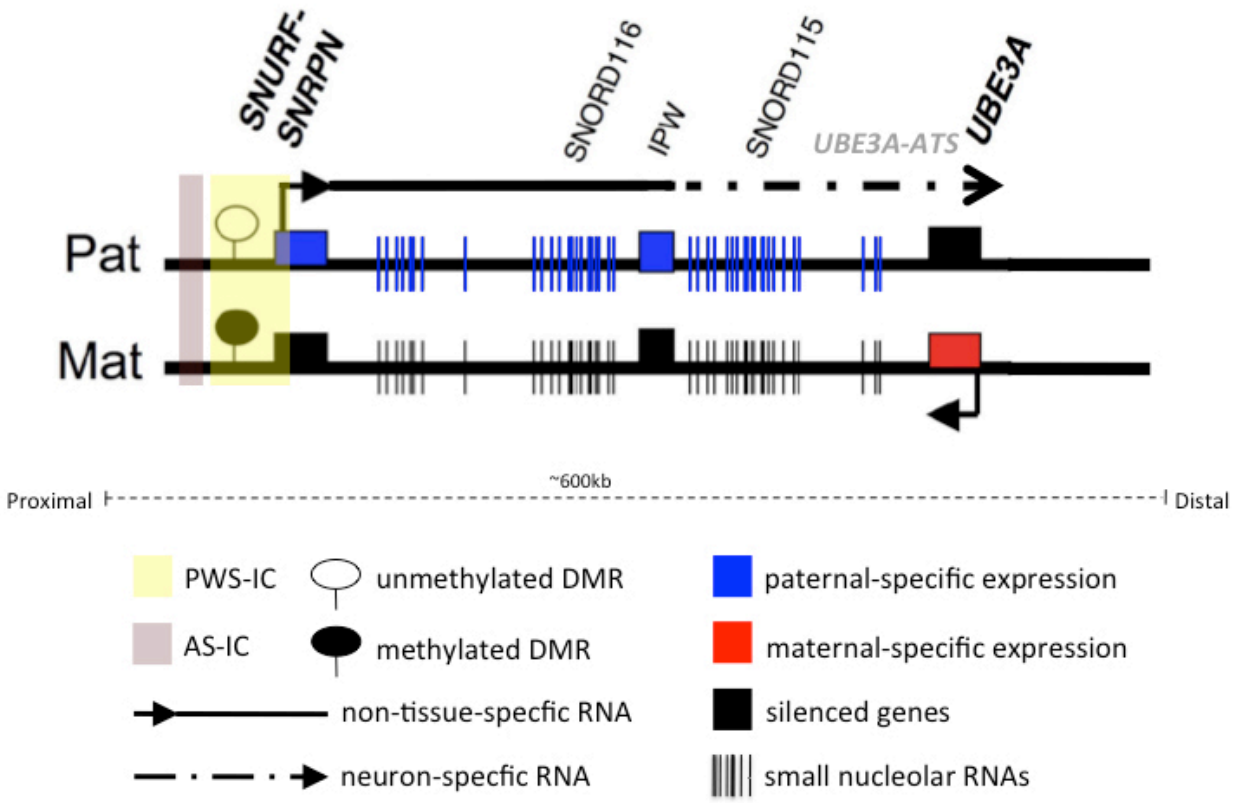

Figure 1. Human chromosome 15q11-q13.1 imprinted cluster at *UBE3A* locus.

Chapter 2

Disease Modeling Using Induced Pluripotent Stem Cells for Angelman, Prader-Willi, and Dup 15q Syndromes

Data presented in this chapter are published in the following papers:

Chamberlain, S.J., Chen, P.F., Ng, K.Y., Bourgois-Rocha, F., Lemtiri-Chlieh, F., Levine, E.S., and Lalande, M. (2010). Induced pluripotent stem cell models of the genomic imprinting disorders Angelman and Prader-Willi syndromes. Proc Natl Acad Sci U S A *107*, 17668-17673.
My Contribution: iPSC characterization, methylation-specific RT-qPCR, RT-PCR

Germain, N.D., Chen, P.F., Plocik, A.M., Glatt-Deeley, H., Brown, J., Fink, J.J., Bolduc, K.A., Robinson, T.M., Levie, E.S., Reiter, L.T.*, et al.* (2014). Gene expression analysis of human induced pluripotent stem cell-derived neurons carrying copy number variants of chromosome 15q11-q13.1. Molecular autism *5*, 44.
My Contribution: neural differentiation, methylation-specific RT-qPCR

Martins-Taylor, K., Hsiao, J.S., Chen, P.F., Glatt-Deeley, H., De Smith, A.J., Blakemore, A.I., Lalande, M., and Chamberlain, S.J. (2014). Imprinted expression of UBE3A in non-neuronal cells from a Prader-Willi syndrome patient with an atypical deletion. Hum Mol Genet *23*, 2364-2373.
License Date: Jan 29, 2016; License Number: 3798290102999
My Contribution: methylation-specific RT-qPCR, RT-qPCR

Chamberlain, S.J., Germain, N.D., Chen, P.F., Hsiao, J.S., and Glatt-Deeley, H. (2016). Modeling Genomic Imprinting Disorders Using Induced Pluripotent Stem Cells. Methods Mol Biol *1353*, 45-64.
License Date: Jan 10, 2016; License Number: 3785350330106
My Contribution: manuscript writing for allele-specific PCR and proof reading.

2.1 Background and Significance

Murine models have provided significant insights on AS, PWS, and Dup 15q syndrome because they are more amenable genetically than human cells and they provide neurons developed in natural context as well as behavioral phenotypes. Murine models were especially instrumental in understanding imprinting regulatory mechanism at AS- and PWS-IC (Chamberlain and Brannan, 2001; Johnstone et al., 2006; Yang et al., 1998), as well as ruling out genes that are not central to disease phenotypes (Bischof et al., 2007; Mercer and Wevrick, 2009; Tsai et al., 1999a; Tsai et al., 1999b). However, cognitive and social impairments in non-primates are hard to assess, and current AS, PWS, and Dup 15q murine models failed to fully recapitulate human phenotypes. The divergence in gene regulation between mouse and human at the homologous region to human chromosome 15q11-q13.1 may explain the phenotypic differences (Chamberlain and Lalande, 2010b). In mice, the entire *SNURF/SNRPN* lncRNA that silences paternal *UBE3A* is only expressed in neurons, while only the second half of *SNURF/SNRPN* lncRNA (i.e. from *SNORD115* to *UBE3A-ATS*) is neuron-specific in human.

The most relevant tissue, fetal brain, for rare neurodevelopmental disorders, such as AS, PWS, and Dup 15q syndromes, has been difficult to obtain and limited to post-mortem samples with varying qualities. Ever since Thomson et al. established the first human embryonic stem cell line in 1998, scientists have been looking for ways to obtain live human neurons through *in vitro* neural differentiation. The first neural differentiation protocol using human embryonic stem cells was established in 2001 (Zhang et al.,

2001), and many more refined protocols for specific neuronal subtype soon followed (Germain et al., 2013; Li et al., 2008; Perrier et al., 2004). In 2007, Takahashi et al. made a Nobel-winning discovery, namely induced pluripotent stem cell (iPSC) technology, which enables scientists to convert human somatic cells back to an embryonic stem cell-like stage (Takahashi et al., 2007). In combination, these two technologies revolutionized the field of neurological disease modeling, providing unlimited and readily accessible patient-derived neuronal tissues.

To address the fundamental question of how imprinting at chromosome 15q11-q13.1 is regulated in human brain, we established patient-derived iPSCs and their neural derivatives as models for AS, PWS, and Dup 15q syndrome (Chamberlain et al., 2010; Germain et al., 2014; Martins-Taylor et al., 2014). Specifically, we took advantage of large deletions that cause AS and PWS to study paternal- and maternal-specific gene expression respectively. With this system, we were able to study the gene regulatory mechanism at chromosome 15q11-q13.1 in an allele-specific manner (manuscript under review and (Cruvinel et al., 2014)). A rare microdeletion from a PWS patient provided us insights on the regulation of neuron-specific portion of the *SNURF/SNRPN* lncRNA (Martins-Taylor et al., 2014). In addition, cells with various chromosome 15q11-q13.1 duplications helped decipher gene contributions to Dup 15q syndrome (Germain et al., 2014). In this chapter, I will discuss the process of reprogramming, iPSC quality control, techniques used to determine the imprinting status at chromosome 15q11-q13.1, and neural differentiation.

2.2 Rationale

Given the differences in phenotypes and *SNURF/SNRPN* lncRNA tissue-specificity between mice and patients with AS, PWS, and Dup 15q syndrome, patient-derived iPSCs and their neural derivatives can provide insights on gene regulation at chromosome 15q11-q13.1 during human neurodevelopment. These cells are also useful for identifying potential therapeutic targets and drug screening.

One concern for modeling human disorders involving genomic imprinting using iPSCs is that the parental imprints may be altered in the process of converting somatic cells to iPSCs (Colman and Dreesen, 2009; Pick et al., 2009). It is known that chromosome modifications and DNA methylation, which are responsible for genomic imprinting, can be erased and re-established at certain loci during reprogramming (Colman and Dreesen, 2009; Pick et al., 2009; Takahashi et al., 2007). However, we do not expect these changes to occur at the PWS-IC because the chromosome modifications and DNA methylation at this locus are established in the male and female germlines, instead of early embryos (Buiting et al., 1995; Dittrich et al., 1996; Ferguson-Smith, 1996). Moreover, DNA methylation at PWS-IC is stably maintained in mouse as well as human embryonic stem cells (Rugg-Gunn et al., 2007; Schumacher and Doerfler, 2004).

To determine whether patient-derived iPSCs and their neural derivatives can be used as a proper disease models for AS, PWS, and Dup 15q syndrome, we carefully assessed the methylation status at PWS-IC and gene expression at chromosome 15q11-q13.1. We measured neuronal activities using electrophysiology and determined

neural cell types using immunocytochemistry to ensure that these neurons are functional and that the neural culture mimics cortical population. We also assessed *UBE3A* imprinting status by measuring UBE3A protein level with Western blotting as well as *UBE3A-ATS* expression using RT-PCR, allele-specific PCR, and RNA fluorescence *in situ* hybridization (RNA-FISH).

2.3 Materials and Methods

iPSC Cell Culture

All iPSCs used in this study were maintained as described before (Chamberlain et al., 2010). Briefly, iPSCs were grown on irradiated mouse embryonic fibroblasts (iMEFs) and fed daily with conventional hESC medium consisting of DMEM-F12 supplemented with knock-out serum replacer, nonessential amino acids, L-glutamine, β-mercaptoethanol, and basic FGF. iPSCs were cultured in a humid incubator at 37 °C with 5% CO_2 and passaged approximately once a week manually.

Methylation-Specific PCR

Genomic DNAs were subjected to bisulfite conversion using the EZ DNA methylation-Gold Kit (Zymo Research) according to the manufacturer's instructions. A multiplex PCR was carried out using the following primers:

15maternalF, 5′-TAATAAGTACGTTTGCGCGGTC-3′;

15maternalR, 5′-AACCTTACCCGCTCCATCGCG-3′;

15paternalF, 5′-GTAGGTTGGTGTGTATGTTTAGGT-3′;

15paternalR, 5′-ACATCAAACATCTCCAACAACCA-3′.

Quantitative Reverse-Transcription PCR

RNA samples were isolated using RNA-Bee (Tel-Test Inc.) and converted into cDNA using High-Capacity cDNA Reverse Transcription Kit (Applied Biosystems) according to the manufacturer's instructions. Expression levels of target genes were measured using Taqman gene expression assays (Applied Biosystems) following the manufacturer's protocol. All genes were normalized to *GAPDH*. Relative quantity (RQ) value was calculated as $2^{-\Delta\Delta Ct}$ using the calibrator sample.

Neural Differentiation

iPSC-derived neuronal culture were generated using either embryoid-body based (Pankratz et al., 2007) or monolayer (Germain et al., 2013) differentiation protocol with some modifications as previously reported (Chamberlain et al., 2010; Germain et al., 2014). Briefly, iPSC colonies were manually cut and lifted when generating embryoid bodies for the embryoid-body protocol. After three weeks of neural differentiation using either protocol, neural progenitors were plated on tissue culture plates coated with poly-ornithine/laminin. The neural differentiation medium consisted of Neurobasal Medium, B-27 supplement, nonessential amino acids, and L-glutamine, and was supplemented with 1 µM ascorbic acid, 200 µM cyclic adenosine monophosphate, 10 ng/mL brain-derived neurotrophic factor, and 10 ng/mL glial-derived neurotrophic factor. Unless otherwise specified, all experiments were conducted on neural cultures that were at least 10 weeks old.

Immunocytochemistry

Immunocytochemistry was carried out as previously described (Chamberlain et al., 2010; Germain et al., 2014). The following antibodies and concentrations were used: rabbit anti-NANOG (1:100, Abcam), mouse anti-SSEA4 (1:20, Developmental Studies Hybridoma Bank), mouse anti-TRA1-60 (1:200, Santa Cruz), mouse anti-TRA1-81 (1:200, Santa Cruz), mouse anti-PAX6 (1:20, Developmental Studies Hybridoma Bank), rabbit anti-MAP2 (1:200, Millipore), chicken anti-MAP2 (1:10,000, Abcam) mouse anti-TUJ1 (1:200, Covance), rabbit anti-SynapsinI (1:200, Millipore), mouse anti-PSD-95 (1:100, NeuroMab), mouse anti-PanNav (1:200, Sigma), rabbit anti-S100β (1:200, Abcam), mouse anti-VGLUT1 (1:100, Synaptic Systems), and rabbit anti-GAD65/67 (1:2000, Sigma). AlexaFluor goat anti-rabbit and anti-mouse 488, 594, and 647 fluorochrome conjugated secondary antibodies (Life Technology) were used at 1:200. A goat anti-chicken IgY-650 secondary antibody (Abcam) was used at 1:250. Nuclei were counterstained with DAPI and coverslips were mounted on slides with Vectashield (Vector Laboratories). Slides were imaged using a Zeiss Axiovision microscope at magnification of 5X, 20X, 40X, and 63X.

DNA Methylation Analysis, Allele-specific PCR, and RNA Fluorescence *in situ* Hybridization (RNA FISH)

Detailed protocols (Chamberlain et al., 2016) are published in a book, titled "Patient-specific Induced Pluripotent Stem Cell Models," shown as following.

2.4 Methods Section for DNA Methylation Analysis, Allele-specific PCR, and RNA Fluorescence in situ Hybridization

---

Modeling Genomic Imprinting Disorders Using Induced Pluripotent Stem Cells

Chamberlain, S.J., Germain, N.D., Chen, P.F., Hsiao, J.S., and Glatt-Deeley, H. (2016). Modeling Genomic Imprinting Disorders Using Induced Pluripotent Stem Cells. Methods Mol Biol *1353*, 45-64.

i. Abstract
Induced pluripotent stem cell (iPSC) technology has allowed for the invaluable modeling of many genetic disorders including disorders associated with genomic imprinting. Genomic imprinting involves differential DNA and histone methylation and results in allele-specific gene expression. Most of the epigenetic marks in somatic cells are erased and reestablished during the process of reprogramming into iPSCs. Therefore, in generating models of disorders associated with genomic imprinting, it is important to verify that the imprinting status and allele-specific gene expression patterns of the parental somatic cells is maintained in their derivative iPSCs. Here, we describe three techniques: DNA methylation analysis, allele-specific PCR, and RNA FISH, that we use to analyze genomic imprinting in iPSC models of neurogenetic disorders involving copy number variations of the chromosome 15q11-q13 region.

ii. Keywords
induced pluripotent stem cells, genomic imprinting, DNA methylation, allele-specific PCR, RNA FISH

1. **Introduction**
Genomic imprinting is an epigenetic phenomenon by which genes are expressed in a parent-of-origin dependent manner. This process occurs primarily in eutherian mammals, although it can also be observed in plants and metatherians. The estimated number of imprinted genes varies from a conservative estimate of 100 genes(Henckel and Arnaud, 2010) to more than 1,000(Gregg et al., 2010), depending on how such imprinted expression was ascertained and the criteria for determining whether a gene is imprinted(Kelsey and Bartolomei, 2012).

DNA cytosine methylation, as well as specific active and repressive histone modifications are involved in mediating the allele-specific gene expression in genes regulated by genomic imprinting. Most imprinted loci have an imprinting control region (ICR) that is an area of differential DNA methylation between the two parental alleles(Henckel and Arnaud, 2010). The ICR is typically methylated on the silent, repressed allele and unmethylated on the expressed,

active allele. Repressive histone modifications, such as trimethylation of histone H3 on lysine 9 (H3K9me3) and histone H3 lysine 79 (H3K79me3) often accompanies DNA methylation on the repressed allele of the ICR(Singh et al., 2011). Active histone modifications such as di- and trimethylation of histone H3 on lysine 4 (H3K4me2 and me3), mono-and dimethylation of histone H3 lysine 79 (H3K79me1 and me2), and acetylation at histone H4 lysine 91 (H4K91Ac) often adorn the unmethylated allele at the ICR(Singh et al., 2011). Altogether, the ICR often controls the imprinted expression of all of the genes within the imprinted cluster, regardless of the parent of origin of their gene expression. Thus, the ICR harbors important epigenetic modifications that ultimately determine the allele-specific expression of several imprinted genes within a cluster.

Imprinted genes, which are expressed from a single parental allele, are functionally haploid in the organism. Deletion or mutation of the single expressed allele leaves an organism null for the imprinted gene. Several human neurogenetic disorders arise from the disruption of the expressed alleles of imprinted genes. Prader-Willi and Angelman syndromes are caused by the loss of function from paternally- and maternally-inherited alleles of the chromosome 15q11-13 region, respectively(Chamberlain and Lalande, 2010a). Beckwith-Wiedemann syndrome is caused by the loss of function from maternal chromosome 11p15(Jacob et al., 2013). Silver-Russell syndrome is caused by disruption of imprinted genes on chromosomes 7(Nakabayashi et al., 2002) and 11(Jacob et al., 2013). Pseudohypoparathyroidism (Albright's hereditary osteodystrophy) and uniparental disomy 14 are also disorders caused by disruption of imprinted genes(Davies and Hughes, 1993). Complex genetic regulation underlies the imprinted genes in each of these disorders, making it difficult to generate cell culture or animal models.

Human induced pluripotent stem cells (iPSCs) are becoming an attractive approach to modeling complex genetic disorders, such as those involving genomic imprinting(Chamberlain et al., 2008). The use of somatic cells derived from patients enables the genetic complexities to be captured in indefinitely self-renewing stem cells that are capable of differentiation into virtually any lineage. Using iPSC technology, copy number variation and uniparental disomy that often leads to disorders involving genomic imprinting can be recapitulated in stem cells. Our group has generated iPSCs from individuals with Prader-Willi syndrome, Angelman syndrome, and Dup15q syndrome, which all involve copy number variation at an imprinted locus(Chamberlain et al., 2010; Germain ND, 2014; Martins-Taylor et al., 2014). However, epigenetic modifications are erased and established during the reprogramming process involved in the establishment of iPSC lines. Since appropriate expression of imprinted genes depends on the maintenance of epigenetic modifications during the reprogramming process, extensive analysis of the relevant epigenetic modifications and gene expression is a stringent requirement for modeling disorders that involve genomic imprinting. Here we detail methods that our lab uses to verify appropriate imprinted expression of genes at the human chromosome 15q11-13 locus.

Differential DNA methylation at the ICR underlies virtually every genomic imprint. We use a quantitative PCR (qPCR) based assay to quantify the fraction of methylated and unmethylated alleles at the human Prader-Willi syndrome imprinting center (PWS-IC). This assay is excellent for quantifying cytosine methylation at ICRs that are relatively stable. It can assay up to seven CpG dinucleotides, but it cannot assay the CpGs individually. In contrast to other protocols for methylation specific PCR, this approach does not require bisulfite conversion to assay

methylation at specific CpGs. Rather, it relies on the digestion of DNA by methylation sensitive and methylation dependent restriction enzymes followed by quantification of the DNA by qPCR (Bruce et al., 2008; Oakes et al., 2006; Yamada et al., 2004). The methylation sensitive enzymes (MSREs) used can only cleave unmethylated DNA since methylated cytosines block enzyme activity. In contrast, methylation dependent restriction enzymes (MDREs) will only digest DNA at methylated cytosine residues. Therefore, digestion with MSREs leaves only methylated DNA and digestion with MDREs leaves only unmethylated DNA available for PCR amplification. Using primer sets designed to flank the specific DNA region of interest, the digested DNA is then analyzed by qPCR. By comparing the cycle threshold (Ct) values generated for each of the digest conditions, the relative amounts of methylated and unmethylated DNA in the region is calculated. Two control reactions are included to allow for more accurate quantitation. A mock digest is performed without either enzyme to quantify the amount of total input DNA amplified with the chosen primer set. A double digest, including both the MSREs and the MDREs, represents background signal from the qPCR reaction as all of the DNA should be digested and unavailable for amplification.

The actual expression of imprinted genes is the single most important factor in determining whether the genomic imprint is correctly established in iPSCs. The collection of epigenetic modifications amalgamates in a precise parent-of-origin gene expression pattern for each imprinted gene. We use allele-specific PCR and/or RNA fluorescence *in situ* hybridization (RNA-FISH) to determine allele specific gene expression. The allele-specific PCR assay can correctly ascribe gene expression to a single parental allele. This can be used to ascertain the allele-specificity across a population of cells. This assay takes advantage of polymorphic sequences on each allele to distinguish the origin of sense and anti-sense RNA transcripts expressed from the same genomic locus. The first step in this approach is to identify existing polymorphism in the target gene. Once the polymorphism is verified, strand-specific reverse transcription is used to distinguish sense and anti-sense transcripts. Followed by PCR amplification across the verified polymorphism, the origin of sense and anti-sense transcripts can be deciphered. RNA-FISH, on the other hand allows one to assay sense versus antisense transcription, which often accompanies imprinted gene expression, on a cell-by-cell basis.

2. Materials

2.1 DNA Methylation Analysis Components

1. Cell lysis buffer: 0.5% Sarcosyl, 200nM NaCl, 10mM EDTA, 10mM Tris pH 8.0
2. Proteinase K (20mg/mL, catalog #P8107S, New England Biolabs)
3. Cell scrapers
4. 1.5mL Eppendorf tubes
5. Phenol-chloroform with isoamyl alcohol
6. 100% ethanol
7. DNase-free distilled water (dH20)
8. Microcentrifuge
9. NanoDrop spectrophotometer
10. EpiTect Methyl II DNA Restriction Kit (catalog #335452, SABiosciences) or individual MSREs / MDREs (e.g., MspI, HpaII, etc., New England Biolabs)
11. 0.2mL PCR microtube strips with caps

12. Thermocycler
13. EpiTect Methyl PCR Primer Assay for the gene of interest. For the PWS-IC, we use a human SNRPN primer (catalog #EPHS104317-1A, SABiosciences). Alternatively, primer sets can be designed that flank the methylation sites to be analyzed using various software programs and ordered from commercial providers.
14. SYBR-Green PCR Master Mix (catalog #330520, SABiosciences or catalog #4334973, Applied Biosystems)
15. 96-well PCR plates
16. Tabletop centrifuge
17. Quantitative PCR instrument

2.2 Allele-specific PCR Components

1. Primers for amplifying polymorphic sequence
2. Phusion® High-Fidelity DNA Polymerase (catalog #M0530S, New England Biolabs)
3. QIAquick PCR Purification Kit (catalog #28104, Qiagen)
4. T7 Endonuclease I (catalog #M0302S, New England Biolabs)
5. Gel electrophoresis apparatus, 2% agarose gel, and matching buffer
6. RNA-Bee (catalog # #CS-104B, Tel Test, Inc.)
7. TURBO DNA-free Kit (catalog #AM1907, Life Technologies)
8. Superscript III (catalog #18080044, Life Technologies)
9. Tagged RT primers (S-RT and ATS-RT)
10. Advantage 2 Polymerase Mix (catalog #639207, Clontech)
11. PCR primers for tag sequences (F' and R')
12. PCR forward and reverse primers (F and R)
13. Novex TBE 6% polyacrylamide gel (catalog #EC6265BOX, Life Technologies)
14. TBE Buffer (catalog #15581-044, Life Technologies)
15. XCell SureLockTM Mini-Cell (catalog #EI0001, Life Technologies)
16. SYBR Gold (catalog #S-11494, Life Technologies)

2.3 RNA FISH Components

1. 12 mm round coverslips (catalog #12-545-80, Fisherbrand)
2. Nick Translation DNA Labeling System (catalog #ENZ-42910, Enzo)
3. ChromaTide Alexa Fluor 594-5-dUTP (catalog #C-11400, Life Technologies)
4. SNORD115 BAC (RP11-37A4, CHORI)
5. MAXIscript T7/T3 Kit (catalog #AM-1324M, Life Technologies)
6. ChromaTide Alexa 488-5-UTP (catalog #C-11403, Life Technologies)
7. Not I (catalog #R0189L, New England Biolabs)
8. Carbonate buffer: 60 mM Na_2CO_3 and 40 mM $NaHCO_3$
9. Micro Bio-Spin P-30 Tris column (catalog #732-6223, Bio-Rad)
10. Human Cot-I DNA 1 µg/µL (catalog #1 581 074, Roche)
11. Salmon sperm DNA
12. 20X SSC (Various SSC dilutions, including 4X SSC, 2X SSC, and 1X SSC, are made from this 20X SSC stock.)
13. 2X hybridization buffer: 1 part 20X SSC, 1 part 10 mg/mL BSA, 1 part nuclease-free water, and 2 parts 50% dextran sulfate.
14. CSK buffer: 100 mM NaCl, 300 mM sucrose, 3 mM MgCl2, and 10mM PIPES pH6.8.

15. 1% Triton X-100/CSK: 100 µL Triton X-100 in 9.9 mL CSK buffer
16. 50% formamide/2X SSC: 1 part 100% formamide in 1 part 4X SSC
17. Vectashield with DAPI (catalog #H-1200, Vector Laboratories)

3. Methods

3.1 DNA methylation analysis

3.1.1 Isolate Genomic DNA

1. Collect iPSCs (approximately $2x10^6$ cells) by scraping with a cell scraper and pellet in a 1.5mL Eppendorf tube.
2. Add 300µL of Cell Lysis Buffer and 20µl of 20mg/mL Proteinase K to pelleted cells. Vortex and incubate in a 55˚C waterbath overnight (at least 18 hours). (See **Note 1**)
3. Add 300µL of phenol-chloroform to lysate and vortex at least 30 seconds.
4. Spin for 3 minutes at maximum speed in a room temperature microcentrifuge.
5. Carefully transfer the upper aqueous phase to a new 1.5mL Eppendorf tube. Avoid contact with the lower phenol phase or the white interphase which may have formed after centrifugation.
6. Add 1mL of 100% ethanol to aqueous phase and invert tube several times. White strands of DNA should be visible as it precipitates.
7. Spin for 5 minutes at maximum speed in a room temperature microcentrifuge.
8. Remove all supernatant and air dry pelleted DNA for approximately 5-10 minutes.
9. Resuspend DNA in 50-100µL of dH20.
10. Check concentration of DNA using a NanoDrop spectrophotometer.
11. Store at 4˚C or at -20˚C for long term storage.

3.1.2 Perform restriction digest with MSREs and MDREs

1. Prepare a solution of 0.5-1.0µg of DNA with the appropriate dilution of restriction digest buffer and dH20. If using the EpiTect Methyl II DNA Restriction Kit, use 26µL of 5X Digestion Buffer and add dH20 to a final volume of 120µL. If using restriction enzymes from another source, prepare a volume of 200µL, which is sufficient for four 50µL individual restriction digest reactions. (See **Note 2**)
2. Thoroughly mix the DNA/buffer solution and divide equally into four separate PCR tubes. (See **Note 3**)
3. Set up the restriction digest reactions and controls by adding the following to each PCR tube: If using the EpiTect Methyl II DNA Restriction Kit, for MSRE reaction– add 1µL of dH20 and 1µL of MSRE (Enzyme A), for MDRE – add 1µL of dH20 and 1µL of MDRE (Enzyme B), for the double digest – add 1µL each of the MSRE and MDRE, and for the mock digest – add 2µL of dH20 in place of restriction enzymes. (See **Note 4**)
4. Mix reactions gently by pipetting and briefly spin samples in a microcentrifuge.
5. Incubate reactions at 37˚C in a thermocycler for at least 6 hours to overnight.
6. Inactivate restriction enzymes by incubating reactions at 65˚C for 20 minutes in a thermocycler.
7. Perform qPCR with digested DNA or store digest reactions at -20˚C until use.

3.1.3 Analyze digested DNA by qPCR

1. Prepare qPCR reaction master mix by combining SYBR-green qPCR Master Mix, EpiTect Methyl PCR Assay Primer, and dH20 sufficient to run each DNA sample in

triplicate (each mock, MSRE, MDRE, and MSRE+MDRE digest is considered a separate sample). To account for pipetting volume error, prepare enough master mix for at least two excess reactions. Each 20µL total PCR reaction will ultimately contain: 10µL SYBR-green qPCR Master Mix, 1µL EpiTect Methyl PCR Assay Primer, 5µL of digest DNA and 4µL dH20. (See **Note 5**)

2. Pipette 15µL of master mix reaction into each well of the qPCR plate. Add 5µL of sample to the individual wells and mix my gentle pipetting.
3. Seal the qPCR plate and spin briefly in a tabletop centrifuge.
4. Perform qPCR amplification. If using EpiTect Methyl PCR Assay primers the following conditions should be used: (1) 95˚C for 10 minutes to activate HotStart DNA polymerase. (2) 3 cycles of 99˚C for 30 seconds and 72˚C for 1 minute. (3) 40 cycles of 97˚C for 15 seconds and 72˚C for 1 minute. (4) Standard melting curve. Record SYBR-green signal at each of the 72˚C cycles in step 3. (See **Note 6**)
5. Calculate percent methylated and percent unmethylated DNA using the Ct values generated from the qPCR run. SABiosciences provides an Excel spreadsheet which can be used to automatically perform these calculations after inserting the mean Ct value for each sample. This spreadsheet takes into account the percentage of DNA resistant to digestion (represented by the double digest reaction) in calculating the percent methylated and unmethylated DNA. Alternatively, several methods have been independently reported to perform these calculations (See **Note 7**).

3.2 Allele-specific PCR

3.2.1 Screening for Polymorphic Sequence

1. Use tracks under the categories of "Variation" or "Repeats" in UCSC Genome Browser (genome.ucsc.edu) to look for reported SNPs or short tandem repeats in the target gene. As an example, a polymorphic region of short tandem repeats in an intron of UBE3A gene was identified using the "Microsatellite" track in **Figure 1**.
2. Carry out T7 E1 assay with the following steps modified from the manufacturer's protocol for T7 Endonuclease I.
    i. Prepare good quality genomic DNA from cells as described in section *3.1.1* (see **Note 8**).
    ii. Design primers to amplify about 1kb region around the polymorphic sequence, preferably with the polymorphic sequence offset from the center as shown in **Figure 1** (see **Note 9**).
    iii. Carry out 50µL PCR reaction using Phusion® High-Fidelity DNA Polymerase or other proofreading DNA polymerase to obtain correct PCR product.
    iv. Clean up PCR product using QIAquick PCR Purification Kit and elute DNA in 30µL elution buffer. When eluting, let the column sit in elution buffer at room temperature for at least 5 minutes before spinning to increase yield.
    v. Measure DNA concentration using a NanoDrop spectrophotometer (see **Note 8**).
    vi. Add 150ng of cleaned PCR product into a 0.2mL PCR tube. Add 1µL of 10x NEBuffer 2 and bring the total volume up to 10µL with water. Save the remaining PCR product as a control for gel electrophoresis in a later step.
    vii. Run the following program in a thermocycler to make heteroduplex:

95°C	10 minutes
95°C to 85°C	decrease 2.0°C per second
85°C	1 minute
85°C to 75°C	decrease 0.3°C per second
75°C	1 minute
75°C to 65°C	decrease 0.3°C per second
65°C	1 minute
65°C to 55°C	decrease 0.3°C per second
55°C	1 minute
55°C to 45°C	decrease 0.3°C per second
45°C	1 minute
45°C to 35°C	decrease 0.3°C per second
35°C	1 minute
35°C to 25°C	decrease 0.3°C per second
25°C	1 minute
4°C	∞

viii. Add 0.5µL of T7 Endonuclease I into the PCR tube and incubate at 37°C for 30 minutes in a thermocycler to cut any heteroduplex that has formed in the previous step.

ix. Stop the reaction by adding 2.5µL of loading dye that contains 0.1M EDTA (see **Note 10**).

x. Run the digested product alongside the original PCR product from step vi on a 2% agarose gel. As an example, a gel for a polymorphic sequence verified by T7 E1 assay is shown in **Figure 2.**

3.2.2 RNA Isolation and DNase Treatment

1. Collect and pellet cells by centrifugation in a 1.5mL Eppendorf tube.
2. Follow manufacturer's protocol (Chomczynski and Sacchi, 1987) using RNA-Bee (see **Note 11**) with the following modifications: 1) For phase separation, shake tube vigorously for 30 seconds. 2) For RNA precipitation, let tube sit at room temperature for 10 minutes before centrifuging at 4°C for 15 minutes. 3) For RNA wash, centrifuge tube at 4°C for 10 minutes. 4) For RNA solubilization, dissolve pellet in nuclease-free water (see **Note 12**).
3. To reduce genomic DNA contamination, treat isolated RNA from the previous step with DNaseI using TURBO DNA-free Kit. Follow manufacturer's protocol exactly, except extend the 37°C incubation time to 45 minutes.
4. Measure the RNA concentration using a NanoDrop spectrophotometer.
5. Store RNA at -80°C until ready to use for reverse transcription.

3.2.3 Primer Design for Strand-specific Reverse Transcription (RT) and PCR

1. Design the following primers surrounding the polymorphic sequence as depicted in **Figure 3**. (See **Notes 13, 14, 15, and 16**)
   i. *Tagged RT Primers for the sense transcript (S-RT) and anti-sense transcript (ATS-RT)*: These primers consist of two parts: a 5' tag and a gene-specific RT primer. For the 5' tag on S-RT, use the following sequence as a template: 5'-

CAGTCGGGCGTCATCA-3'(Shirk et al., 2013a). For the 5' tag on ATS-RT, use the following sequence from M13R as a template: 5'-GGAAACAGCTATGACCAT-3'. Add or remove nucleotides from the ends of the primer sequence to optimize the melting temperature and minimize secondary structure formation (see **Note 17**). For the gene-specific RT primers, use Primer3 (Koressaar and Remm, 2007; Untergasser et al., 2012) or other similar software to design a primer located upstream of the polymorphic sequence on the sense and anti-sense transcripts. The melting temperature for these sequences should be around or slightly below 55°C (See **Note 18**). Check the tag sequence, the gene-specific RT primer sequence, and the final combined sequence using BLAST or UCSC genome browser for mis-priming.

ii. *PCR primer for the tag sequence on S-RT (A)*: This primer is the same sequence as the tag sequence on S-RT.

iii. *PCR primer for the tag sequence on ATS-RT (C)*: This primer is the same sequence as the tag sequence on ATS-RT.

iv. *PCR primer B*: This primer is located upstream of the polymorphic sequence on the sense transcripts.

v. *PCR primer D*: This primer is located upstream of the polymorphic sequence on the anti-sense transcripts.

3.2.4 Strand-specific Reverse Transcription (RT)

1. Follow manufacturer's protocol for Superscript III.
2. Set up two RT reactions: one using S-RT as the gene-specific primer and another using ATS-RT as the gene-specific primer. For each reaction, include a no RT control that contains the same ingredients except for the reverse transcriptase. The no RT controls (S-noRT and ATS-noRT) will indicate any genomic DNA contamination in the following PCR reaction.
3. Heat the primer/dNTP/DNase-treated RNA mixture in a thermocycler at 65°C for 5 minutes and cool on ice for at least 1 minute.
4. After adding the remaining reaction components as instructed, place the tubes in a thermocycler and run the following program for reverse transcription: 25°C for 5 minutes, 55°C for 60 minutes, and 70°C for 15 minutes.
5. Keep the tubes on ice or store at -20°C until ready to use for the allele-specific PCR.

3.2.5 Allele-specific PCR

1. Follow manufacturer's protocol for Advantage 2 Polymerase Mix (or other high-fidelity proof-reading DNA polymerase).
2. Set up two sets of PCR reactions for each S-RT, ATS-RT, S-noRT, ATS-noRT, as well as a genomic DNA control (see **Note 19**). For the first set, use A and B as PCR primers. These two primers amplify the sense transcripts specifically. For the second set, use C and D as PCR primers which will specifically amplify the anti-sense transcripts. The PCR result with different primer combinations is summarized in **Figure 4A**.
3. Once the PCR result is verified with strand-specific primers as stated above, you can carry out a PCR using primers B and D to obtain an image that is easier to interpret visually as shown in **Figure 4B** (see **Note 20**).

3.3 RNA FISH

3.3.1 Plate iPSC colonies on coverslips

1. Plate irradiated mouse embryonic fibroblasts (MEFs) onto 12mm round coverslips 1-2 days before seeding iPSC colonies on them.
2. Cut iPSC colonies mechanically and place them on MEF-coated coverslips and let them grow in human embryonic stem cell medium for 4-6 days.

3.3.2 Make SNORD115 BAC probes using Nick Translation DNA Labeling System (See **Note 21**)

1. Dilute Alexa Fluor 594-5-dUTP to 0.3 mM (10 µL of 1 mM Alexa Fluor 594-5-dUTP in 23.3 uL of nuclease-free water). Keep the unused portion in -20°C and avoid light.
2. Prepare diluted DNase I freshly (80 µL of 1X DNase dilution buffer and 1 µL of DNase I). Gently flick to mix. DO NOT VORTEX!!!
3. Add the following reagents from the Nick Translation DNA Labeling system accordingly.

SNORD115 BAC	1 µg (Adjust volume to 25 µL with Nuclease-free water)
Reaction Buffer	5 µL
dNTP Mix	5 µL
dTTP	2.5 µL
0.3 mM Alexa 594-dUTP	2.5 µL
DNA Polymerase I	5 µL
Fresh diluted DNase I	5 µL
Total Volume	50 µL

4. Carefully mix the reagents by flicking and briefly centrifuge.
5. Incubate the mixture for 2 hours at 15°C.
6. After incubation, place the reactions on ice.
7. Terminate the reaction by adding 5 µL of Stop Buffer and heat up for 5 minutes at 65°C. *Pause point*: Labeled BAC probes can be stored at -20°C prior to use.

3.3.3 Make UBE3A riboprobes using MAXIscript T7/T3 Kit (See **Note 22**)

1. Clone UBE3A cDNA C7-3 (Kishino and Wagstaff, 1998) into pBluescript SK+.
2. Linearize the plasmid with Not I (See **Note 23**).
3. Add the following reagents from the MAXIscript T7/T3 kit accordingly.

Linearized UBE3A plasmid	1 µg
10X Transcription Buffer	2 µL
10 mM ATP	1 µL
10 mM CTP	1 µL
10 mM GTP	1 µL
10 mM UTP	1 µL
1 mM Alexa 488-UTP	2.5 µL
T7 or T3 Enzyme (**see Note 24**)	2 µL
Nuclease-free water	to 20 µL

4. Carefully mix the reagents by flicking and briefly centrifuge.
5. Incubate the mixture for one hour at 37°C.
6. Add 1 µL of DNase I and incubate at 37°C for 15 minutes to remove any residual DNA. Pause point: Labeled riboprobes can be stored at -20°C prior to use.
7. Take 5 µL of *in vitro* transcribed riboprobes and hydrolyze it by adding 20 µL carbonate buffer and 20 µL of nuclease-free water (See **Note 25**).
8. Incubate at 60°C for 30 minutes to obtain the optimal size of riboprobes (See **Note 26** and **Figure 5**).
9. Neutralize with 2.5 µL (or 1/20 volume) of 10% acetic acid.
10. Purify riboprobes by running through a Micro Bio-Spin P-30 Tris column to remove the unlabeled Alexa Fluro 488-5-UTP.

3.3.4 Precipitate probes

1. Add 5 µL of labeled SNORD115 BAC probes to the purified riboprobes (See **Note 26**).
2. Add 5 µL of Cot-1 DNA and 5 µL of salmon sperm DNA to the combined probes.
3. Add 2.5X volume of 100% ice-cold EtOH to the mix.
4. Mix well and precipitate the probes for 30 minutes at -20°C.
5. Centrifuge at 12,000 rpm for 30 minutes at 4°C.
   (While waiting for the centrifuge, prepare coverslips and 2X hybridization buffer, See 3.3.5)
6. Carefully remove the supernatant and air dry in the dark for at least 15 minutes.

3.3.5 Prepare coverslips and 2X hybridization buffer

1. Aspirate iPSC medium and wash with PBS once.
2. Incubate the coverslips with ice-cold CSK buffer for 30 seconds at room temperature.
3. Incubate the coverslips with ice-cold 1% Triton X-100/CSK buffer for 5-10 minutes at room temperature (See **Note 27**).
4. Incubate the coverslips with ice-cold CSK buffer for 30 seconds.
5. Fix the coverslips with 4% paraformaldehyde/PBS for 10 minutes at room temperature. *Pause point*: The coverslips can be stored in 70% EtOH at 4°C until use.
6. Dehydrate the coverslips with 85%, 95%, and 100% EtOH for 2 minutes each.
7. Airdry for 10-15 minutes until everything evaporates.
8. Make 2X hybridization buffer.

3.3.6 Hybridization

1. Resuspend the dry pellet in 5 µL 100% formamide and denature the probes at 90-95°C for 10 minutes (for 2 coverslips).
2. Meanwhile, create a humid chamber with 50% formamide /2X SSC.
3. Add equivalent amount of 2X hybridization buffer to denatured probes, mix well, and spin it down.
4. Wrap a slide with parafilm and apply ~5 µL of denatured probes on the film (avoid bubbles).
5. Put coverslips upside down and make sure iPS colonies are well covered.
6. Place the slide in the humid chamber and incubate at 37°C overnight.

3.3.7 Post-hybridization wash

1. Take the coverslip and put the side with iPSC colonies up on a new parafilm wrapped slide.
2. Wash with 50% formamide/2X SSC three times at 39°C for 7 minutes.
3. Wash with 2X SSC three times at 39°C for 7 minutes.
4. Wash with 1X SSC two times at 39°C for 7 minutes (wash more or less with 1X SSC to have best signal/noise ratio).
5. Airdry the coverslips in the dark until everything evaporates.
6. Mount it with 3-4 µL Vectashield with DAPI and seal it.
7. The coverslips are ready for imaging (see **Figure 6**).

4. Notes

1. Alternatively, any commercially available kit can be used to isolate high quality genomic DNA.
2. We often reduce the reaction volume by half when performing this assay using the EpiTect Methyl II Restriction Enzyme kit. This results in 15µL of each digested DNA which is sufficient to run triplicate qPCR technical replicates using 5µL of DNA per qPCR reaction.
3. It is very important to ensure that each digest tube contains the same amount of DNA.
4. If using MSREs and MDREs from another source, follow manufacturer guidelines for running a standard restriction digest with appropriate volumes of enzyme.
5. If using PCR primers other than the EpiTect assay, adjust volume of water to accommodate volume of PCR primers used.
6. If using primer sets other than an EpiTect assay, qPCR conditions such as annealing temperature will need to be optimized.
7. According to Bruce et al. (Bruce et al., 2008), in order to calculate percent methylation, first subtract the mean Ct value of the Mock digest from the mean Ct value of the MSRE reaction to yield value *x*. Then use the equation: % meth = $100*1/P^M$ where $P^M = 2^x$. Oakes et al. (Oakes et al., 2006) use a slightly modified equation. Again, subtract the mean Ct of the Mock digest from the mean Ct of the MSRE or MDRE reaction to yield ΔCt. Then using the ΔCt of MSRE, use the equation: % meth = $100*(e^{-0.7(\Delta Ct)})$ or using the ΔCt of MDRE, use the equation: % meth = $100*(1-e^{-0.7(\Delta Ct)})$.
8. DNA with good quality has a 260/280 ratio of 1.8-2.0 when measured by a NanoDrop spectrophotometer.
9. If there are known heterozygous and homozygous regions for polymorphism, it is a good practice to include a positive and a negative control for the T7 E1 assay.
10. Alternatively, add 0.5ul of 0.5M EDTA if loading dye does not contain EDTA.
11. Alternatively, use any RNA isolation kit that produces high quality RNA. Note the 260/280 ratio when measuring RNA concentration with a NanoDrop spectrophotometer. High quality RNA extracted by RNA-Bee typically has a ratio of 1.6-1.9.
12. Do not use DEPC-treated water as it may not be compatible with following experiments.
13. The RT primers should be within a few hundred nucleotides of the polymorphic region for reverse transcription, yet far enough from the polymorphic region to accommodate the PCR primers downstream.

14. For ease of analysis, the polymorphic region should preferably be located at the center of all three primer-pairs so that the resulting PCR products from sense and anti-sense strand are similar in size for each allele.
15. The four PCR primers (A, B, C, and D) should have similar melting temperature so that they can be used interchangeably during PCR.
16. If the polymorphism is a single nucleotide change or the difference in repeat numbers is too small to be resolved using gel electrophoresis, sequencing is required to decipher the origin of the sense and anti-sense transcripts. In this case, PCR primers B and D can be used as sequencing primers and should be located at least 40 nucleotides away from the polymorphic region to avoid the initial low quality sequencing reads.
17. As PCR primers A and C are dependent on the tag sequences in the RT primers, it is important to check melting temperatures and secondary structures of the tag sequences. Software such as Primer Express® 3.0 is recommended for this purpose. Ideally, these sequences should be unique and do NOT align to the host genome to avoid non-specific PCR amplification.
18. The melting temperature of gene-specific RT primer sequences should be similar to the optimal working temperature of the reverse transcriptase used. According to manufacturer's protocol, Superscript III works the best at 55°C for gene-specific reverse transcription.
19. When the polymorphic sequence is not centered, the band size between PCR product from sense and anti-sense specific PCR amplification will be different. If your polymorphism leads to size differences between two alleles, it may be slightly harder to interpret visually on a gel. In this case, try carrying out PCR using B and D. This primer set is not as specific and may give you false result if the reverse transcription step is not specific enough. Other than changing the band size, it should give you similar result in terms of number of bands and intensity as using strand-specific primers.
20. It is advised to do a serial dilution for the genomic DNA control to match the band intensity to a similar level as the other samples.
21. The following steps are adapted from Nick Translation DNA Labeling System protocol (catalog #ENZ-42910, Enzo).
22. The following steps are partially adapted from MAXIscript T7/T3 Kit protocol (catalog #AM-1324M, Life Technologies) and Cold Spring Harbor protocol (Ferrandiz and Sessions, 2008)
23. A restriction enzyme that cuts downstream of the template strand of the cDNA plasmid should be used to linearize your plasmid. If the plasmid DNA is not linearized completely, heterogeneous and extremely long RNA transcripts will be generated due to the processiveness property of RNA polymerases.
24. Depending on how cDNA is cloned into your vector plasmid, T3 or T7 enzyme would be used to produce the right orientation of riboprobes. For example, if cDNA is cloned in the T3-T7 direction, T7 enzyme would be used to generate riboprobes that would detect sense transcript.
25. The volume of riboprobe and BAC probe used can be adjusted to obtain optimal FISH signal.
26. Run 1 uL of *in vitro* transcribed riboprobes (product from step 3.3.3.6) and 5 uL hydrolyzed riboprobes (product from step 3.3.3.8) on a 1% agarose gel to obtain optimal size for hybridization. The optimal probe size should be less than 250 nucleotides.

Larger size of probes cause low penetration of probes. The incubation time can be calculated using the following formula: $t = (L_0-L_1) / 0.11 \times (L_0)(L_1)$, where L_0 is the original length of transcript and L_1 is the desired riboprobe length (Ferrandiz and Sessions, 2008).

27. Increasing the incubation time of 1% Triton X-100/CSK will increase penetration of probes into the nuclei.

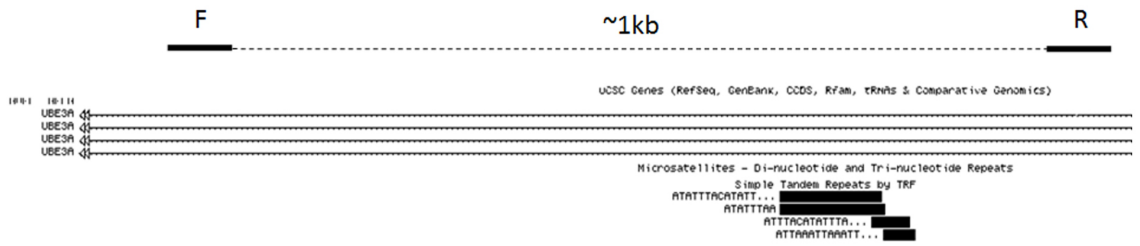

Figure 1. Short tandem repeats in an intron in *UBE3A* gene shown in USCS genome browser. Ideal PCR primers for T7 E1 assay is depicted on top (F: forward primer; R: reverse primer).

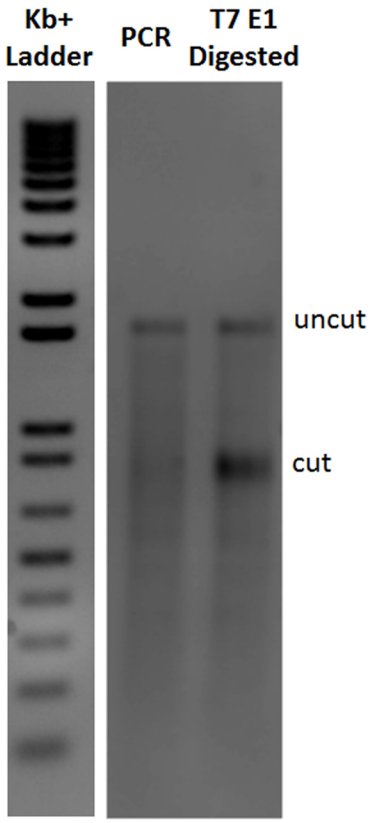

Figure 2. A polymorphism in *UBE3A* gene verified by T7 E1 assay in a patient iPS cell line. The PCR product is around 1.7kb, with the polymorphic sequence located at the center (left lane). The non-perfectly matched DNA resulted from the polymorphism is cut by T7 Endonuclease I and leads to a 850bp band (right lane).

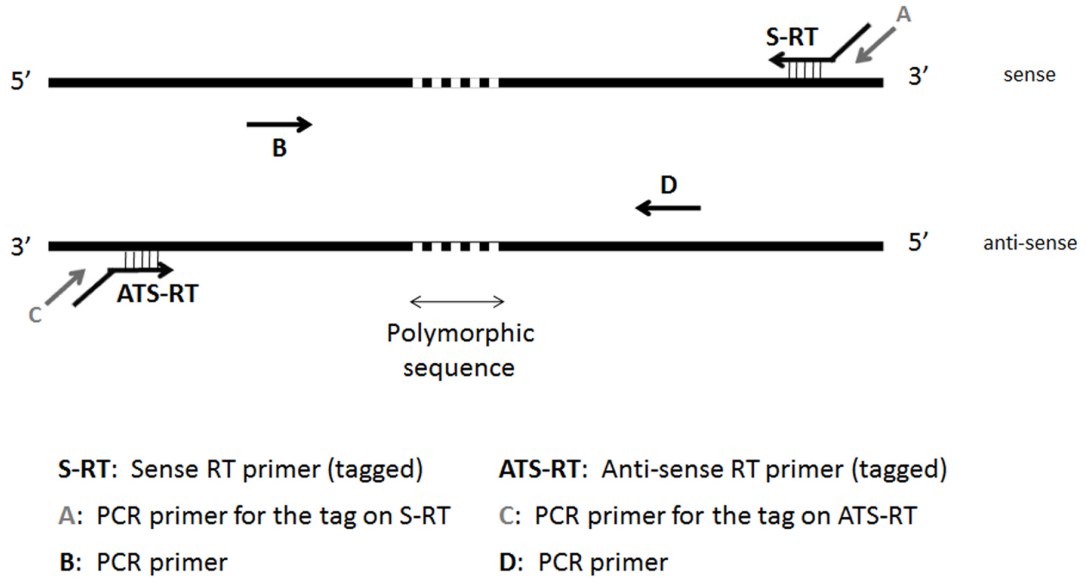

Figure 3. Primer designs for strand-specific reverse transcription and the following PCR amplification. The arrow head in each primer points towards the primer's 3' direction.

A

PCR Primers	S-RT	ATS-RT	gDNA	S-noRT	ATS-noRT
A and B	✔	✖	✖	✖	✖
C and D	✖	✔	✖	✖	✖
B and D	✔	✔	✔	✖	✖

B

Figure 4. Allele-specific PCR for sense and anti-sense transcripts across polymorphism. (A) The summary of PCR amplification results with different primer combinations. (B) This gel shows allele-specific PCR using primer B and D across the polymorphism identified in Fig. 2. The data indicates that the allele that expresses UBE3A-ATS transcripts expresses UBE3A sense transcripts at a lower level than the other allele. Genomic DNA serves as a positive control for PCR amplification (S-RT: reverse transcription using S-RT primer; ATS-RT: reverse transcription using ATS-RT primer; gDNA: genomic DNA; S-noRT: no reverse transcriptase control for RT using S-RT primer; ATS-noRT: no reverse transcriptase controls for RT using ATS-RT primer).

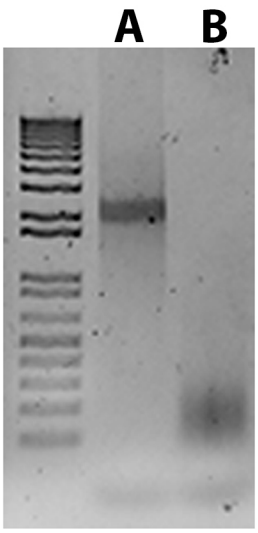

Figure 5. Gel electrophoresis of riboprobes. (A) *In vitro* transcribed and labeled riboprobes. (B) Hydrolyzed riboprobes. DNA ladder is used to approximately estimate the size of riboprobes.

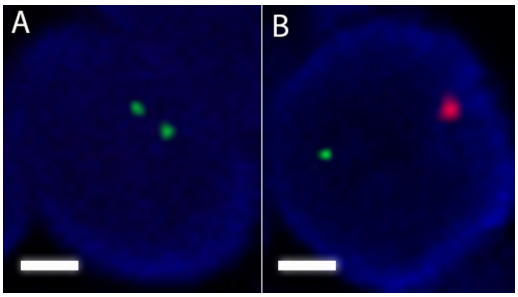

Figure 6. Representative RNA-FISH images. (A) A normal iPSC with UBE3A (green) transcribed from both alleles. SNORD115 (red) is not expressed in normal iPSCs. (B) The paternal UBE3A is silenced due to aberrant SNORD115 expression in the atypical Prader-Willi Syndrome iPSCs. Scale bar: 2μm.

5. References

1. Henckel A & Arnaud P (2010) Genome-wide identification of new imprinted genes. *Briefings in functional genomics* 9(4):304-314.
2. Gregg C*, et al.* (2010) High-resolution analysis of parent-of-origin allelic expression in the mouse brain. *Science* 329(5992):643-648.
3. Kelsey G & Bartolomei MS (2012) Imprinted genes ... and the number is? *PLoS genetics* 8(3):e1002601.
4. Singh P*, et al.* (2011) Chromosome-wide analysis of parental allele-specific chromatin and DNA methylation. *Molecular and cellular biology* 31(8):1757-1770.
5. Chamberlain SJ & Lalande M (2010) Neurodevelopmental disorders involving genomic imprinting at human chromosome 15q11-q13. *Neurobiol Dis* 39(1):13-20.
6. Jacob KJ, Robinson WP, & Lefebvre L (2013) Beckwith-Wiedemann and Silver-Russell syndromes: opposite developmental imbalances in imprinted regulators of placental function and embryonic growth. *Clinical genetics* 84(4):326-334.
7. Nakabayashi K*, et al.* (2002) Identification and characterization of an imprinted antisense RNA (MESTIT1) in the human MEST locus on chromosome 7q32. *Hum Mol Genet* 11(15):1743-1756.
8. Davies SJ & Hughes HE (1993) Imprinting in Albright Hereditary Osteodystrophy. *0022-2593* 30(2):101-103.
9. Chamberlain SJ, Li XJ, & Lalande M (2008) Induced pluripotent stem (iPS) cells as in vitro models of human neurogenetic disorders. *Neurogenetics* 9(4):227-235.
10. Chamberlain SJ*, et al.* (2010) Induced pluripotent stem cell models of the genomic imprinting disorders Angelman and Prader-Willi syndromes. *Proc Natl Acad Sci U S A* 107(41):17668-17673.
11. Germain ND CP, Plocik AM, Glatt-Deeley H, Brown J, Fink JJ, Bolduc KA, Robinson TM, Levine ES, Reiter LT, Graveley BR, Lalande M, Chamberlain SJ. (2014) Gene expression analysis of human induced pluripotent stem cell-derived neurons carrying copy number variants of chromosome 15q11-q13.1. *Molecular autism* 5(44).
12. Martins-Taylor K*, et al.* (2014) Imprinted expression of UBE3A in non-neuronal cells from a Prader-Willi syndrome patient with an atypical deletion. *Hum Mol Genet* 23(9):2364-2373.
13. Yamada Y*, et al.* (2004) A comprehensive analysis of allelic methylation status of CpG islands on human chromosome 21q. *Genome Res* 14(2):247-266.
14. Bruce S, Hannula-Jouppi K, Lindgren CM, Lipsanen-Nyman M, & Kere J (2008) Restriction site-specific methylation studies of imprinted genes with quantitative real-time PCR. *Clin Chem* 54(3):491-499.
15. Oakes CC, La Salle S, Robaire B, & Trasler JM (2006) Evaluation of a quantitative DNA methylation analysis technique using methylation-sensitive/dependent restriction enzymes and real-time PCR. *Epigenetics* 1(3):146-152.

16. Chomczynski P & Sacchi N (1987) Single-step method of RNA isolation by acid guanidinium thiocyanate-phenol-chloroform extraction. *Anal Biochem* 162(1):156-159.

17. Shirk RY, Glenn TC, Chang S-M, & Hamrick J (2013) Development and characterization of microsatellite primers in Geranium carolinianum (Geraniaceae) with 454 sequencing. *Applications in Plant Sciences* 1(8).

18. Untergasser A*, et al.* (2012) Primer3--new capabilities and interfaces. *Nucleic Acids Res* 40(15):e115.

19. Koressaar T & Remm M (2007) Enhancements and modifications of primer design program Primer3. *Bioinformatics* 23(10):1289-1291.

20. Kishino T & Wagstaff J (1998) Genomic organization of the UBE3A/E6-AP gene and related pseudogenes. *Genomics* 47(1):101-107.

21. Ferrandiz C & Sessions A (2008) Preparation and hydrolysis of digoxygenin-labeled probes for in situ hybridization of plant tissues. *CSH Protoc* 2008:pdb prot4942.

2.5 Results

2.5.1 *Generation of iPSCs, Pluripotency Characterization, and Karyotype Analysis*

AS del 1-0, PWS del 1-1, and PWS del 1-7 were generated following previously published retroviral protocols (Chamberlain et al., 2010; Takahashi et al., 2007). PWS SD 2-4, 2-8, and 2-9 were derived from patient fibroblasts using the human polycistronic STEMCCA lentiviral vector (Martins-Taylor et al., 2014; Somers et al., 2010). For Dup 15q syndrome, two idic(15) cell lines—idic 1-8 and idic CB-09—were generated with retrovirus using patient fibroblasts and with episome using patient umbilical cord blood cells, respectively (Germain et al., 2014; Mack et al., 2011). Mat. int dup(15)-02/-12 and pat. int dup(15)-04 were generated by using the aforementioned STEMCCA lentiviral vector to reprogram patient fibroblasts harboring paternal and maternal interstitial duplication of chromosome 15q11-q13.1, respectively (Germain et al., 2014). Chromosome 15q11-q13.1 copy number variations and deleted/duplicated locus in all cell lines are shown in **Figure 2.1**.

Reprogrammed iPSC colonies with human embryonic stem cell morphology were identified and subsequently validated using immunocytochemistry for pluripotency markers, NANOG, SSEA4, TRA1-60, and TRA1-81 (**Figure 2.2 A-D**). Taqman® qRT-PCR-based gene expression arrays were used to analyze the expression of lineage markers for endoderm, ectoderm, and mesoderm in embryoid bodies (EBs) spontaneously differentiated for 14-16 days (**Figure 2.2 E-F**). These data demonstrated that all iPSC lines derived here were indeed pluripotent and capable of multi-lineage

differentiation. Additionally, karyotyping was carried out by UConn Chromosome Core and showed that all iPSCs presented the expected karyotypes (**Figure 2.2 G**).

2.5.2 *iPSCs Maintain Appropriate DNA Methylation at PWS-IC*

To confirm that the methylation imprint at PWS-IC was maintained following reprogramming, we carried out methylation-specific PCR as well as qRT-PCR based DNA methylation analysis. In **Figure 2.3 A-C**, bisulfite-converted genomic DNA was subjected to a multiplex PCR using primers at PWS-IC specific for unmethylated paternal allele (bottom band) and methylated maternal allele (top band). As expected, only the unmethylated allele was present in AS iPSCs, while only the methylated allele was present in PWS iPSCs. In **Figure 2.3 D-F**, we utilized a more quantitative DNA methylation analysis using methylation-sensitive/methylation-dependent restriction endonuclease digestion to demonstrate that DNA methylation at PWS-IC was largely unchanged between the fibroblasts and their iPSC counterparts. In normal cells with one methylated and one unmethylated allele, we observed 50% to 60% methylation (50% expected). Less than 1% of methylation was observed in AS cells with one unmethylated allele (0% expected), while more than 95% was found in PWS cells with one methylated allele (100% expected). In PWS SD cells, PWS-ICs on both alleles were present, and 42% to 50% methylation was observed in all but one iPSC line (50% expected). The iPSC line with aberrant methylation status (20%) was excluded from further study. For pat. int dup(15)-04, which contained one copy of methylated allele and two copies of unmethylated allele, the methylation averaged around 25% (33% expected). For Mat. int dup(15), which contained two copies of methylated allele and

one copy of unmethylated allele, the methylation averaged around 66% (66% expected). Finally, for idic 1-8 and idic CB-09, both carrying three copies of methylated allele and one copy of unmethylated allele, averages of 76% and 77% methylation were observed, respectively (75% expected).

2.5.3 *AS and Dup 15q iPSCs Can Be Differentiated into Functional Neurons*

AS and Dup 15q syndrome are neurodevelopmental disorder that affect cortical functions. We sought to generate functional neurons from AS and Dup15q iPSCs *in vitro* that mimic the cortical population. Using previously published EB protocol (**Figure 2.4 A**), we obtained AS and normal neural epithelial cells that expressed PAX6 and formed neural rosettes (**Figure 2.4 CA, CB, DA**). After six weeks of differentiation, neurons were positive for MAP2 and TUJ1 (**Figure 2.4 BB, CC, DB, DD**). S100β-positive astrocytes were detected after six weeks of differentiation (**Figure 2.4 BC, DB**). Concomitantly, Synapsin-I-positive cells also appeared around six weeks post-differentiation, indicating synaptic development (**Figure 2.4 CD, DC**). After 10 weeks of development, extensive neurite outgrowth was observed (**Figure 2.4 BA**) and some neurons exhibited proper localization of voltage-gated channels in the axonal initial segments (AIS) shown by PanNav immunostaining (**Figure 2.4 CE, CF, DE**). Importantly, we determined that these neurons are functional by electrophysiology (Chamberlain et al., 2010).

Similarly, using a modified monolayer protocol (**Figure 2.4 A**), we obtained Dup 15q neurons that are MAP2-positive, composed of both VGLUT1-positive excitatory neurons as well as GAD65-positive inhibitory neurons, after 10 weeks of differentiation

(**Figure 2.4 Ea, Ec, Ed**). These MAP2-positive neurons also showed co-localization of the postsynaptic density protein PSD-95 and the presynaptic marker Synapsin-I, indicating functional synaptic formation (**Figure 2.4 Ee-Ee''**). S100β-positive astrocytes were detected in the monolayer neural culture (**Figure 2.4 Eb**). Importantly, these neurons are electrophysiologically functional and comparable to neurons generated using the EB protocol (Germain et al., 2014).

2.5.4 *UBE3A Is Imprinted In AS iPSC-Derived Neurons*

In order to model AS and Dup 15q syndrome using iPSCs and iPSC-derived neurons, it was necessary to ensure that *UBE3A* was imprinted in neurons as observed *in vivo*. Using qRT-PCR, we compared *UBE3A* expression of AS cells, which contained a single paternal copy of *UBE3A*, to that of normal cells, which contained both copies of *UBE3A*. We showed that *UBE3A* expression level was lower in AS iPSCs when compared to normal iPSCs, and was further decreased in AS iPSC-derived neurons, demonstrating the epigenetic silencing of paternal *UBE3A* upon neural differentiation (**Figure 2.5 A**). *UBE3A* expression levels were not significantly different between normal iPSCs and normal iPSC-derived neurons, which were consistent with the UBE3A protein levels assayed by Western blotting (**Figure 2.5 B**). Lower levels of *UBE3A* expression in AS iPSCs and AS iPSC-derived neurons were also reflected in the protein level. Using Western blotting, we showed that UBE3A protein was drastically reduced in AS iPSCs compared to normal iPSCs, and that it was almost undetectable in AS iPSC-derived neurons (**Figure 2.5 B**).

Although the mechanism is yet to be elucidated, neuron-specific paternal *UBE3A* repression is thought to be regulated by active transcription of *UBE3A-ATS*, which is part of the *SNURF/SNRPN* lncRNA. To determine whether transcripts resulted from *SNURF/SNRPN* lncRNA demonstrate expected tissue-specificity, we analyzed spliced exons in the *SNORD116* cluster, the *SNORD115* cluster, as well as *UBE3A-ATS* using RT-PCR (**Figure 2.5 C**). We showed that *SNORD116* was expressed in iPSCs, neural precursors, and neurons. *SNORD115* was not expressed in iPSCs, but in both neural precursors and neurons. As expected, *UBE3A-ATS* expression was restricted to iPSC-derived neurons. Due to the fact that the AS iPSCs and iPSC-derived neurons harbor a large deletion on maternal chromosome 15q11-q13.1, we were able to study gene expression in an allele-specific fashion. For other cells, such as normal, PWS SD, and Dup 15q, that contain more than one copy of chromosome 15q11-q13.1, it is essential to study genomic imprinting using tools that can distinguish one allele from another. Two of the techniques we utilized for this purpose are allele-specific PCR and RNA FISH, as described previously in Section 2.4 (Chamberlain et al., 2016).

2.5 Discussion

We derived patient-specific iPSCs carrying a variety of copy number variations at chromosome 15q11-q13.1 that led to AS, PWS, and Dup 15q syndrome. To address whether iPSC models are appropriate for studying these imprinting disorders, we demonstrated that DNA methylation at PWS-IC is resistant to the global erasure during the reprogramming process. Our observation supports the notion that epigenetic marks at this locus are established prior to or during early stage of preimplantation (El-Maarri

et al., 2001). Although the AS and Dup 15q iPSCs we derived carry mutations that lead to neurodevelopmental disorders, we were able to differentiate all cell lines into mature and functional neurons. The developmental timing of neural differentiation for these diseased iPSCs closely followed that for normal iPSCs. This is in agreement with the fact that, other than micro/macrocephaly, there is no gross brain structural difference between AS and Dup 15q patients compared to normal individuals (Battaglia, 2008; Williams et al., 2010a).

Using AS iPSCs and iPSC-derived neurons, we demonstrated that *UBE3A* on the paternal allele is properly silenced in a neuron-specific manner. We did not observe a decrease in *UBE3A* RNA and protein level in normal iPSC-derived neurons compared to normal iPSCs. This could be attributed to upregulated maternal UBE3A expression in mature neurons (Dindot et al., 2008). Moreover, we found that different parts of *SNURF/SNRPN* lncRNA exhibit different tissue-specificity—the more distal, the more neuron-specific. The most distal part of *SNURF/SNRPN* lncRNA, *UBE3A-ATS*, plays an important role in paternal UBE3A silencing in neurons.

Techniques that distinguish allele-specific gene expression are instrumental in understanding gene regulation at imprinted locus. For example, we found that PWS SD iPSCs carrying an atypical microdeletion aberrantly express *SNORD115* and *UBE3A-ATS* (Martins-Taylor et al., 2014). This observation suggests the presence of a boundary element in non-neuronal cells that suppresses downstream *SNURF/SNRPN* lncRNA expression. We speculate polyadenylation signals in *IPW* and several CTCF binding sites downstream of *IPW* may be responsible for this boundary function. We

also concluded that the expression of *UBE3A-ATS* alone is sufficient to silence *UBE3A in cis* and that additional neural factors are not necessary (Martins-Taylor et al., 2014).

In conclusion, we demonstrated that iPSCs and iPSC-derived neurons are great tools for understanding gene regulation at human chromosome 15q11-q13.1. This *in vitro* model system is not only useful for understanding disease mechanism for AS, PWS, and Dup 15q syndrome, but also can be used for drug screening to develop therapies (Germain et al., 2014; King et al., 2013; Martins-Taylor et al., 2014).

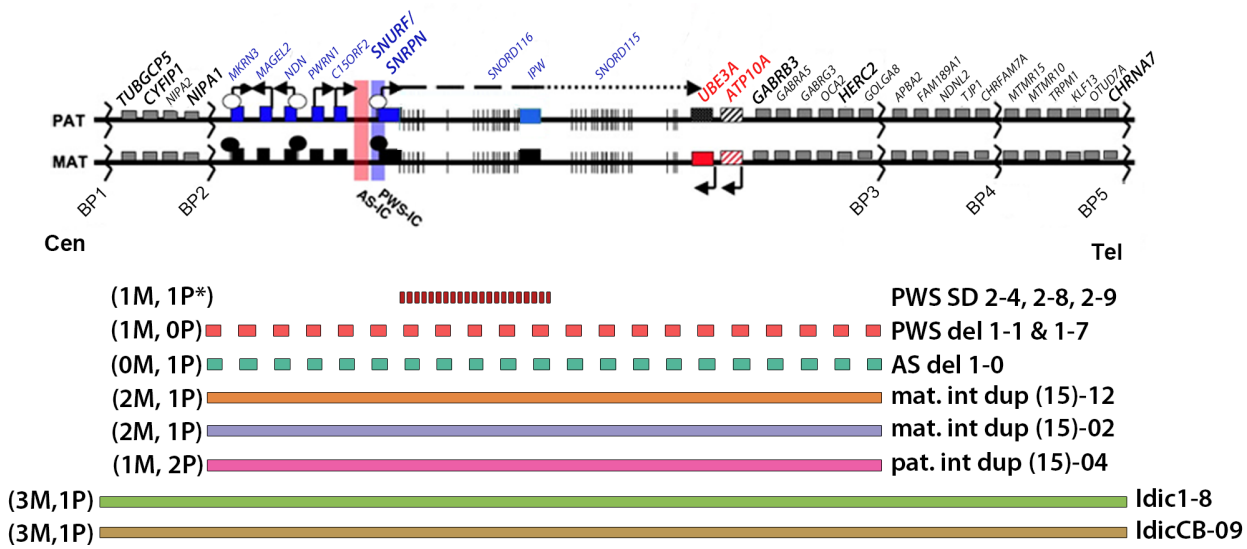

Figure 2.1. Map of the chromosome 15q11-q13.1 region (adapted from Germain et al., 2014). Genes are displayed as rectangles (grey: biallelically expressed; red: maternally expressed; blue: paternally expressed; black: silenced). Small nucleolar RNA clusters are shown as vertical lines. Stripes marking *ATP10A* indicates variable imprinting status depending on individuals. The dotted line represents *UBE3A-ATS* long non-coding RNA transcript. Red and blue shaded areas are the Angelman syndrome and Prader-Willi syndrome imprinting centers (AS-IC and PWS-IC), respectively. Differentially methylated regions are denoted with ovals (white: unmethylated CpG islands; black: methylated CpG islands). Right below the map is a list of AS, PWS, and Dup 15q patient-derived iPSC lines. Regions deleted (dashed rectangles) or duplicated (continuous rectangles) as well as the respective maternal (M) or paternal (P) chromosome 15 allele copy numbers are indicated [PAT: paternal allele; MAT: maternal allele; BP: breakpoint; Cen: centromere; Tel: telomere; *mutated].

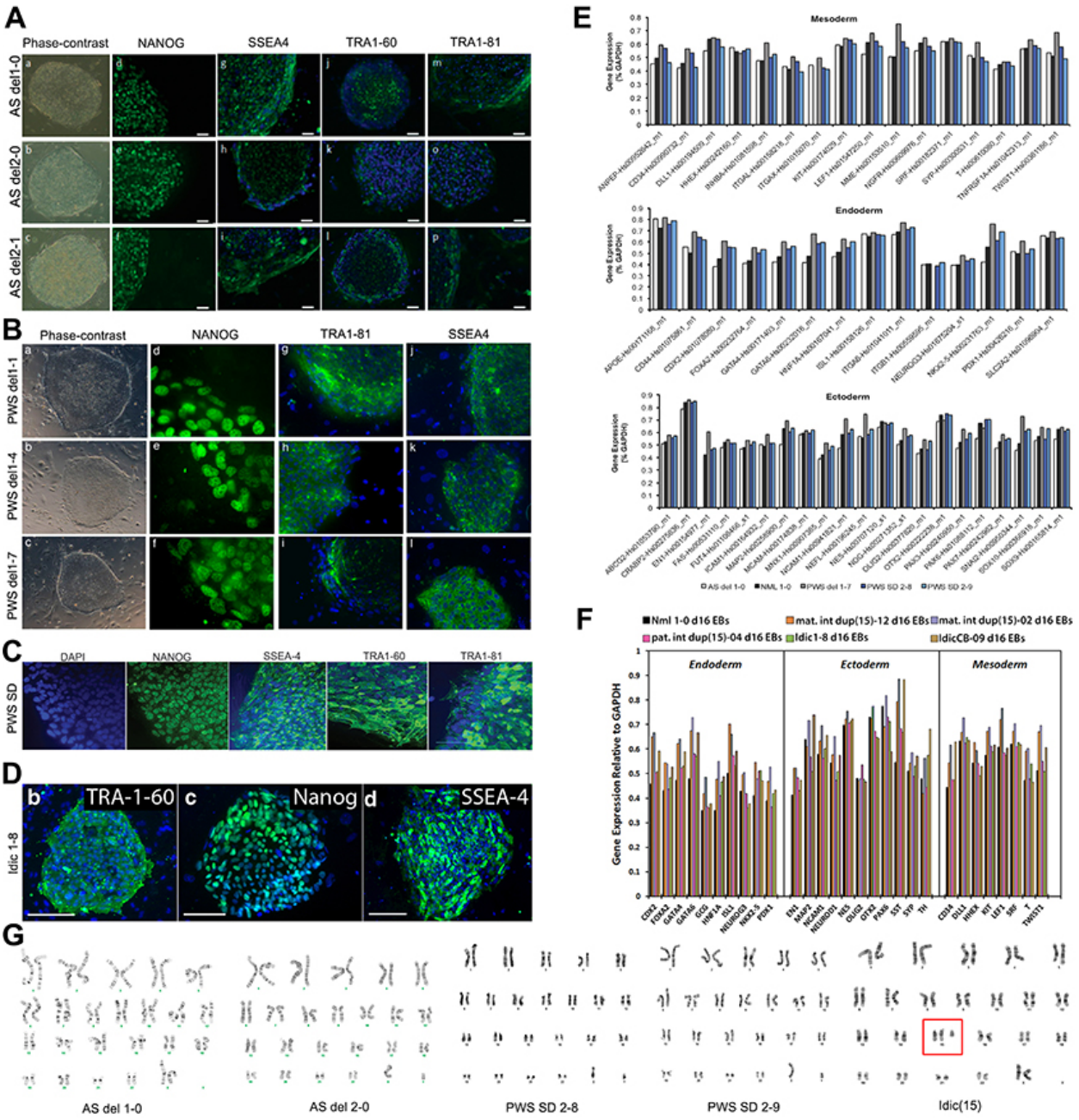

Figure 2.2. AS, PWS, and Dup 15q iPSCs are pluripotent and have expected karyotypes (Chamberlain et al., 2010; Germain et al., 2014; Martins-Taylor et al., 2014)**. A-D)** AS, PWS, and Dup 15q iPSCs show hESC-like morphology and express pluripotency markers, NANOG, SSEA4, TRA1-60, and TRA1-81. **E-F)** AS, PWS, and Dup 15q iPSCs are capable of multi-lineage differentiation. Spontaneously differentiated

14- to16-day AS, PWS, and Dup 15q EBs express early lineage markers for all three embryonic germ layers by qRT-PCR. **G)** Karyotype analysis show expected chromosome counts in representative AS, PWS, and Dup 15q iPSC lines. Red box indicates the expected supernumerary isodicentric chromosome 15.

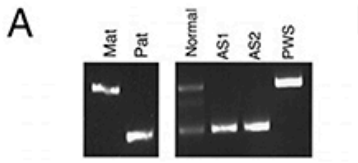

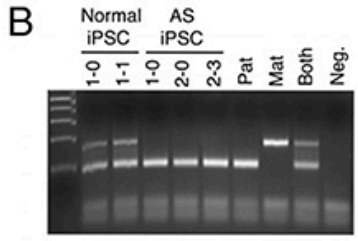

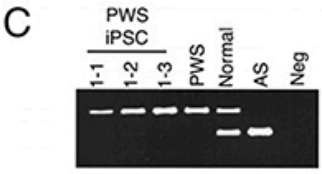

D

Cell line	Percent methylation
Normal fibroblast	58.77±1.49
Normal iPS 1-0	60.06±2.41
Normal iPS 1-1	50.00±0.00
AS 1-0 fibroblast	0.21 ±0.08
AS iPS del 1-0	0.17±0.14
AS iPS del 1-1	1.10±0.85
AS iPS del 2-0	0.33±0.17
AS iPS del 2-3	0.38±0.32
PWS fibroblast	95.17±3.53
PWS iPS del 1-1	96.92 ±0.50
PWS iPS del 1-2	97.68 ±0.88
PWS iPS del 1-3	99.66 ±0.57
PWS iPS del 1-4	98.45 ±0.44
PWS iPS del 1-5	98.49 ±1.36
PWS iPS del 1-6	98.34 ±0.76
PWS iPS del 1-7	99.03±1.24
PWS iPS del 1-8	98.81±1.03
PWS iPS del 1-9	95.15 ±0.82

E

Cell Line	Percent Methylation
AS del 1-0 iPSCs	0.10 ± 0.16
PWS del 1-7 iPSCs	99.70 ± 0.31
PWS SD fibroblasts	43.38 ± 3.96
PWS SD 2-1 iPSCs	20.58 ± 1.34
PWS SD 2-2 iPSCs	46.95 ± 5.28
PWS SD 2-3 iPSCs	50.00 ± 0.00
PWS SD 2-4 iPSCs	42.23 ± 5.33
PWS SD 2-5 iPSCs	50.00 ± 0.00
PWS SD 2-6 iPSCs	42.62 ± 4.89
PWS SD 2-7 iPSCs	46.70 ± 3.19
PWS SD 2-8 iPSCs	48.42 ± 2.74
PWS SD 2-9 iPSCs	50.00 ± 0.00

F

Cell line	% methylated at PWS-IC*
mat. Int dup(15)	**66.57 ± 0.92**
mat. Int dup(15)-02	66.15 ± 2.12
mat. Int dup(15)-12[b]	65.64 ± 3.25
pat. Int dup(15)	**25.31 ± 1.46**
pat. Int dup(15)-04	23.53 ± 2.93
Idic	**76.94 ± 5.02**
Idic1-8	72.43 ± 1.00
IdicCB	**77.35 ± 3.52**
IdicCB-07	79.49 ± 5.03
IdicCB-09	72.29 ± 9.69

Figure 2.3. DNA Methylation imprint at the PWS-IC is maintained during reprogramming (Chamberlain et al., 2010; Germain et al., 2014; Martins-Taylor et al., 2014)**. A-C)** Methylation-specific PCR analysis of genomic DNA from normal, AS, PWS fibroblasts (A) and iPSCs (B-C). Primers specific for the methylated allele amplify a 174 bp band, while those for the unmethylated allele a 100 bp band [Mat: maternal allele; Pat: paternal allele; Neg.: negative control]. **D-F)** qRT-PCR-based DNA methylation analysis using genomic DNA shows expected methylation status at PWS-IC predicted by allele copy number and parental origin. The averages of percent methylation plus or minus the standard deviation from three replicates are shown.

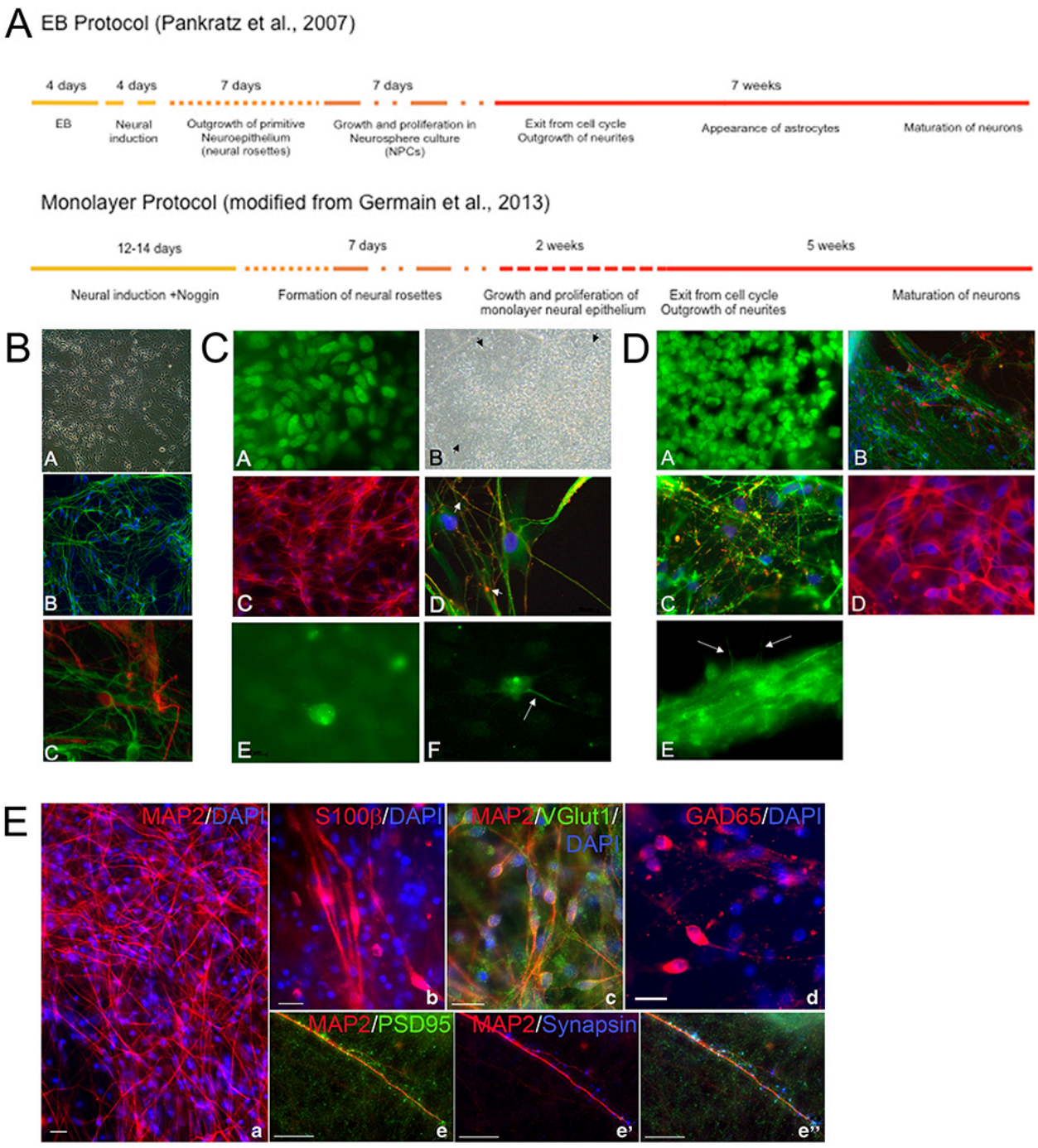

Figure 2.4. Characterization of neurons derived from AS and Dup 15q iPSCs (Chamberlain et al., 2010; Germain et al., 2014)**. A)** Schematics of neural differentiation process using EB and monolayer protocols. **BA)** Phase-contrast of 10-week-old AS iPSC-derived neurons. **BB)** AS iPSC-derived neurons stain positively for βIII-TIBULIN

(TUJ1, in green) **BC)** S100β-positive astrocytes are present in AS iPSC-derived neuron cultures after 6 weeks of differentiation. **CA)** AS iPSC-derived neural epithelial cells are PAX6-positive (green). **CB)** Neural rosette formation in AS iPSC-derived neural epithelial culture. **CC-CD)** 6-week-old AS iPSC-derived neurons express MAP2 (CC, in red) and βIII-TIBULIN (CD, in green), and show SynapsinI-positive puncta (CD, in red, arrows). **CE-CF)** Immunocytochemistry for PanNav (green) shows lack of voltage-gated sodium channel localization in the AIS in most neurons (CE), but proper localization in some neurons (CF, arrow). **DA)** normal iPSC-derived neural epithelial cells are PAX6-positive (green). **DB-DC)** 6-week-old normal iPSC-derived neuron cultures contain S100β-positive astrocytes (DB, in red) and βIII-TIBULIN-positive neurons (green), which show SynapsinI-positive puncta (DC, in red). **DD-DE)** 10-week-old normal iPSC-derived neurons express MAP2 (red) and show lack of voltage-gated sodium channel localization in the AIS in most but not all (arrows) neurons by PanNav immunocytochemistry (green). **Ea)** 10-week-old Dup 15q iPSC-derived neurons express MAP2 (red). **Eb-Ed)** 10-week-old Dup 15q iPSC-derived neuron cultures contain S100β-positive astrocytes (Eb, in red), VGLUT1-positive excitatory neurons (Ec, in green), and GAD65-positive inhibitory neurons (Ed, in red). **Ee-Ee')** MAP2-positive neurons (red) show PSD-95-positive (Ee, in green) and SynapsinI-positive (Ee', in blue) puncta. **Ee'')** Merged image shows formation of functional synapses with of PSD-95 and SynapsinI co-localization.

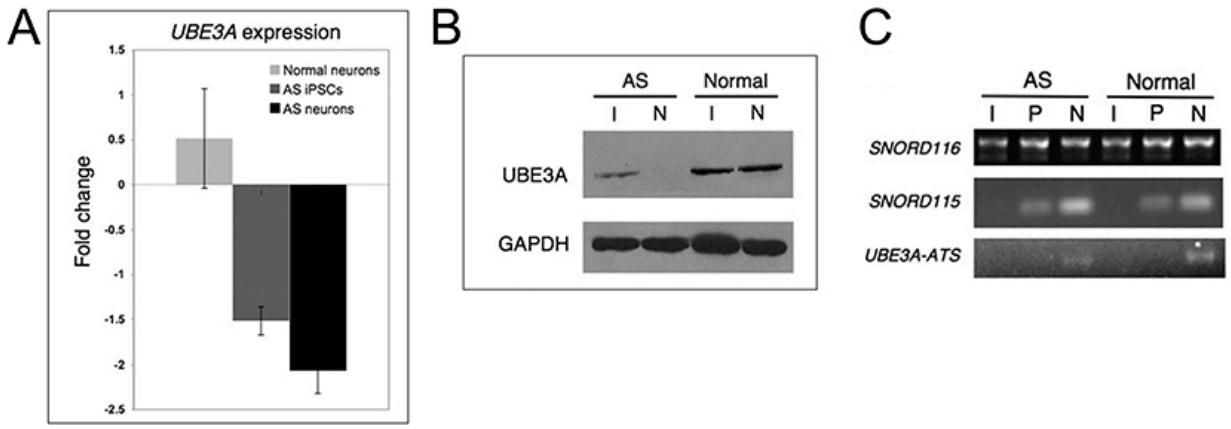

Figure 2.5. AS iPSC-derived neurons show paternal *UBE3A* silencing (Chamberlain et al., 2010)**. A)** qRT-PCR analysis showing relative *UBE3A* expression levels in normal iPSC-derived neurons, AS iPSCs, and AS iPSC-derived neurons when compared to *UBE3A* expression level in normal iPSCs. **B)** Western blot analysis showing UBE3A protein level in normal and AS iPSCs (I) and 10-week-old iPSC-derived neurons (N). **C)** RT-PCR analysis showing *SNORD116*, *SNORD115*, and *UBE3A-ATS* expression in iPSCs (I), 3-week-old iPSC-derived neural precursors (P), and 10-week-old iPSC-derived neurons (N).

Chapter 3

Generation of a UBE3A Reporter Cell Line by Genome Editing

3.1 Background and Significance

Observations made in murine models indicate that Ube3a protein expression and localization is dynamic during neurodevelopment (Dindot et al., 2008; Judson et al., 2014). Specifically, Judson et al. utilized knockin mice expressing yellow fluorescent protein (YFP) fused to the C-terminus of Ube3a to demonstrate the spatiotemporal characteristic of Ube3a expression from paternal or maternal allele in developing postnatal brain. In addition to showing maternal-specific Ube3a expression in mature neurons, they identified postnatal neural stem cells and oligodenrocytes to be the two cell populations expressing Ube3a biallelically. Interestingly, some characteristic phenotype of AS patients, such as cognitive impairment and white matter abnormalities, may be related to aberrant neural stem cells and oligodendrocyetes, respectively (Judson et al., 2014). Further study is required to determine whether loss of maternal Ube3a expression/function in these two cell types can lead to haploinsufficiency and, therefore, contribute to AS manifestation.

In addition, Judson et al. reported a shift in subcellular localization of Ube3a, from cytoplasmic to nuclear, during the first postnatal month. Ube3a expression at embryonic stage rescues phenotypes across multiple domains in AS mice, including behavioral phenotypes that cannot be rescued at postnatal stages (Silva-Santos et al., 2015). Taken together, this suggests that cytoplasmic Ube3a may play a major role in early brain development. Incidentally, impaired dendrite polarity caused by Ube3a knockdown in mice could only be rescued by expressing full-length cytoplasmic Ube3a isoform 2

(Miao et al., 2013). These observations suggest that cytoplasmic Ube3a may be the most relevant isoform for developing therapies for AS.

Studies mentioned above are informative in determining affected cell populations, treatment windows, and UBE3a isoform selection for treating AS. However, mouse brain is fundamentally different from human brain and lacks gyrification, which is important for higher cognitive functions. In order to translate these findings into treatments for AS patients, it is necessary to understand whether UBE3A protein expression and subcellular localization are similarly regulated in human neural tissues. It is also important to determine the timing of paternal *UBE3A* silencing in human, so that neurodevelopmental stages critical for AS between human and mice can be better correlated. To address these issues, we attempted to create an UBE3A-GFP fusion protein reporter using AS iPSCs, using a design similar to the YFP knockin mice previously mentioned. However, we were unable to detect abundant UBE3A-GFP fusion proteins in these cells, most likely caused by low expression or instability at the protein level. Nevertheless, a successful UBE3A-GFP reporter AS iPSC line would be informative on spatiotemporal regulation of UBE3A expression during human neurodevelopment as well as a useful tool for high throughput drug screening for AS treatments.

3.2 Rationale

One difficulty that scientists faced when determining allele-specific Ube3a protein expression and subcellular localization using immunofluorescent staining was poor assay sensitivity. Judson et al. was able to improve immunofluorescent staining protocol

to detect low level of endogenous Ube3a expression from paternal allele in mice. However, currently available UBE3A antibody does not work well in human neurons. Since Ube3a-YFP fusion protein was stable in mice, and its subcellular localization agreed with native Ube3a localization observed using immunofluorescent staining (Judson et al., 2014), we utilized a recently developed gene-editing technology, CRISPR/Cas9, to create a cell line expressing enhanced green fluorescent protein (GFP) fused to the C-terminus of Ube3a. We chose to use AS iPSCs to construct this reporter cell line, because of the ease in targeting the single paternal copy of *UBE3A* gene. The detailed targeting vector and CRISPR/Cas9 construct design is described below (**Figure 3.1A**).

3.3 Materials and Methods

iPSC line and Maintenance

AS del 1-0 iPSCs were used in this study and maintained as described before (Chamberlain et al., 2010). Briefly, iPSCs were grown on irradiated mouse embryonic fibroblasts (iMEFs) and fed daily with conventional hESC medium consisting of DMEM-F12 supplemented with knock-out serum replacer, nonessential amino acids, L-glutamine, β-mercaptoethanol, and basic FGF. iPSCs were cultured in a humid incubator at 37 °C with 5% CO_2 and passaged approximately once a week manually.

sgRNA and UBE3A-GFP Construct Design for Gene Editing

CRISPR/Cas9 and UBE3A-GFP vectors were designed and constructed by Christopher Stoddard of the hESC/iPSC Targeting Core at the University of

Connecticut Health Center. AGGCCATCACGTATGCCAA is the small guide RNA sequence targeting the last exon of *UBE3A*, and it was cloned into a human codon-optimized SpCas9 and chimeric guide RNA expression plasmid, pX330 (Addgene plasmid #42230) (Cong et al., 2013). The UBE3A-GFP targeting vector contains a loxP-flanked neomycin resistance gene for drug selection and a diphtheria toxin A gene for negative selection. The targeting vector also lacks the guide sequence to prevent CRISPR/Cas9-mediated cutting. The detailed design for the targeting construct is depicted in Figure 3.1.

Nucleofection and Drug Selection

10μM ROCK inhibitor, Y-27632, was added to iPSC colonies overnight prior to nucleofection. iPSCs were singlized with Accutase and counted using a hemocytometer. 1~2 million cells were used for each experiment. Cells were pelleted by centrifugation at 1400rpm and preplated into one well of a 6-well tissue culture plate for 1~2 hours to remove feeder cells. Nucleofection was carried out following the manufacturer's protocol for Human Stem Cell Nucleofector Kit 1 and 2 (Lonza). 3μg of sgRNA/Cas9 vector and 3μg of UBE3A-GFP targeting construct were used for each nucleofection. Nucleofector programs A-023 and B-016 were used in combination with Human Stem Cell Nucleofector Kit 1 and 2, respectively. Cells were then plated into one well of a 6-well tissue culture plate coated with DR4-iMEF feeders in the presence of 10μM ROCK inhibitor overnight. The morning after nucleofection, old medium was removed and fresh hESC medium with 10μM ROCK inhibitor was added to the

cells. ROCK inhibitor was removed from the culture medium the following day. 96 hours post-nucleofection, cells were drug selected using 25µg/mL G418 for one passage. Single colonies were manually split into a 24-well tissue culture plate coated with DR4-iMEF feeders and numbered. Half of each iPSC colony was saved for genotyping. One-day post splitting, G418 concentration was increased to 50µg/mL to eliminate false positive clones. Targeted clones were drug selected with G418 at 50µg/mL for an additional passage and then cultured in regular hESC medium on normal iMEFs. Neomycin resistance gene containing a polyadenylation signal sequence was removed from the last intron of *UBE3A* by Cre-Lox recombination. 5 µg of Cre-IRES-PuroR vector (Addgene plasmid #30205) was nucleofected in to about 1 million cells as described above to transiently express Cre (Somers et al., 2010). Nucleofected cells were seeded into one 6-well tissue culture plate coated with DR4-iMEF feeders. 24 hours post-nucleofection, cells were drug selected using 1µg/mL puromycin for 48 hours. Individual colonies were manually split onto regular iMEFs and genotyped.

Genotyping Targeted Clones

Genomic DNA from half of each iPSC colony was prepared using hot sodium hydroxide and tris (HotSHOT) (Truett et al., 2000) (protocol available on http://gttf.uchc.edu/protocols/hotshot.html). Briefly, cells were pelleted in a microcentrifuge tube by spinning at top speed in a tabletop centrifuge for 30 seconds. Excess culture medium was carefully removed by aspiration without perturbing the pellet. Pelleted cells were incubated in 30µL Alkaline Lysis

Reagent (25mM NaOH; 0.2mM EDTA) at 95°C for at least one hour and chilled on ice. Then, 30µL of Neutralization Reagent (40mM Tris-HCl) was added to each tube and mixed well. For each sample, 1~3µL of HotSHOT DNA per PCR reaction was used for genotyping. Primers for HotSHOT PCR were designed to produce products smaller than 500bp. Presences of *GFP* and neomycin resistance gene (*Neo*) were used in the initial screening to rule out untargeted cells. GFP^+/Neo^+ colonies were expanded and high quality genomic DNA was prepared using phenol/chloroform extraction. Proper integration of UBE3A-GFP targeting vector was assayed by sequential PCR amplification for 5' and 3' homologous recombination. Presence of wild type *UBE3A* was assayed using sequential PCR amplification. DNA sequencing was done at the fusion site of *UBE3A* and *GFP*. The resulting clones were expanded and subjected to Cre-Lox recombination. HotSHOT PCR with various primer sets were used to genotype wildtype, targeted Neo^+, and targeted Neo^- clones. For primers used in this project, see Appendix A.

RNA Isolation and Reverse Transcription

RNA samples were isolated using RNA-Bee (Tel-Test Inc.) and converted into cDNA using High-Capacity cDNA Reverse Transcription Kit (Applied Biosystems) according to the manufacturer's instructions.

Immunocytochemistry

Immunocytochemistry was carried out as previously described (Chamberlain et al., 2010). Mouse anti-GFP (1:150, MAB3580, Chemicon) was used as primary

antibody and AlexaFluor 488 conjugated goat anti-mouse (1:300, Life Technologies) was used as secondary antibody. Nuclei were counterstained with DAPI and coverslips were mounted on slides with Vectashield (Vector Laboratories). Slides were imaged using a Zeiss Axiovision microscope.

Western Blotting

Cells were lysed on ice using RIPA buffer (150mM NaCl; 50mM Tris, pH 8.0; 1% TritonX-100; 0.5% Sodium Deoxycholate; 0.1% SDS) supplemented with proteinase inhibitor II. Protein concentrations were measured using Peirce BCA Protein Assay Kit (Thermo Scientific). Total cell lysates were resolved on 10% handcast SDS-PAGE gels and transferred to nitrocellulose membranes using wet/tank blotting system (Bio-Rad). The membranes were blocked in 5% nonfat dry milk in TBST (0.5% Tween-20 in TBS containing 20mM Tris and 500mM NaCl), followed by overnight incubation with primary antibody, rabbit anti-UBE3A (1:1000, A300-352A, Bethyl). After washing with TBST three times, membranes were blotted with goat anti-rabbit secondary antibody conjugated with horseradish peroxidase for one hour. Membranes were washed and then developed in Immobilon Western Chemiluminescent HRP Substrate (Millipore), detected using X-ray films (Kodak).

3.4 Results

GFP was inserted into the last exon of *UBE3A* on the paternal allele in AS iPSCs using CRISPR/Cas9-mediated gene editing (**Figure 3.1A**). Primers for genotyping are depicted in **Figure 3.1B** and all primers used in this chapter are listed in **Appendix A**.

For initial screening, *GFP*$^{+}$/*Neo*$^{+}$ clones were identified using HotSHOT PCR (**Figure 3.2A**). Purity of UBE3A-GFP clones was assayed by endogenous *UBE3A*-specific sequential PCR on genomic DNA (**Figure 3.2B**). This data suggests that the clones were targeted and no wild type *UBE3A* existed in their genome.

Successful targeting events were confirmed by sequential PCR for 5' and 3' homologous recombination (**Figure 3.2C**). Clones with both 5' and 3' homologous recombination were selected and subjected to Cre-Lox recombination to remove neomycin resistance gene (**Figure 3.3**). Based on this PCR result, we had technical difficulties in acquiring pure Neo^{-} UBE3A-GFP clones. However, we thought that the presence of neomycin resistance gene was unlikely to have adverse effect on UBE3A-GFP expression, as it resides in an intron. In-frame GFP insertion in these clones was confirmed by DNA-sequencing (**Figure 3.4A**). RNA expression of wild type *UBE3A* and *UBE3A-GFP* transcripts was assessed by conventional PCR (**Figure 3.4B**). Unexpectedly, we saw a low level of wild type *UBE3A* expression in the UBE3A-GFP clones that do not have wild type *UBE3A* based on genotyping. This artifact is likely caused by inappropriate primer design that non-specifically amplifies *UBE3A-GFP* transcripts at low efficiency.

UBE3A-GFP fusion protein expression was determined by immunocytochemistry (**Figure 3.5A**) and western blotting (**Figure 3.5B**). Fluorescence from UBE3A-GFP fusion proteins was not visible without antibody amplification under fluorescence microscope. This is expected because antibody amplification was also required to detect protein expression in the Ube3a-YFP knockin mice (Dindot et al., 2008; Judson

et al., 2014). However, to our surprise, we were unable to detect UBE3A-GFP fusion proteins by western blot using antibody against UBE3A, which differed from previously published data (Dindot et al., 2008).

3.5 Discussion

CRISPR/Cas9-mediated UBE3A-GFP gene targeting was successful. No wild type *UBE3A* was detected by genotyping. The last two base pairs at the 3' end of reverse primer designed to specifically detect wild type *UBE3A* RNA transcript overlaps with *UBE3A-GFP* transcript, and therefore may bind and amplify *UBE3A-GFP* at a low efficiency. This indicates that the low level wild type UBE3A expression in **Figure 3.4B** may be an artifact.

The reporter cell lines created here are not as useful for studying spatiotemporal regulation of UBE3A expression and drug screening than we expected initially because of the following two reasons. First, GFP florescence level in these cells was undetectable without immunofluorescent staining and only visible at high magnification (63x with oil) even with GFP antibody amplification. To study the timing of paternal *UBE3A* silencing, immunofluorescent staining would have to be carried out at multiple time points during neural differentiation, and paternal *UBE3A* expression in individual cells can not be followed by live cell imaging. Having to amplify the fluorescent signal also increases the difficulty to use these cell lines for high-throughput drug screening. Second, we could not detect UBE3A-GFP fusion protein using an antibody against native UBE3A protein. This antibody recognizes the middle section of UBE3A protein, 400~450aa, which should be identical between wild type UBE3A and UBE3A-GFP

fusion proteins. As proteins were denatured for western blotting, it is unlikely that structural changes interfere with protein detection. This suggests that the UBE3A-GFP fusion protein was either expressed at a very low level or unstable and degraded soon after translation.

There are several prospects that can lead to low UBE3A-GFP fusion protein expression or stability. At RNA level, one possibility is that we were unable to efficiently remove neomycin resistance gene through Cre-Lox recombination. The neomycin resistance gene contained a polyadenylation signal sequence, and, although residing in an intron and should be removed by splicing, its presence may still affect *UBE3A-GFP* RNA transcription or stability. In Ube3a-YFP mice, loxP-flanked neomycin resistance gene was positioned after YFP stop codon and before the native 3' UTR of *UBE3A*, which may reduce its interference on RNA transcription or stability. In **Figure 3.4B** we assessed *UBE3A-GFP* RNA level by conventional PCR. Despite the fact that this method was not quantitative, we showed a strong *UBE3A-GFP* expression. This suggests that low expression and instability of UBE3A-GFP may occur at the protein level.

In our targeting construct, GFP was inserted into a cut site located within the last exon of *UBE3A*, separating the final six amino acids from the rest of UBE3A protein sequence. Additionally, five amino acids were deleted at the cut site to protect targeting construct from CRISPR/Cas9-mediated cutting. As a result, the last 11 amino acids of UBE3A were disrupted by the GFP insertion in our targeting construct. The UBE3A C-terminus encodes for a HECT domain, which is important for UBE3A ligase activity.

Many non-truncating mutations right before these 11 amino acids are linked to AS, indicating that any changes at this locus may affect UBE3A function or integrity. Furthermore, this protein sequence is 100% conserved in all species available on UCSC genome browser, from human to lamprey. We speculate that disruption at the UBE3A C-terminus was the cause for low UBE3A-GFP expression and/or instability in the reporter cell lines we derived. In Ube3a-YFP mice, the YFP was fused in-frame to a full length Ube3a protein without any sequence perturbation, other than removal of the *Ube3a* stop codon.

To create a better UBE3A-GFP reporter cell line, two changes should be made in the construct designs. First, the small guide RNA should be designed to target the 3'-UTR of *UBE3A* for CRISPR/Cas9-mediated cutting. The resulting 3'-UTR will miss 15 nucleotides to protect targeting construct from CRISPR/Cas9-mediated cutting, but no sequence alteration will be introduced to UBE3A-GFP protein. Second, the targeting construct should be designed according to that used for Ube3a-YFP mice, with a full-length UBE3A fused to GFP and neomycin resistance gene between GFP and the 3' UTR (Dindot et al., 2008). This experimental design should lead to reporter cell lines that express stable UBE3A-GFP fusion protein.

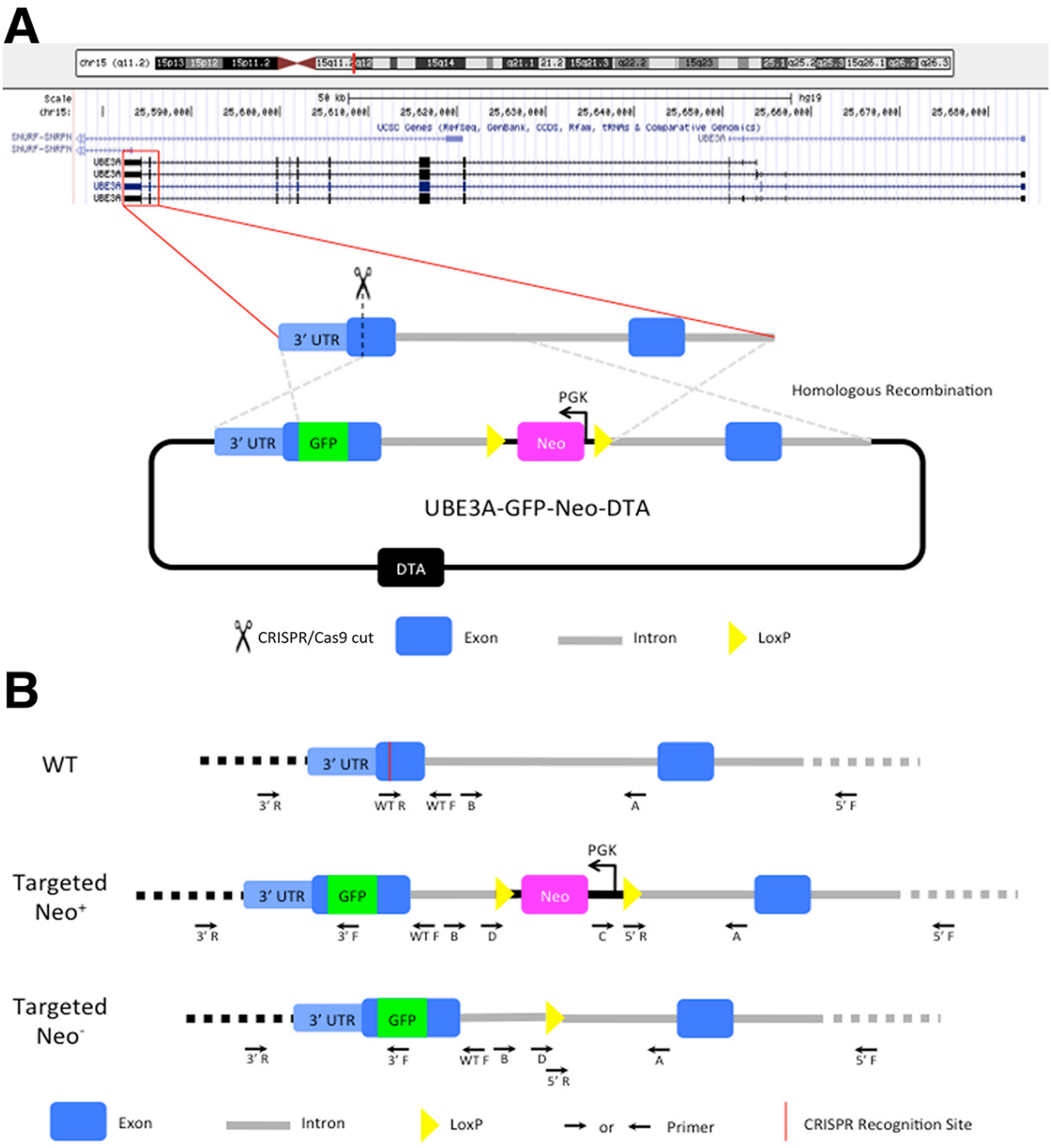

Figure 3.1. UBE3A-GFP construct and genotyping primer design. A) UBE3A-GFP targeting vector showing CRISPR/Cas9-mediated homologous recombination. UCSC genome browser on top shows edited *UBE3A* locus. **B)** Genotyping primers used to determine 5'/3' homologous and Cre-Lox recombination. Dashed lines indicate endogenous genomic sequences outside of homologous arms.

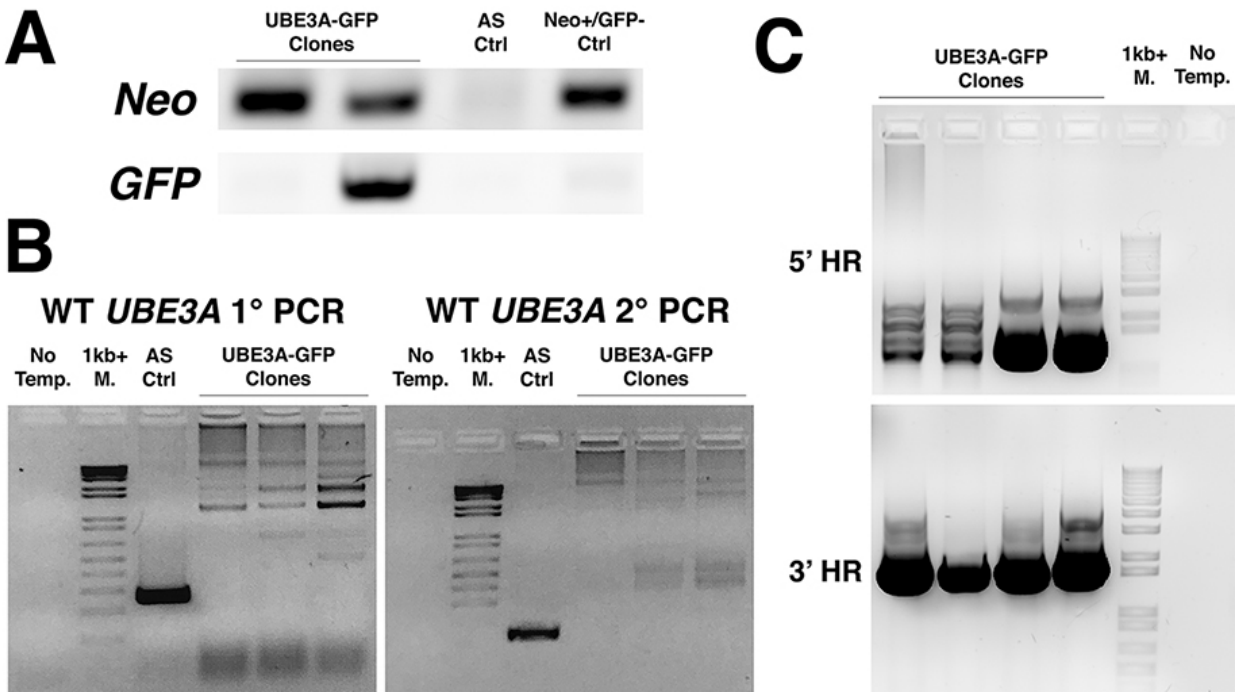

Figure 3.2. UBE3A-GFP genotyping result using PCR and gel electrophoresis. A) HotSHOT PCR screening for *GFP*$^{+}$/*Neo*$^{+}$ clones. One UBE3A-GFP clone showed only Neo cassette integration (left) and another showed correct targeting with both Neo and GFP integration (second to the left). **B)** Sequential PCR on genomic DNA using wild type *UBE3A* specific primers showed that wild type *UBE3A* was not present in UBE3A-GFP clones. **C)** PCR shows proper homologous recombination on 5'- and 3'- arms (HR) [Ctrl: control; 1°: primary; 2°: secondary; No Temp.: no template control; 1kb+ M.: 1kb+ DNA marker].

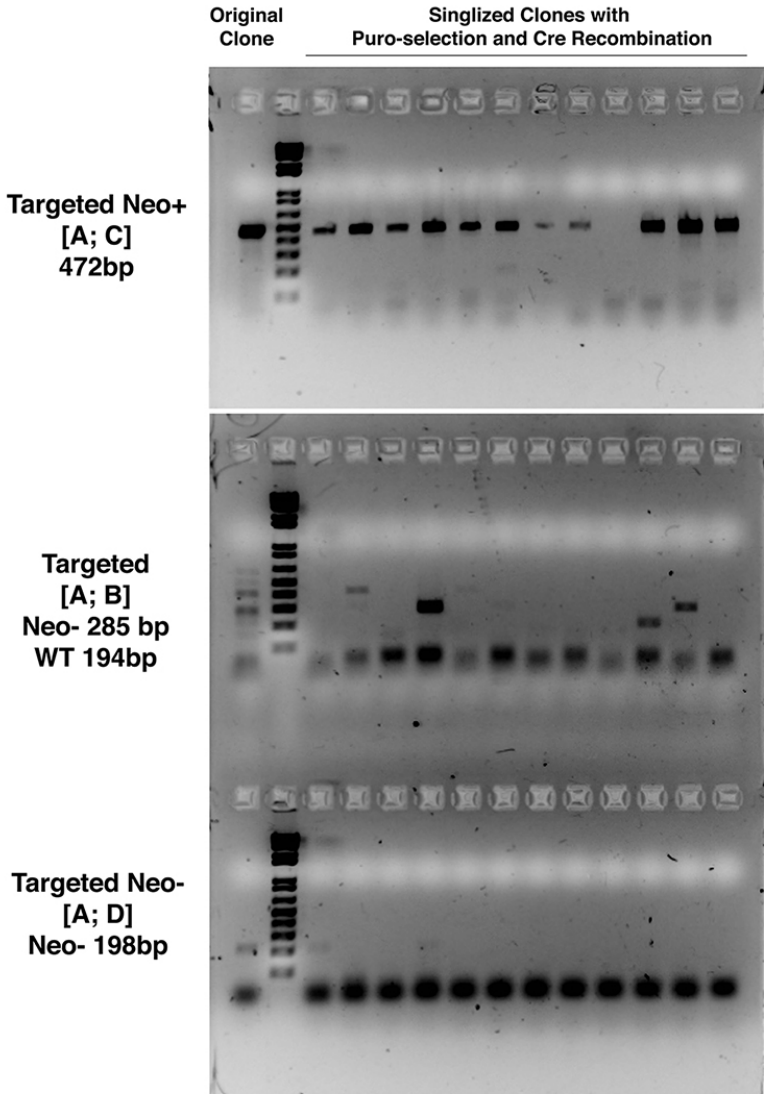

Figure 3.3. Genotyping PCR result for Cre-Lox recombination. Example gel images for Cre-Lox recombination to remove neomycin resistance gene from *UBE3A* intron. PCR products from the original UBE3A-GFP targeted clone were ran on the left of 1kb+ DNA ladder. PCR products from 12 daughter clones that were nucleofected and drug selected to transiently express Cre were ran on the right-hand side of the ladder. Primer sets indicated in the brackets correspond to Figure 3.1B and Appendix A.

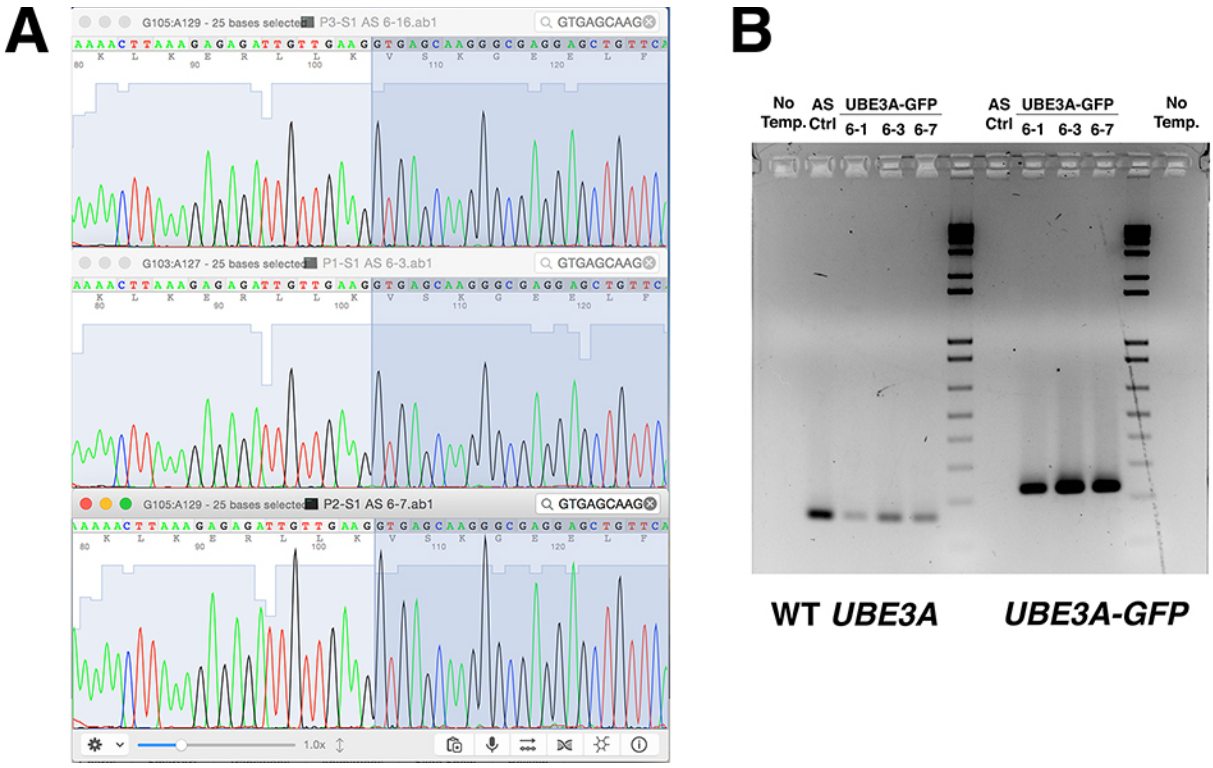

Figure 3.4. *UBE3A-GFP* DNA sequencing and RNA expression. A) Genomic DNAs from targeted clones were subjected to PCR amplification using primers across *UBE3A* and *GFP* fusion site and sequenced using a nested sequencing primer. *GFP* sequences are shaded in blue. **B)** RNA isolated from *UBE3A-GFP* targeted clones were reverse transcribed and amplified by PCR using wild type *UBE3A* or *UBE3A-GFP* primers. Wild type *UBE3A* expression in UBE3A-GFP clones is likely an artifact caused by poor primer specificity to wild type *UBE3A*.

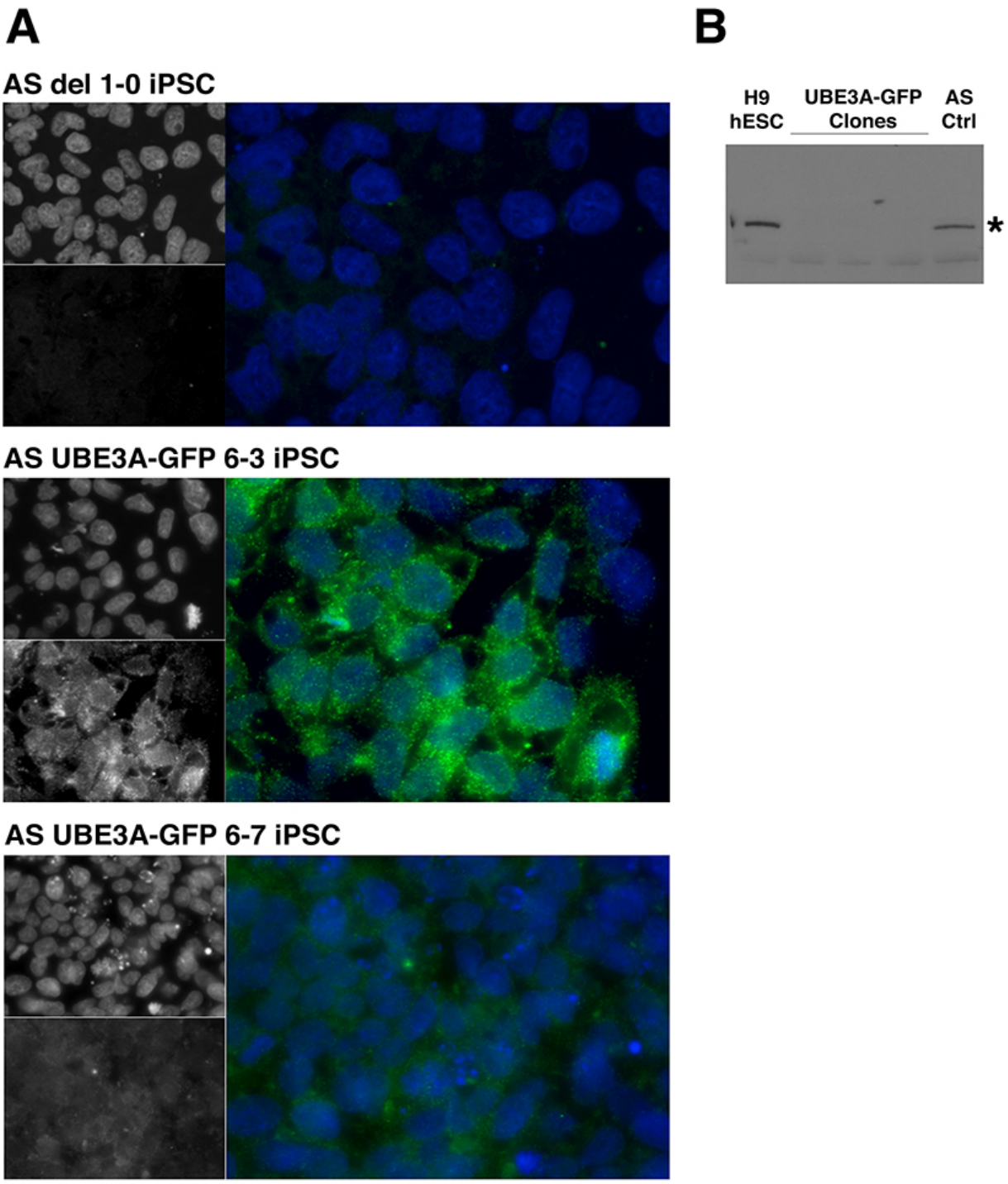

Figure 3.5. UBE3A-GFP protein expression. A) Immunocytochemistry using antibody against GFP (green) to amplify UBE3A-GFP fluorescent signals. **B)** Western blot using antibody against UBE3A to detect UBE3A-GFP (not observed) in targeted clones and wild type UBE3A (*) in H9 hESC and AS del 1-0 iPSC controls.

Chapter 4

RBFOX1 and RBFOX2 are dispensable in iPSCs and iPSC-derived neurons and do not contribute to neural-specific paternal *UBE3A* silencing

This chapter is a manuscript under review.

4.1 Abstract

Angelman Syndrome (AS) is a rare neurodevelopmental disorder caused by loss of function of the maternally inherited copy of *UBE3A*, an imprinted gene expressed biallelically in most tissues, but expressed exclusively from the maternal allele in neurons. Active transcription of the neuron-specific long non-coding RNA (lncRNA), *UBE3A-ATS,* has been shown to silence paternal *UBE3A*. We hypothesized that alternative splicing factors, RBFOX2 and RBFOX1, might mediate splicing changes and result in the transcription of *UBE3A-ATS* in neurons. We found that RBFOX2 and RBFOX1 both bind to *UBE3A-ATS* transcript in neurons, but are not required for gene expression and/or neuron-specific processing in the *SNURF/SNRPN-UBE3A* region. However, we found that depletion of RBFOX2 causes a proliferation phenotype in immature neural cultures, suggesting that RBFOX2 is involved in division versus differentiation decisions in iPSC-derived neural progenitors. Absence of RBFOX2 also altered the expression of some genes that are important for glutamatergic neocortical development and Wnt-Frizzled signalling in mature neuronal cultures. Our data show that while RBFOX1 and RBFOX2 do not mediate neuron-specific processing of *UBE3A-ATS*, these proteins play important roles in developing neurons and are not completely functionally redundant.

4.2 Introduction

Angelman syndrome (AS), a neurodevelopmental disorder affecting approximately 1/15,000-1/30,000 live births (Chamberlain and Lalande, 2010b), is characterized by microcephaly, seizures, ataxia, lack of speech, happy demeanor, and

severe cognitive disability (Lossie et al., 2001). AS is caused by the loss of function from the maternal copy of the *UBIQUITIN PROTEIN LIGASE E3A* (*UBE3A*) gene (Kishino et al., 1997). *UBE3A* is imprinted, and expressed preferentially from the maternal allele in neurons, but is expressed from both parental alleles in other tissues. This tissue-specific imprinting—or silencing of paternal *UBE3A*—occurs due to the neuron-specific expression of an antisense transcript (*UBE3A-ATS*) from the paternal allele (Chamberlain et al., 2010). *UBE3A-ATS* is one of several lncRNAs that are processed from the *SNURF/SNRPN* gene. In addition to the protein-coding *SNURF* and *SNRPN* transcripts, this gene also produces several members of the *SNORD116* and *SNORD115* snoRNA clusters, as well as lncRNAs of unknown function, such as *IMPRINTED IN PRADER-WILLI* (*IPW*) and *UBE3A-ATS* (Runte et al., 2001). The neuron-specific regulation of *UBE3A-ATS* is poorly understood, but likely differs between mouse and human. In mouse, the entire lncRNA portions of the *Snurf/Snrpn* transcript are neuron-specific (Landers et al., 2004). In human, the lncRNAs between *SNURF/SNRPN* protein-coding portion and the *IPW* lncRNA are expressed broadly in many tissue types, but the lncRNA downstream of *IPW*, including the *SNORD115* cluster and *UBE3A-ATS* are neuron-specific (Chamberlain et al., 2010). It is important to understand the regulation of the neuron-specific portion of *SNURF/SNRPN* lncRNA, since it, in turn, controls *UBE3A* imprinted expression (Huang et al., 2012; Meng et al., 2015).

A previous crosslinking-immunoprecipitation-sequencing (CLIP-Seq) study in human embryonic stem cells (hESCs) showed that the *SNURF/SNRPN* lncRNA is

highly bound by an alternative splicing factor, RBFOX2 (data available at http://genome.ucsc.edu) (Yeo et al., 2009). RBFOX2, also known as RBM9, belongs to the RBFOX1 family of RNA-binding proteins (Nakahata and Kawamoto, 2005). RBFOX2 and its paralogs, RBFOX1 (A2BP1) and RBFOX3 (HRNBP3), are known to be key regulators of alternative splicing in neurons and regulate exon exclusion/inclusion as well as intron retention (Kim et al., 2010; Nakahata and Kawamoto, 2005; Underwood et al., 2005). All three RBFOX proteins are known to bind to the hexanucleotide sequence UGCAUG, a common *cis*-regulatory element in pre-mRNAs. Mouse studies suggest that RBFOX1 is highly expressed in heart, brain, and muscles while RBFOX2 is expressed in a broader range of tissues, including the aforementioned as well as ovary, kidney, lung epithelium, and embryo (Underwood et al., 2005). In comparison, RBFOX3 is not as well characterized and is identified to encode a neuron-specific nuclear protein that is recognized by NeuN antibody (Kim et al., 2009). Recent studies indicate that RBFOX proteins may be involved in alternative polyadenylation regulation and affect functions related to 3' untranslated regions (UTRs), such as mRNA stability, localization, and translation (Shi et al., 2009; Wang et al., 2008). Interestingly, RBFOX1 haploinsufficiency is linked to autism, intellectual disability, and epilepsy (Bill et al., 2013).

High-throughput sequencing studies of 3' polyadeylated ends (polyA-Seq) in human tissues revealed two polyadenylation sites at the 3' end of *IPW* near the end of the *SNURF/SNRPN* lncRNA transcript in non-neuronal cells (Derti et al., 2012). We hypothesized that the neuron-specific expression of RBFOX1 regulates an alternative

splicing event that results in the skipping of the polyadenylation sites at *IPW*, leading to the neuron-specific expression of *UBE3A-ATS* and subsequent imprinted expression of *UBE3A*. In this paper, we investigated whether depletion of RBFOX1 and RBFOX2 altered *SNURF/SNRPN* lncRNA expression and/or processing during neural differentiation. We mutated RBFOX1 and RBFOX2 singly and in combination using lentiCRISPRs in AS and normal patient-derived iPSCs and differentiated them into neurons. We found that RBFOX1 and RBFOX2 are not required for the neuron-specific expression or processing of the *SNURF/SNRPN*. However, we found a neural differentiation defect in RBFOX2-null iPSCs, suggesting that RBFOX2 is involved in division versus differentiation decisions in iPSC-derived neural progenitors.

4.3 Materials and Methods

iPSC Culture

iPSCs were maintained as described before (Chamberlain et al., 2010). Briefly, iPSCs were grown on irradiated mouse embryonic fibroblasts and fed daily with conventional hESC medium consisting of DMEM-F12 supplemented with knock-out serum replacer, nonessential amino acids, L-glutamine, β-mercaptoethanol, and basic FGF. iPSCs were cultured in a humid incubator at 37 °C with 5% CO_2 and passaged approximately once a week manually.

Neural Differentiation

iPSC-derived neuronal culture were generated using either embryoid-body based (Pankratz et al., 2007) or monolayer (Germain et al., 2013) differentiation protocol with some modifications as previously reported (Chamberlain et al.,

2010; Germain et al., 2014). Briefly, iPSC colonies were manually cut and lifted when generating embryoid bodies for the embryoid-body protocol. After three weeks of neural differentiation using either protocol, neural progenitors were plated on tissue culture plates coated with poly-ornithine/laminin. The neural differentiation medium consisted of Neurobasal Medium, B-27 supplement, nonessential amino acids, and L-glutamine, and was supplemented with 1 μM ascorbic acid, 200 μM cyclic adenosine monophosphate, 10 ng/mL brain-derived neurotrophic factor, and 10 ng/mL glial-derived neurotrophic factor. Unless otherwise specified, all experiments were conducted on neural cultures that were at least 10 weeks old.

Lentiviral Production, Transduction, and Clone-screening

sgRNAs were designed using web-based CRISPR design tool (http://crispr.mit.edu) and cloned into lentiCRISPR (Addgene Plasmid 49535 and 52961) and lentiGuidePuro (Addgene Plasmid 52963) as instructed (Sanjana et al., 2014; Shalem et al., 2014). lentiviral particles were made by transfecting 293FT cells with 2nd generation packaging systems using lipofectamine 2000 (Life Technologies). iPSCs were singlized using Accutase (Millipore) and transduced with lentivirus in suspension in the presence of 8μg/mL polybrene for two hours. The iPSCs/lentivirus mixture were diluted 1:1 in hESC medium and plated on DR4 MEF feeders at a low density, supplemented with 10μM ROCK inhibitor, Y-27632, overnight. Attached cells were cultured in hESC medium for an additional 72 hours before drug selection using puromycin at 0.5μg/mL during

the first week and at 1 μg/mL during the second week. Puromycin-resistant iPSC colonies were individually picked into a new feeder well and screened for indels by sequencing genomic DNA.

RNA Isolation and Reverse Transcription

RNA samples were isolated using RNA-Bee (Tel-Test Inc.), DNase-treated with Amplification Grade DNaseI (Invitrogen) at 37°C for 45 minute, and converted into cDNA using High-Capacity cDNA Reverse Transcription Kit (Applied Biosystems) according to the manufacturer's instructions.

Quantitative Reverse Transcription PCR

All RT-qPCR assays were performed in biological triplicate from independent cultures. Expression levels of target genes were measured using Taqman gene expression assays (Applied Biosystems) following the manufacturer's protocol. In the case of *sno-lncRNAs*, gene expression levels were measured using published primers (Yin et al., 2012) in combination with SYBR Green PCR master mix (Applied Biosystems). All genes were normalized to *GAPDH*. Relative quantity (RQ) value was calculated as $2^{-\Delta\Delta Ct}$ using un-manipulated AS or normal cell lines as the calibrator sample.

Western Blotting

Cells were lysed on ice using RIPA buffer (150mM NaCl; 50mM Tris, pH 8.0; 1% TritonX-100; 0.5% Sodium Deoxycholate; 0.1% SDS) supplemented with proteinase inhibitor II. Protein concentrations were measured using Peirce BCA Protein Assay Kit (Thermo Scientific). Total cell lysates were resolved on 10%

handcast SDS-PAGE gels and transferred to nitrocellulose or polyvinylidene difluoride membranes using wet/tank blotting system (Bio-Rad). The membranes were blocked in 5% nonfat dry milk in TBST (0.5% Tween-20 in TBS containing 20mM Tris and 500mM NaCl). The following primary antibodies and concentrations were used: mouse anti-GAPDH (1:3000, MAB374, Millipore), rabbit anti-RBFOX2 (1:2000, A300-864A, Bethyl), rabbit anti-RBFOX1 (1:1000, ab83574, Abcam). After washing with TBST three times, membranes were blotted with corresponding secondary antibodies conjugated with horseradish peroxidase. Membranes were washed and then developed in Immobilon Western Chemiluminescent HRP Substrate (Millipore), visualized using ChemiDoc Touch (Bio-Rad).

Cross-linking Immunoprecipitation (CLIP)

CLIP experiments are carried out according to published protocols (Ule et al., 2005; Yeo et al., 2009). Briefly, RNA-binding proteins are cross-linked to RNA transcripts by UV irradiation at 400mJ/cm^2. Irradiated cells are lysed and subjected to DNase treatment. RBFOX1 and RBFOX2 bound transcripts are magnetically pulled down using Protein A Dynabeads (Dynal), which are pre-conjugated to rabbit anti-RBFOX1 (Abcam) and rabbit anti-RBFOX2 (Bethyl, (Yeo et al., 2009)) respectively. An antibody against rabbit IgG is used to assay for non-specific binding. After purification steps, transcripts are released by proteinase K and isolated as described before. RNA products are reverse-transcribed followed by conventional PCR analysis.

Immunocytochemistry

Immunocytochemistry was carried out as previously described (Chamberlain et al., 2010). The following antibodies and concentrations were used: rabbit anti-RBFOX2 (1:250, A300-864A, Bethyl), mouse anti-OCT3/4 (1:100, sc-5279, Santa Cruz Biotechnology), rabbit anti-Activated-Caspase3 (1:400, #9661, Cell Signaling Technology), mouse anti-Ki67 (1:100, M7240, Dako), rabbit anti-TBR1 (1:500, ab31940, Abcam). AlexaFluor 488 and 594 fluorochrome conjugated secondary antibodies (Life Technologies) were used at 1:500. Nuclei were counterstained with DAPI and coverslips were mounted on slides with Vectashield (Vector Laboratories). Slides were imaged using a Zeiss Axiovision microscope or a Zeiss LSM 780 confocal microscope. Cell counting was carried out in a double-blind fashion on independent cultures in triplicates.

Cell Death and Cell Cycle Flow Cytometry

Cell death analysis was done using Dead Cell Apoptosis Kit with Annexin V Alexa Fluor 488 and propidium iodide (Molecular Probes). Seven days after splitting, iPSCs were singlized using Accutase (Millipore). Staining was carried out according to the manufacturer's protocol. All experiments were run in triplicates using independent cultures. Negative control with no Annexin V and propidium iodide staining, Annixin V only control, and propidium iodide only control were included using corresponding cell lines to set up gates. Flow cytometry analysis was carried out by UCONN Health Flow Cytometry Core, using a MACSQuant Analyzer 10.

Cell cycle analysis was done using Click-iT Plus EdU Alexa Fluor 647 Flow Cytometry Assay Kit (Molecular Probes). Four days after splitting, iPSCs were synchronized using 0.2μM of nocodazole for 18 hours. The cells were then released into cell cycle for 3.5 hours in hESC medium, followed by 10μM EdU labeling for 30 minutes. Cells were then washed and singlized using TrypLE Express (Gibco). Staining was carried out according to the manufacturer's protocol. All experiments were run in duplicates or triplicates using independent cultures. In addition to EdU-labeling and propidium iodide, iPSCs were also stained with mouse anti-OCT3/4 (1:100, sc-5279, Santa Cruz Biotechnology) in combination with goat anti-mouse AlexaFluor 488 fluorochrome conjugated secondary antibody (1:200, Life Technologies) for pluripotency. Negative control (with no EdU, Oct3/4, or propidium iodide staining), EdU-labeling only control, Oct3/4 only control, and propidium iodide only control were included using corresponding cell lines to set up gates. AlexaFluor 488 fluorochrome conjugated secondary antibody was present in all four controls. Flow cytometry analysis was carried out by UCONN Health Flow Cytometry Core, using a Becton-Dickinson LSR II Flow Cytometer.

RNA FISH

RNA fluorescence *in situ* hybridization was carried out as previously described (Martins-Taylor et al., 2014). *SNORD116* probes were made from BAC RP11-186C7 (BACPAC Resources Center). Slides were imaged using a Zeiss LSM 780 confocal microscope.

4.4 RESULTS

4.4.1 *RBFOX2 is expressed ubiquitously throughout in vitro neural differentiation while RBFOX1 is expressed in a neuron-specific manner in human.*

Previous studies indicated that *RBFOX2* and its protein product are expressed in a broad spectrum of tissues and cell types, including hESCs (Underwood et al., 2005; Yeo et al., 2009), while *RBFOX1* and its protein product are specifically expressed in brain and muscle cells (Underwood et al., 2005). We sought to determine the expression patterns of RBFOX2 and RBFOX1 RNA and protein during *in vitro* differentiation of human iPSCs into neurons. Conventional PCR and western blotting in iPSCs and their neural-derivatives revealed that RBFOX2 is expressed abundantly in iPSCs and at all time points during neural differentiation (**Figure 4.1A-B**). On the other hand, *RBFOX1* RNA is first evident in the neural precursor stage, but is markedly upregulated in 6-week and 10-week neuronal cultures (**Figure 4.1A**). RBFOX1 protein is detectable only in neural cultures that have been maturing *in vitro* for over 6 weeks (**Figure 4.1B**). Robust expression of *RBFOX1* RNA and detectable expression of RBFOX1 protein is coincident with the appearance of *UBE3A-ATS* (**Figure 4.1A**) (Chamberlain et al., 2010).

4.4.2 *SNURF/SNRPN lncRNA transcripts are bound by RBFOX1 and RBFOX2 in iPSCs and neurons.*

Since RBFOX1 and RBFOX2 are both RNA-binding proteins (Kuroyanagi, 2009) and RBFOX2 was previously shown to bind the *SNURF/SNRPN* lncRNA, we carried out cross-linking immunoprecipitation (CLIP) to see whether the RBFOX proteins bind

SNURF/SNRPN in iPSCs and 10-week-old iPSC-derived neurons (**Figure 4.1C**). We found abundant RBFOX2-binding on the *SNURF/SNRPN* lncRNA expressed in iPSCs (i.e. from *SNURF/SNRPN* to *IPW*). This finding agrees with previously published RBFOX2 CLIP-seq data in hESCs (Yeo et al., 2009). In neurons, where both RBFOX1 and RBFOX2 are expressed, we found both factors bound to the entire *SNURF/SNRPN* lncRNA, including neuron-specific *SNORD115* and *UBE3A-ATS*. Since RBFOX1 expression correlated with the appearance of *UBE3A-ATS,* and since RBFOX proteins bind to *SNURF/SNRPN* lncRNA transcripts, we hypothesized that RBFOX1, by itself or together with RBFOX2, may play a role in regulating the expression of the neuron-specific portion of *SNURF/SNRPN* transcripts via alternative splicing.

4.4.3 *Loss of RBFOX2 does not affect expression of the lncRNA in iPSCs and neurons.*

To investigate the role of RBFOX2 in the regulation of *SNURF/SNRPN* lncRNA, we knocked out RBFOX2 in AS iPSCs harboring a large deletion of maternal 15q11-q13 using CRISPR/Cas9. Specifically, we transduced AS iPSCs with lentiviruses carrying both Cas9 and sgRNA components (Shalem et al., 2014) to create non-homologous end-joining (NHEJ)-mediated insertions/deletions (indels). To account for potential off-target effects, we designed two different sgRNAs targeting the two most upstream exons of *RBFOX2* that are common amongst all *RBFOX2* transcripts (**Figure 4.2A**). As a control for lentiviral transduction and CRISPR/Cas9 integration and expression, we designed a scrambled sgRNA that has no match in the human genome (Shirk et al., 2013b). For RBFOX2 knockouts (KOs), we amplified and sequenced the genomic DNA near the predicted CRISPR/Cas9 cut site to identify small indels that shifted the reading

frame, leading to a premature stop codon. We selected two clonal iPSC lines for further study.

We then quantified *RBFOX2* mRNA and protein and found reduced levels of *RBFOX2* mRNA (**Figure 4.2C**) and undetectable levels of RBFOX2 protein in RBFOX2 KO iPSCs (**Figure 4.2D, F**). We also confirmed the functional loss of RBFOX2 by assaying splicing changes in previously reported RBFOX2-splicing targets, *PICALM* and *TSC2* (**Figure 4.2E**) (Yeo et al., 2009). Even though RBFOX2 is the only available RBFOX paralog expressed in iPSCs, the absence of RBFOX2 did not affect gene expression at any portion of the *SNURF/SNRPN* lncRNA assayed (**Figure 4.2G, H**). Specifically, we quantified *SNORD116* host transcript and *sno-lncRNAs*, which are most enriched for RBFOX2 binding (Yeo et al., 2009; Yin et al., 2012), as well as an individual processed snoRNA, *SNORD116-29*, and found no expression differences between non-transduced, scrambled and RBFOX2 KO iPSCs.

Following 10-week *in-vitro* neural differentiation, we reassessed *RBFOX2* mRNA and protein levels, and ensured that functional loss of RBFOX2 was still evident in RBFOX2 KO neurons (**Figure 4.3A-C**). Since it is known that RBFOX paralogs affect each other's splicing and expression, we also quantified the RNA levels of *RBFOX1* and *RBFOX3*, which are expressed in neurons. We observed a slight downregulation of *RBFOX1* and upregulation in *RBFOX3* in RBFOX2 KO neurons. However, these changes were also observed in the scrambled control (**Figure 4.3A**), and are thus unlikely to be related to RBFOX2 depletion. As in iPSCs, the absence of RBFOX2 did not overtly affect the expression of the *SNURF/SNRPN* lncRNA (**Figure 4.3D, E**).

To rule out the possibility that RBFOX2 might play a different role in normal iPSCs and neurons, we also mutated RBFOX2 in normal iPSCs and differentiated them into neurons (**Supplementary figure 1**). Although we found slight increases in the levels of *RBFOX1* and *RBFOX3* mRNAs as well as small, but significant increases in 4 out of 5 *sno-lncRNAs* in the RBFOX2 KO neurons, we determined that the RBFOX2 KO neurons also had increased *MAP2* and *VGLUT2* levels, suggesting that there are more mature neurons in the RBFOX2 KO cultures. This variability in the neuronal cultures may account for the increases in *RBFOX1* and *RBFOX3* mRNAs and the *sno-lncRNAs* independent of RBFOX2 depletion (**Supplementary figure 1I**).

4.4.4 *Loss of RBFOX1 does not affect the expression of the SNURF/SNRPN lncRNA in neurons.*

We hypothesized that tissue-specific expression of RBFOX1 might play a critical role in processing the *SNURF/SNRPN* lncRNA, leading to the neuron-specific expression of *UBE3A-ATS* and repression of paternal *UBE3A*. Therefore, we knocked out RBFOX1 in AS iPSCs and in RBFOX2 KO AS iPSCs using the lentiCRISPR/Cas9 approach. The details of the specific mutations further studied are shown in **Figure 4.2B**. Following differentiation into 10-week neurons, we found that *RBFOX1* mRNA was significantly reduced in RBFOX1 KO and RBFOX1/2 double knockout (dKO) iPSC-derived neurons (**Figure 4.3A**). However, *RBFOX1* was reduced in neurons derived from iPSCs transduced with the scrambled lentiCRISPR as well. We were not able to obtain the same lot of RBFOX1 antibody that had worked for Western blot previously. Therefore, to assure the absence of functional RBFOX1 protein, we cloned cDNAs from

the RBFOX1 KO and RBFOX1/2 dKO neurons to ensure that the remaining RNA transcripts harbored frame-shift mutations and lead to premature stop codons (**Supplementary figure 2**). Unexpectedly, in RBFOX1 KO2, we found a subpopulation of neurons expressing *RBFOX1* cDNA with a complex 57nt deletion that was not identified in the original iPSC gDNA. By designing primers specific to the unique DNA sequence created by this deletion, we found a very small population of iPSCs presenting the same mutation (**Supplementary figure 2F**). This indicates that RBFOX1 KO2 was a mixed clone, with the majority harboring a 4nt frame-shift deletion in *RBFOX1*. The functional loss of RBFOX1 in neurons was confirmed by splicing changes in previously reported RBFOX1 targets, *KCND3* and *ABLIM1* (**Supplementary figure 2G**) (Gehman et al., 2011). To our surprise, the expression of the *SNURF/SNRPN* lncRNA and *UBE3A* was not significantly affected in RBFOX1 KO and RBFOX1/2 dKO neurons (**Figure 4.3D, E**).

4.4.5 *RBFOX2 KO iPSCs are viable with normal cell cycle and have no increase in apoptosis*

Contrary to Yeo et al. (Yeo et al., 2009), we found that RBFOX2 KO iPSCs in both AS and normal background were viable and did not exhibit increased apoptosis (**Figure 4.4A, Supplementary figure 3A**). To confirm this finding, we performed immunocytochemistry using an antibody against activated-caspase3 and found no significant differences between the controls and RBFOX2 KO iPSCs (**Figure 4.4B, Supplementary figure 3B**). We also tested whether the absence of RBFOX2 affects cell cycle. RBFOX2 KO and control iPSCs were synchronized using a nocodazole block

and labeled using EdU. We found no differences between RBFOX2 KO iPSCs and controls at any stage of the cell cycle (**Figure 4.4C, Supplementary figure 3C**). This indicated that RBFOX2 KO iPSCs also have a normal cell cycle length.

4.4.6 *RBFOX2 KOs exhibit increased proliferation during in vitro neural differentiation.*

Although the iPSCs appeared to be normal, we consistently saw increased proliferation of RBFOX2 KO neurons at approximately 7 weeks of differentiation when compared to scrambled controls in both normal and AS background. Immunocytochemistry using an antibody against Ki67 confirmed that the proliferating population is significantly increased in RBFOX2 KO 7-week neuronal cultures when compared to controls (**Figure 4.5A-B, Supplementary figure 4A-B**). This proliferation phenotype in RBFOX2 KO neurons is likely to be caused by splicing changes in exon 12 of *NUMB* (**Figure 4.3C**). Exon 12 alternative splicing in NUMB is mediated by RBFOX2 (Lu et al., 2015), the inclusion of which is pro-proliferation while the exclusion is pro-differentiation during neural development (Verdi et al., 1999).

To determine whether this increase in proliferation affects neural cell-fate and, hence, the cell population in the 10-week culture, we quantified mRNA levels of neural markers in 10-week-old AS neurons (**Supplemental figure 5**). Markers representing neuronal precursors (*SOX2*, *PAX6*, and *DCX*), neurons (*TUBB3* and *CTIP2*), and mature astrocytes (*S100B*) were largely unchanged in RBFOX2 KO neurons. However, significant increases in *TBR1* and *TBR2* were observed in RBFOX2 KO neurons (**Figure 4.5C, Supplementary figure 4C**). *TBR2* is a marker of intermediate progenitor cells, while *TBR1* is a marker for post-mitotic cortical plate neurons (Englund et al.,

2005). By counting the number of cells that express TBR1 in **Figure 4.5D**, we found that the percentage of TBR1 positive cells in the neuronal culture was comparable between the controls and RBFOX2 KO neurons (**Figure 4.5E, Supplementary figure 4D-E**), suggesting that TBR1 may be upregulated in individual cells and that the proportion of post-mitotic cortical plate neurons was not increased.

4.4.7 *FRZB mRNA is upregulated in RBFOX2.*

Gene expression changes were previously seen in RBFOX1 knockdown human neural progenitor cells (Fogel et al., 2012). We sought to determine whether these changes could also be seen in RBFOX1 and RBFOX2 KO neurons. We observed no significant expression changes in *SV2B*, *NRXN1*, *GABRA3*, and *FRZB* in AS RBFOX1 KO and RBFOX1/2 dKO neurons compared to the controls (**Supplementary figure 6**). However, we observed an increase in *FRZB* expression in normal and AS RBFOX2 KO neurons (**Figure 4.5F, Supplementary figure 4F**). FRZB protein competes with FRIZZLED receptors for Wnt-binding (Harterink et al., 2011; Leyns et al., 1997). Increased *FRZB* levels suggest that Wnt/β-cat signaling may be attenuated in RBFOX2 KO neurons. Therefore, we quantified *AXIN2* expression, which is transcriptionally activated by Wnt/β-cat signaling (Lustig et al., 2002). Unexpectedly, we found a subtle increase *AXIN2* expression, rather than the expected decrease (**Figure 4.5F, Supplementary figure 4F**). These data suggest that although an increase in *FRZB* mRNA is observed in RBFOX2 KO neurons, there may not be an increase in FRZB protein because there is not an attenuation of Wnt/β-cat signaling.

4.5 DISCUSSION

RBFOX2 and its paralog, RBFOX1 are RNA binding proteins known to regulate alternative splicing in brain (Gehman et al., 2012; Gehman et al., 2011). Yeo at al. showed abundant RBFOX2-binding on the *SNURF/SNRPN* lncRNA in hESCs (Yeo et al., 2009). We hypothesized that RBFOX1, the neuron-specific paralog of RBFOX2, may regulate alternative splicing of the *SNURF/SNRPN* lncRNA, leading to the skipping of the polyadenylation sites in *IPW* and neuron-specific expression of the distal portion of the lncRNA, also known as *UBE3A-ATS*. We first determined that expression of the RBFOX1 protein is coincident with the appearance of *UBE3A-ATS*, while RBFOX2 protein is more broadly expressed, and a third paralog, RBFOX3, is only expressed in 10-week neuronal cultures, weeks after the initial detection of *UBE3A-ATS* (**Supplementary figure 7**). Because RBFOX3 was expressed at a time point later than the first appearance of *UBE3A-ATS*, it is unlikely to play a role in regulating *UBE3A-ATS* expression. Subsequently, we found abundant RBFOX2 and RBFOX1 binding across the entire *SNURF/SNRPN* lncRNA in human iPSC-derived neurons, including *IPW* and *UBE3A-ATS*. These observations supported our initial hypothesis that RBFOX1, by itself or together with RBFOX2, may play a role in regulating the expression of the neuron-specific portion of *SNURF/SNRPN* transcripts via alternative splicing.

To directly test whether RBFOX1 and/or RBFOX2 played a role in the neuron-specific processing of the *SNURF/SNRPN* lncRNA, we knocked out RBFOX2 and RBFOX1 alone and in combination in AS iPSCs. These cells have a deletion of the maternal allele of chromosome 15q11-q13, allowing us to focus on the RNA transcripts originating from the paternal allele. We used lentiCRISPR/Cas9 technology to generate

indels that would create a frameshift and prematurely stop RBFOX protein translation. Although puromycin-resistant clones were carefully screened manually and using online TIDE (Tracking of Indels by Decomposition) software (Brinkman et al., 2014) to ensure that they were clonal populations with the desired deleterious mutations, we found that at least one clone harbored a mutation larger than 50 nucleotides, which was not readily detectable by TIDE or manual efforts. The RBFOX1 KO2 clone carried a small portion of cells with a 57 nt in-frame deletion, which likely produces a small amount of potentially functional RBFOX1 protein (**Supplementary figure 2**). All other clones were demonstrated to have either loss of RBFOX protein and/or showed only the presence of a mutated cDNA that is predicted to make a prematurely terminated protein (**Supplementary figure 2**).

Upon knocking out RBFOX2 and RBFOX1, individually and in combination, we found that *SNURF/SNRPN* lncRNA expression levels, including the steady-state levels of the *SNORD116* host gene, an individual processed *SNORD116* snoRNA, the *sno-lncRNAs*, and the *SNORD115* host gene were not altered in iPSCs and in neurons. This indicates that even though RBFOX2 and RBFOX1 bind to *SNURF/SNRPN* lncRNA, they are not essential for its processing and neuron-specific expression as we hypothesized. In addition, we found that the absence of RBFOX2 did not change *SNORD116* localization in the nucleus (**Supplementary figure 8**), indicating that RBFOX2 does not have an obvious role in in nuclear organization of this locus. The unaltered steady-state levels of *SNORD115* RNA in RBFOX1KO and RBFOX1/2 dKO neurons suggest that RBFOX1 is not regulating alternative polyadenylation as we had

originally hypothesized. It is possible that alternative polyadenylation is regulated by a different RNA binding protein, or alternatively, the *SNURF/SNRPN* lncRNA is truncated in non-neurons by a different mechanism.

In agreement with our results, Yin et al. reported that RBFOX2 knockdown did not affect *sno-lncRNA* levels in PA1 cells (Yin et al., 2012), and further hypothesized that RBFOX proteins may be sequestered by the *lncRNA*-binding. Our data did not address the latter notion. Yeo et al. reported a positive correlation between the amount of RBFOX2 binding and transcript abundance (Yeo et al., 2009), thus, the enrichment for RBFOX binding on *SNURF/SNRPN* lncRNA and its processed products may reflect the abundance of these RNA transcripts. We did not observe increased cell death in RBFOX2 knockout iPSCs as previously reported in RBFOX2 knockdown hESCs (Yeo et al., 2009). The disparity in viability may be due to differences between RBFOX2 knockdown versus knockout, but is most likely either caused by differences in the culture system (i.e. feeder-free versus MEF feeders) for the pluripotent stem cells or shRNA toxicity.

Despite the fact that many important neuronal genes are targets of RBFOX2 and RBFOX1 for alternative splicing, we were able to differentiate all of the RBFOX knockout iPSC lines into mature cortical neurons, demonstrating that the proteins are dispensible for neuronal differentiation. CNS-specific RBFOX2 and/or RBFOX1 knockout mice were viable and had morphologically normal cortical layers, which supports our observation (Gehman et al., 2012; Gehman et al., 2011). However, there was a significant increase in proliferation at around 7-weeks of neural differentiation in RBFOX2 KO neurons,

despite normal cell cycle in iPSCs (**Figure 4.4C, Supplementary figure 3C**). This suggests that RBFOX2 may play an important role in the decision between self-renewal and differentiation during neural development. We found increased inclusion of the pro-proliferative exon 12 of *NUMB* in RBFOX2 KO neurons, which may provide an underlying mechanism for this proliferation phenotype. We measured mRNA levels of neural markers in mature RBFOX2 KO neurons to determine whether this increase in proliferation affects neural cell-fate. While most neural markers remained unchanged, we found that *TBR1* and *TBR2* were significantly upregulated in 10-week-old RBFOX2 knockout neurons. *PAX6, TBR2*, and *TBR1* are expressed sequentially during glutamatergic neocortical development (Englund et al., 2005). With no change in *PAX6* level and significant increases in both *TBR2* and *TBR1* levels in RBFOX2 knockout neurons, we hypothesized that there was an over-proliferation in the *TBR2*$^+$ intermediate progenitor population, leading to an increase in the post-mitotic *TBR1*$^+$ neurons. However, the percentage of TBR1$^+$ neurons was not increased in RBFOX2 KO neuron cultures, although many TBR1$^+$ neurons reside in multi-layered hubs that are hard to image and quantitate using microscopy (**Supplementary figure 9**).

We also sought to verify previously reported gene expression changes that were observed in RBFOX1 knockdown human neural precursor cells (Fogel et al., 2012). One of the genes analyzed, *FRZB*, was reported to be downregulated in RBFOX1 knockdown human neural progenitor cells (Fogel et al., 2012). While we did not see a change in *FRZB* in RBFOX1 knockout neurons, we observed a significant increase in *FRZB* in RBFOX2 knockout neurons (**Figure 4.5F, Supplementary figure 4F**). FRZB

protein is a Wnt signaling antagonist that competes with FRIZZLED receptors for Wnt-binding (Harterink et al., 2011; Leyns et al., 1997). The canonical Wnt/β-cat pathway was not attenuated in RBFOX2 knockout neurons based on the level of *AXIN2* (**Figure 4.5F, Supplementary figure 4F**). It is possible that despite increased *FRZB* mRNA, FRZB protein was not increased. However, since Wnt-Frizzled signaling can activate various non-canonical pathways in addition to the β–catenin pathway (Cadigan and Liu, 2006; Lu et al., 2004), other aspects of Wnt signaling may be altered in RBFOX2 KO neurons. As Wnt-Frizzled signaling regulates many aspects in neurodevelopment, such as neuronal migration (Pan et al., 2006), neuronal polarity (Hilliard and Bargmann, 2006), and axon guidance (Wolf et al., 2008), it will be interesting to determine whether other Wnt signaling pathways function normally in RBFOX2 KO neurons.

Our previously published transcriptome data shows that the FPKM values for RBFOX1, RBFOX2, and RBFOX3 are 16.5, 50.2, 5.8, respectively, in AS neurons and 16.5, 63.9, 6.8, respectively, in normal neurons (Germain et al., 2014). The fact that RBFOX2 is much more abundant than RBFOX1 in neurons at the developmental stage we assessed may explain why more severe phenotypes were observed in the absence of RBFOX2. Because of the highly conserved RNA-binding-motif between RBFOX1 and RBFOX2, we expected that they functionally compensate each other to a certain extent. However, the RBFOX1/2 dKO neurons presented milder gene expression changes in trend with RBFOX2 KO neurons, and showed similar splicing changes to RBFOX2, rather than RBFOX1, knockout neurons (**Figure 4.3C, Supplementary figure 2G**). This observation supports our notion that RBFOX2, the most abundant RBFOX paralog,

plays a larger role than the other RBFOX proteins in these neurons. It is curious that the RBFOX1/2 dKO neurons have a slightly milder phenotype compared to RBFOX2 KO neurons. However, the most apparent phenotype in the RBFOX2 KO neurons is the increased proliferation in immature neural cultures. Perhaps the loss of RBFOX1 counteracts this increased proliferation.

In conclusion, RBFOX1 and RBFOX2 are not required for processing of *SNURF/SNRPN* lncRNA, despite the fact that the lncRNA is highly bound by the RBFOX proteins. The absence of RBFOX1 did not overtly affect expression or splicing for genes assayed here and did not present observable phenotypes in *in vitro* derived human neurons. On the other hand, the absence of RBFOX2 led to a proliferation phenotype in immature neural cultures and altered the expression of some genes that are important for glutamatergic neocortical development and Wnt-Frizzled signaling. These data support the idea that RBFOX1 and RBFOX2 are not completely functionally redundant (Gehman et al., 2012).

4.6 ACKNOWLEDGEMENT

The authors would like to thank the members of the Chamberlain and Lalande labs for helpful discussions. We thank Christopher Stoddard and Leann Crandall of the University of Connecticut Stem Cell Core for advice and support. We also thank Drs. Nada Zecevic, James Li, and Xuejun Li of the University of Connecticut Neuroscience Department for their generosity in sharing reagents and suggestions.

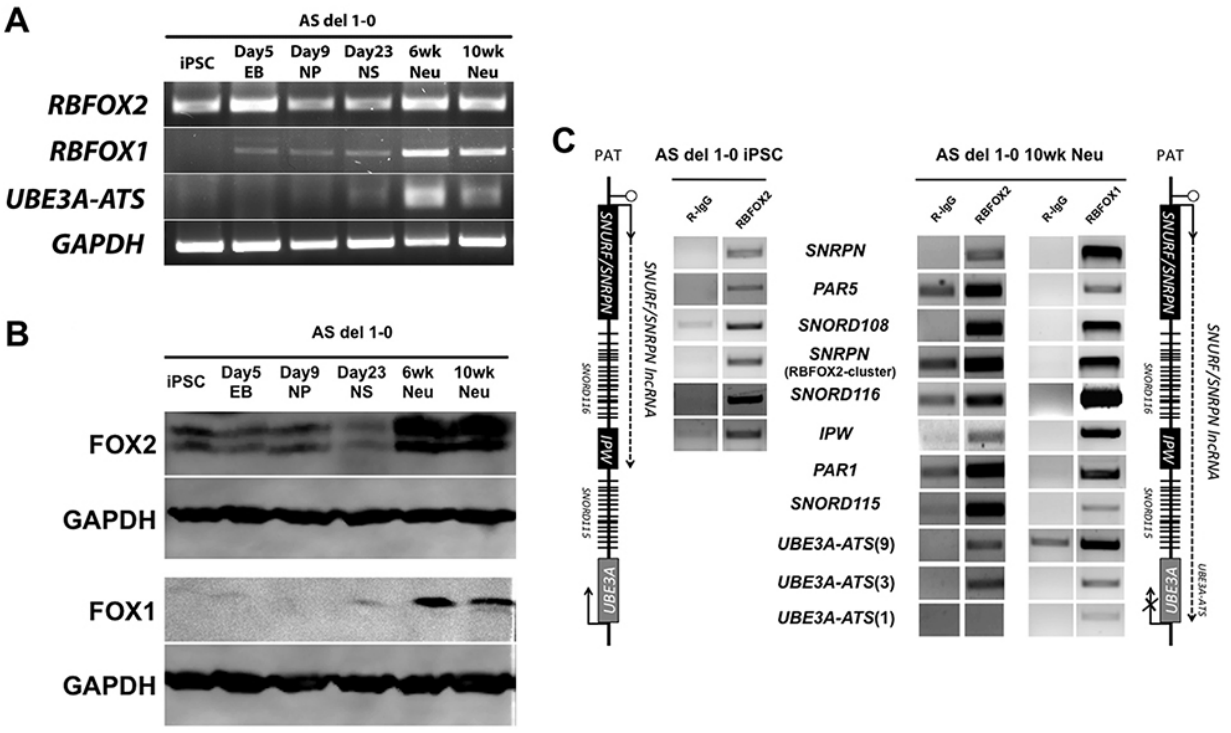

Figure 4.1. RBFOX expression and binding during neural differentiation (iPSC: induced pluripotent stem cell; EB: embryoid body; NP: neural precursor; NS: neural sphere; Neu: neuron). **A)** Conventional RT-PCR showing RNA expression of *RBFOX2*, *RBFOX1*, *UBE3A-ATS*, and *GAPDH* over 10 weeks of *in vitro* neural differentiation. **B)** Western blots showing protein expression of RBFOX2 and RBFOX1. GAPDH was used as a loading control. **C)** RBFOX2 and RBFOX1 bind to *SNURF/SNRPN* lncRNA in iPSCs and 10-week-old neurons. Rabbit IgG served as a negative control for non-specific binding.

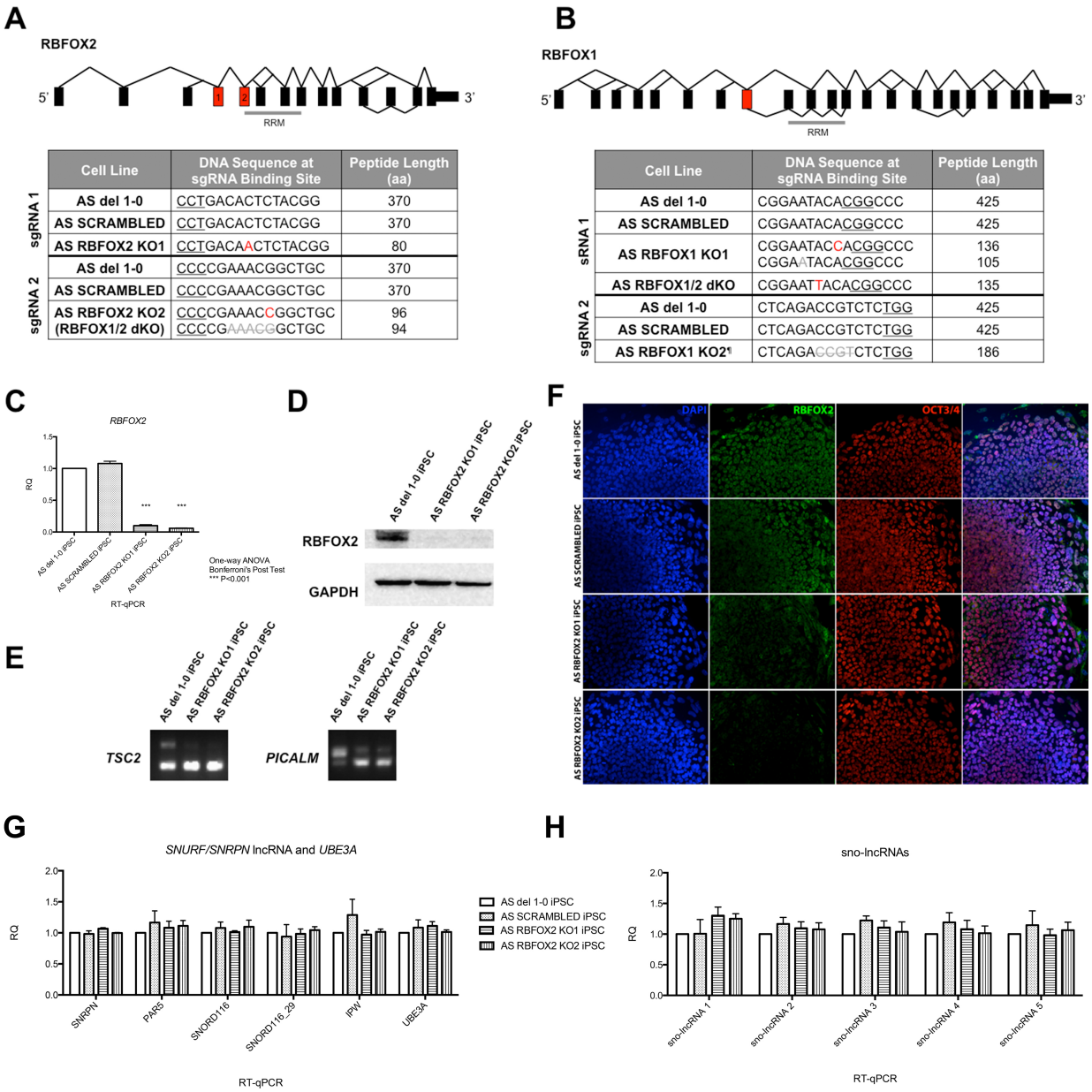

	Cell Line	DNA Sequence at sgRNA Binding Site	Peptide Length (aa)
sgRNA 1	AS del 1-0	CCTGACACTCTACGG	370
	AS SCRAMBLED	CCTGACACTCTACGG	370
	AS RBFOX2 KO1	CCTGACAACTCTACGG	80
sgRNA 2	AS del 1-0	CCCCGAAACGGCTGC	370
	AS SCRAMBLED	CCCCGAAACGGCTGC	370
	AS RBFOX2 KO2 (RBFOX1/2 dKO)	CCCCGAAACCGGCTGC CCCCGAAACGGCTGC	96 94

	Cell Line	DNA Sequence at sgRNA Binding Site	Peptide Length (aa)
sRNA 1	AS del 1-0	CGGAATACACGGCCC	425
	AS SCRAMBLED	CGGAATACACGGCCC	425
	AS RBFOX1 KO1	CGGAATACCACGGCCC CGGAATACACGGCCC	136 105
	AS RBFOX1/2 dKO	CGGAATTACACGGCCC	135
sgRNA 2	AS del 1-0	CTCAGACCGTCTCTGG	425
	AS SCRAMBLED	CTCAGACCGTCTCTGG	425
	AS RBFOX1 KO2¶	CTCAGACCGTCTCTGG	186

Figure 4.2. Lentiviral CRISPR/Cas9-mediated RBFOX KO in AS iPSCs. A and B) Schematic of *RBFOX2* and *RBFOX1* splicing patterns according to the alternative splicing graph from Swiss Institute of Bioinformatics on UCSC genome browser. Targeted exons are colored in red and the numbers correspond to respective sgRNAs. gDNA sequencing shows frameshift indels leading to premature stop codon in two RBFOX2 KOs, two RBFOX1 KOs, and one RBFOX1/2 dKO (¶see supplemental figure

2). **C)** RT-qPCR, **D)** western blot, and **F)** immunocytochemistry showing RBFOX2 mRNA or protein expression in RBFOX2 KO iPSCs. **E)** Splicing changes in *TSC2* and *PICALM* showing functional loss of RBFOX2. **G and H)** The expression of transcripts from *SNURF/SNRPN* lncRNA, including *SNORD116* and *sno-lncRNAs*, was not altered in RBFOX2 KO iPSCs.

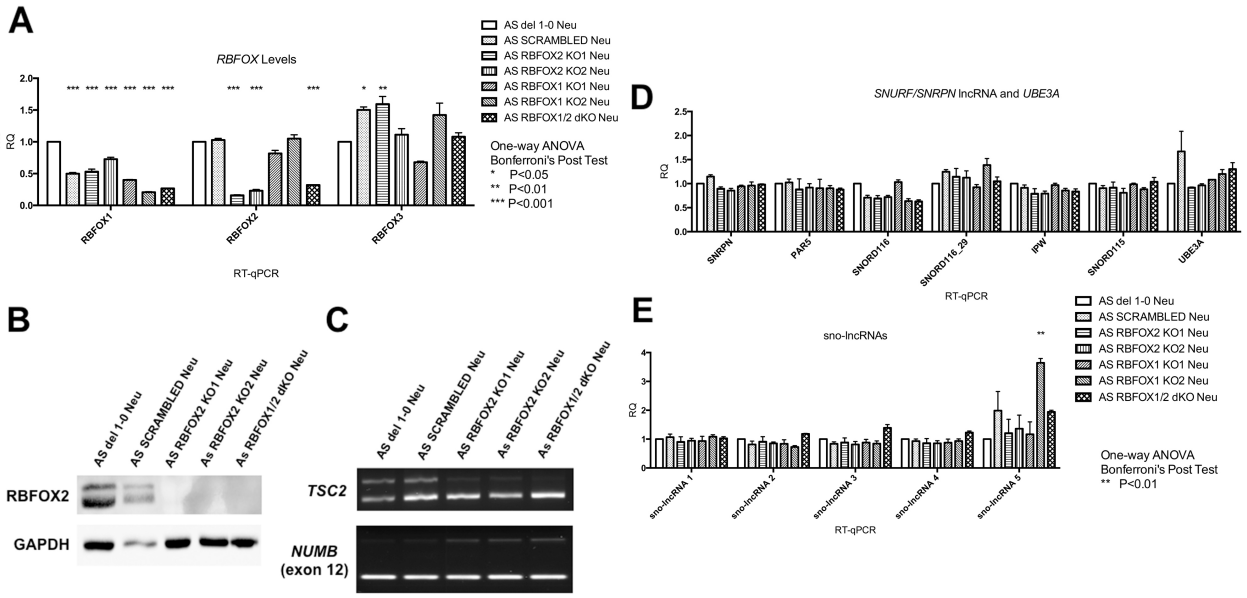

Figure 4.3. Expression of transcripts from *SNURF/SNRPN* lncRNA was not altered in RBFOX KO AS iPSC-derived neurons. A) RT-qPCR showing *RBFOX2* and *RBFOX1* expression in respective KO neurons. **B)** Western blot of RBFOX2 protein in KO neurons. **C)** Splicing changes in *TSC2* and *NUMB* in RBFOX2 KO neurons. **D and E)** Expression of transcripts from *SNURF/SNRPN* lncRNA, including *SNORD116* and *sno-lncRNA,* in RBFOX KO neurons.

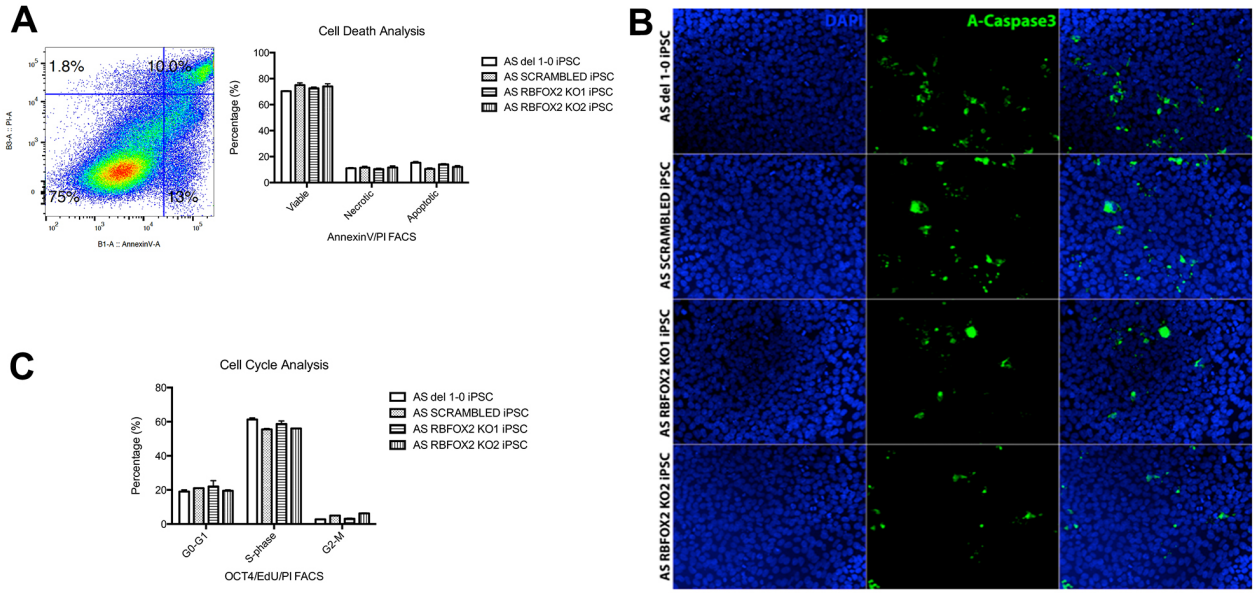

Figure 4.4. Cell death and cell cycle analysis in RBFOX2 KO AS iPSCs. A) Flow cytometry analysis using Annexin V and propidium iodide, to identify viable, necrotic, or apoptotic cells. **B)** Apoptotic cells labeled with activated caspase-3 (green). **C)** Flow cytometry was used to analyse cell cycle in synchronized iPSCs. Cells were labeled with EdU during S-phase, and then stained with propidium iodide.

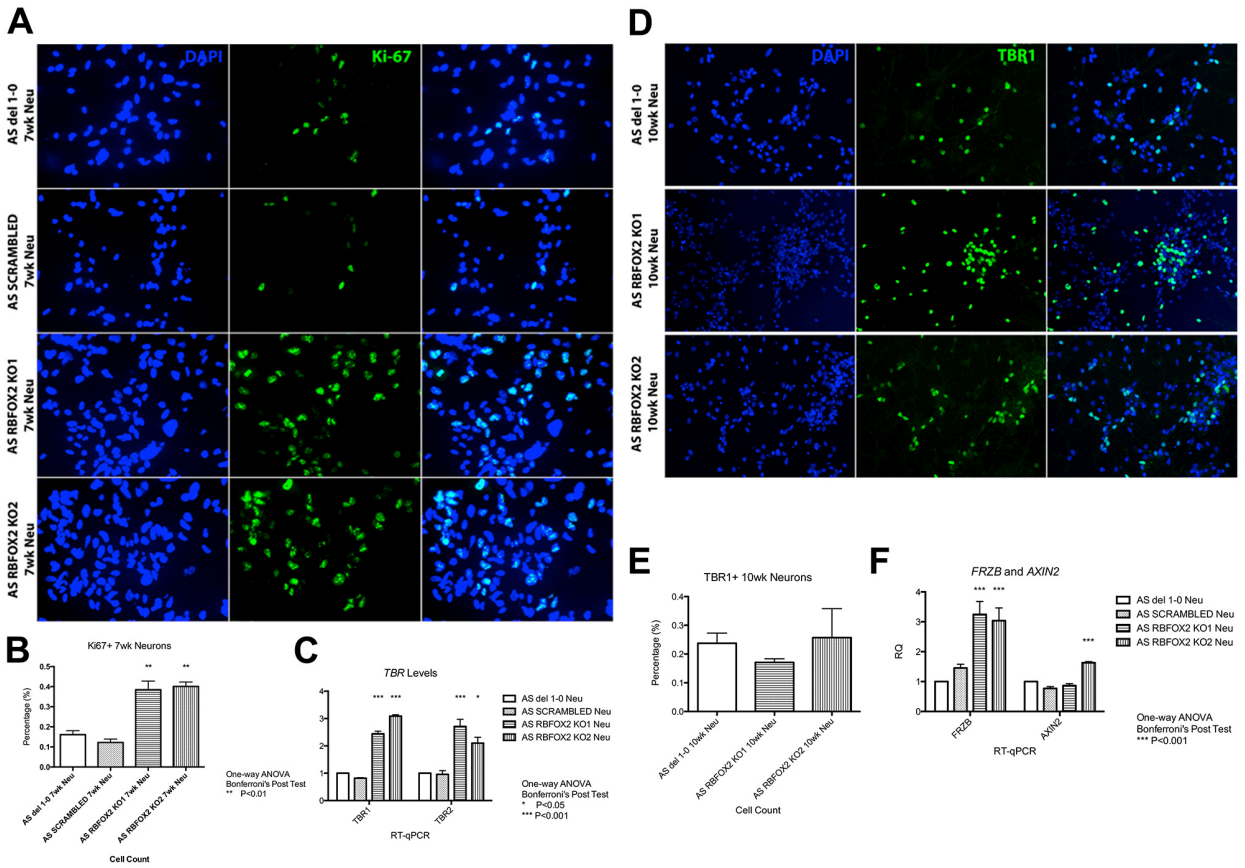

Figure 4.5. 7-week-old AS RBFOX2 KO neurons showed increased proliferation and 10-week-old AS RBFOX2 KO neurons showed increased *TBR1*, *TBR2*, and *FRZB* expression. A) Proliferating cells in 7-week-old neural culture labeled with antibody against Ki67 (green). **B)** Quantification of Ki67+ cells in A. **C)** RT-qPCR showing *TBR1* and *TBR2* expression in 10-week-old RBFOX2 KO neurons. **D)** 10-week-old RBFOX2 KO neurons labeled with antibody against TBR1 (green). **E)** Quantification of TBR1+ cells in D. **F)** RT-qPCR showing *FRZB* and *AXIN2* expression in 10-week-old RBFOX2 KO neurons.

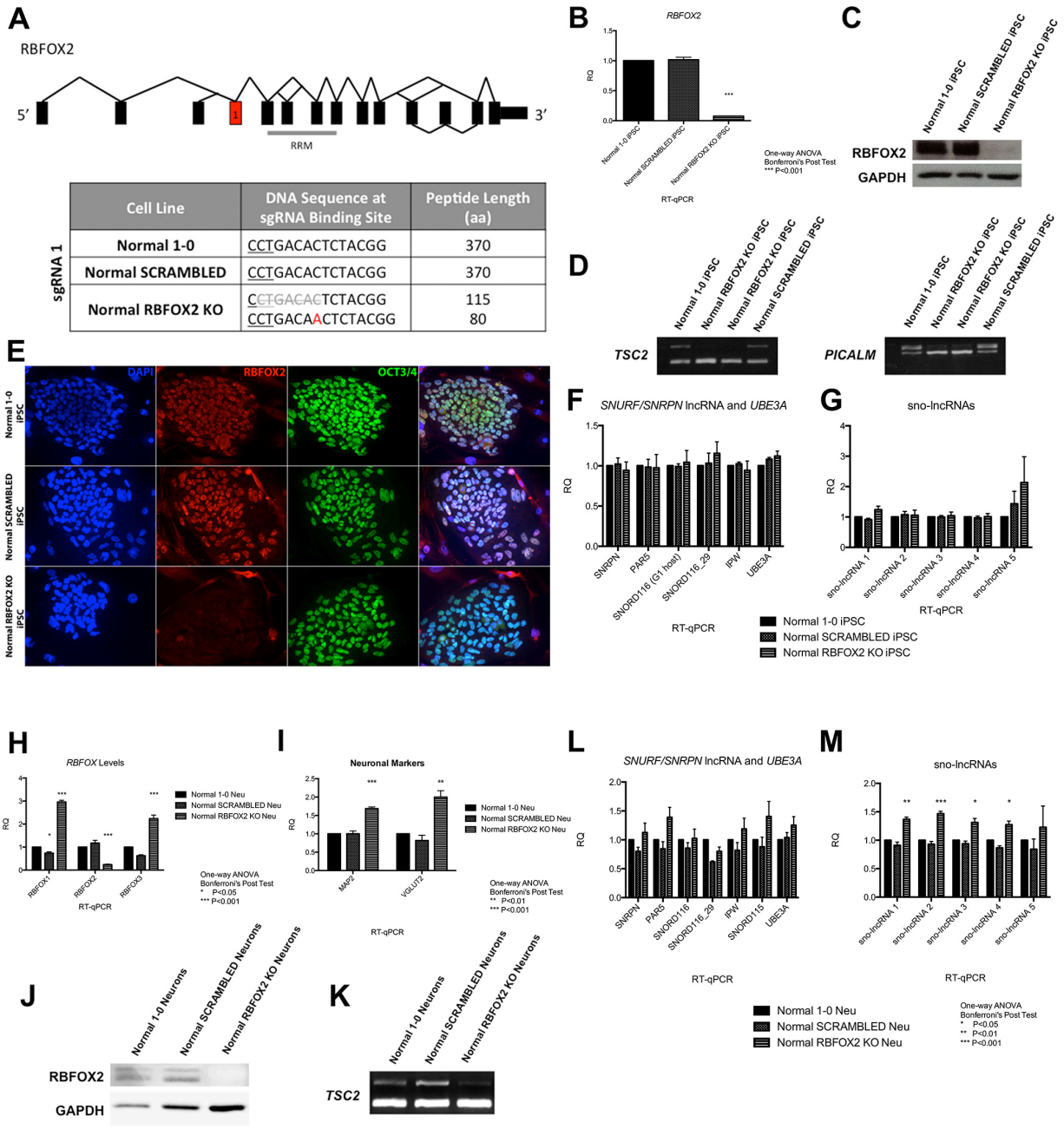

Supplementary Figure 1. Lentiviral CRISPR/Cas9-mediated RBFOX2 KO in Normal iPSCs. The expression of *SNURF/SNRPN* lncRNA was not altered in RBFOX KO AS iPSCs and iPSC-derived neurons. **A)** Schematic of *RBFOX2* splicing pattern according to alternative splicing graph from Swiss Institute of Bioinformatics on UCSC genome browser. Targeted exon is colored in red. gDNA sequencing shows frameshift indels

leading to premature stop codon in the RBFOX2 KO. **B, C, and E)** RT-qPCR, western blot, and immunocytochemistry showing *RBFOX2*/RBFOX2 expression in the RBFOX2 KO iPSCs. **D)** Splicing changes in *TSC2* and *PICALM* showing functional loss of RBFOX2. **F and G)** RT-qPCR to quantify transcripts from the *SNURF/SNRPN* lncRNA, including *SNORD116* and *sno-lncRNAs* in RBFOX2 KO iPSCs. **H)** RT-qPCR showing reduced *RBFOX2* expression in RBFOX2 KO neurons. **I)** Increased *MAP2* and *VGLUT2* expression corresponded with increased *RBFOX1* expression in H. **J)** Western blot showing loss of RBFOX2 in KO neurons. **K)** Splicing changes in *TSC2* showing functional loss of RBFOX2 in KO neurons. **L and M)** RT-qPCR to quantify transcripts from *SNURF/SNRPN* lncRNA, including *SNORD116* and *sno-lncRNAs*, in RBFOX KO neurons.

A

AS RBFOX1 KO1		
Sequence Source	Sequence	Nucleotide Indel
iPSC gDNA	CGGAATACCACGGCCC CGGAATACACGGCCC	+1, -1
Neuron gDNA	CGGAATACCACGGCCC CGGAATACACGGCCC	+1, -1
Neuron cDNA Clone 1	CGGAATACCACGGCCC	+1
Neuron cDNA Clone 2	CGGAATTACCACGGCCC	+1
Neuron cDNA Clone 3	CGGAATACCACGGCCC	+1
Neuron cDNA Clone 4	CGGAATACCACGGCCC	+1

B

AS RBFOX1 KO2		
Sequence Source	Sequence	Nucleotide Indel
iPSC gDNA	CTCAGACCGTCTCTGG	-4
Neuron gDNA	CTCAGACCGTCTCTGG AGCACAC//GA//GACACGAGCG//CTCTGG	-4, -57*
Neuron cDNA Clone 1	AGCACAC//GA//GACACGAGCG//CTCTGG	-57
Neuron cDNA Clone 2	AGCACAC//GA//GACACGAGCG//CTCTGG	-57
Neuron cDNA Clone 3	AGCACAC//GA//GACACGAGCG//CTCTGG	-57

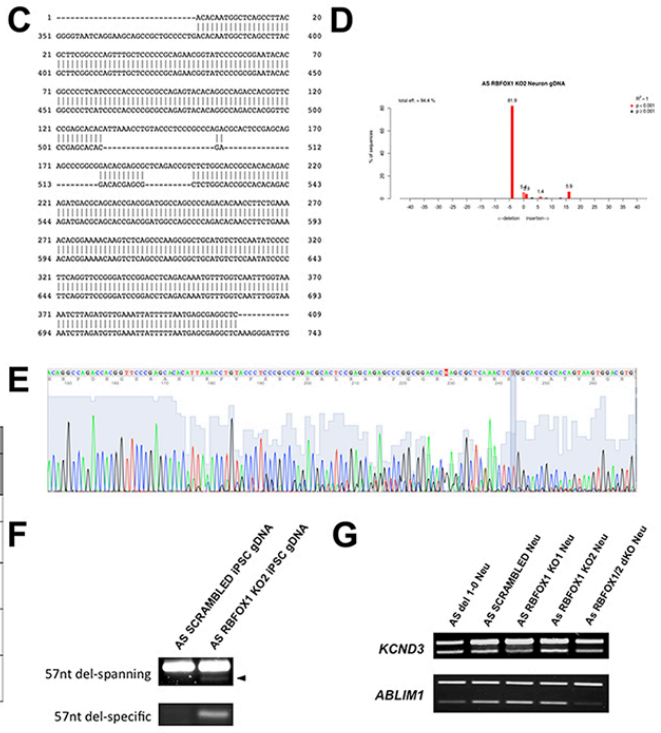

Supplementary Figure 2. Sequencing analysis for *RBFOX1* mutations in AS RBFOX1 KO iPSCs and neurons. A and B) gDNA sequencing in iPSCs and neurons as well as cDNA sequencing by pBluescript cloning of PCR products in AS RBFOX1 KO1 and KO2. **C)** Sequencing alignment between representative AS RBFOX1 KO2 pBluecript cloning product and control wild type sequence, showing a complex 57 nucleotide deletion. **D)** The 57 nucleotide deletion in C was not picked up by TIDE in AS RBFOX1 KO2 neuronal gDNA due to the software's size limitation on indels. **E)** AS RBFOX1 KO2 neuronal gDNA trace file showing mutations that can be resolved into the 57 nucleotide deletion by hand. **F)** By conventional PCR, 3% agarose gel image showed a small population of AS RBFOX1 KO2 iPSCs harbors the 57 nucleotide deletion (arrowhead), which was better detected using primers specific to the deletion. **G)** Splicing changes in *KCND3* and *ABLIM1* showing functional loss of RBFOX1 in AS

RBFOX1 KO and RBFOX1/2 dKO neurons. Differences in these spliced isoform ratio were observed in the scrambled neurons, which has lower RBFOX1 expression than the control neurons (Figure 3A).

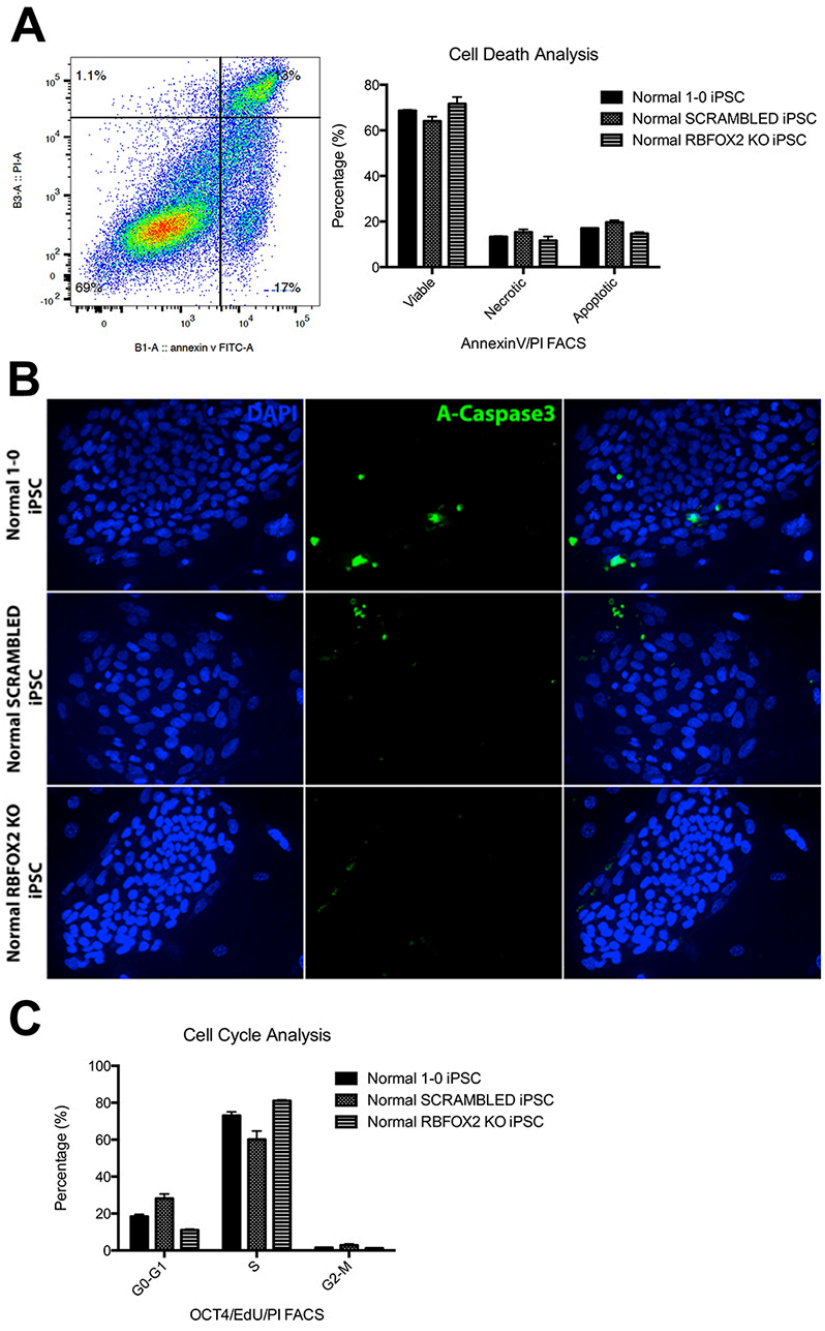

Supplementary Figure 3. Cell death and cell cycle analysis in RBFOX2 KO normal iPSCs. A) Flow cytometry analysis using Annexin V and propidium iodide, to identify viable, necrotic, or apoptotic cells. **B)** Apoptotic cells labeled with activated caspase-3 (green). **C)** Flow cytometry was used to measure cell cycle in synchronized iPSCs. Cells were labeled with EdU during S-phase, and then stained with propidium iodide.

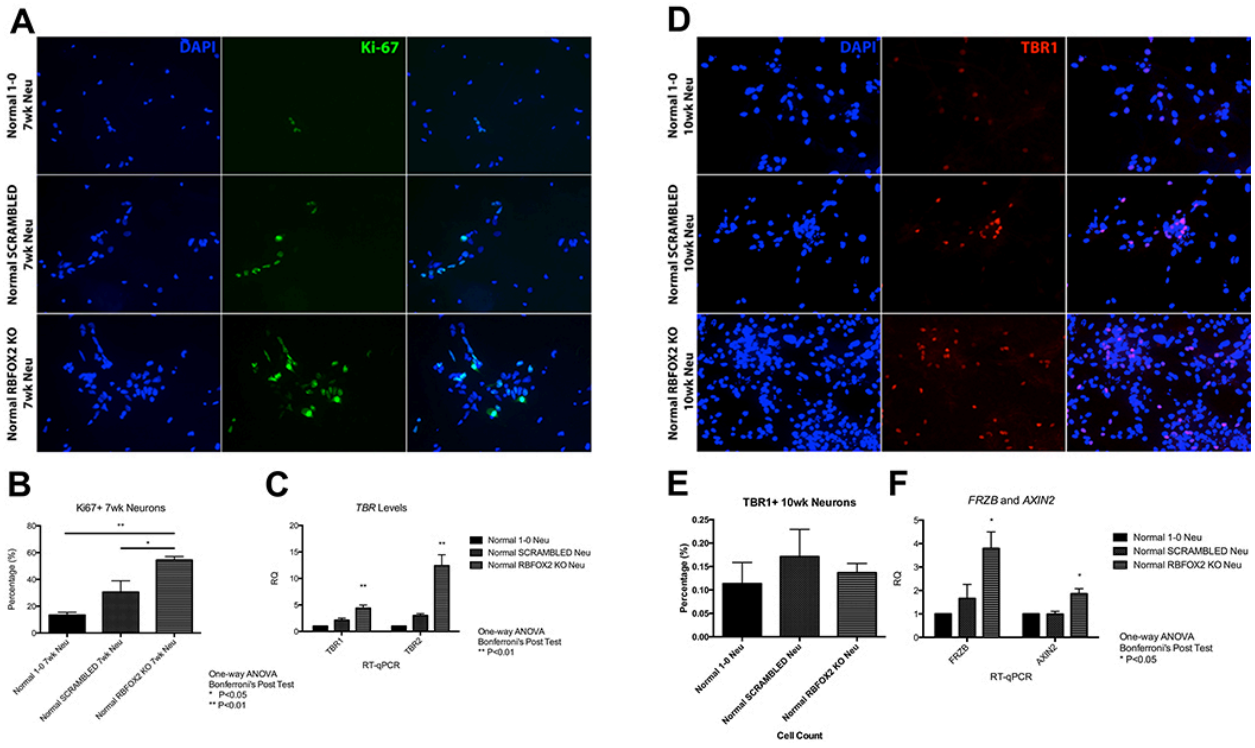

Supplementary Figure 4. 7-week-old normal RBFOX2 KO neurons showed increased proliferation and 10-week-old normal RBFOX2 KO neurons showed increased *TBR1*, *TBR2*, and *FRZB* expression. A) Proliferating cells in 7-week-old neural culture labeled with antibody against Ki67 (green). **B)** Quantification of Ki67+ cells in A. **C)** RT-qPCR showing *TBR1* and *TBR2* expression in 10-week-old RBFOX2 KO neurons. **D)** 10-week-old RBFOX2 KO neurons labeled with antibody against TBR1 (red). **E)** Quantification of TBR1+ cells in D. **F)** RT-qPCR showing *FRZB* and *AXIN2* expression in 10-week-old RBFOX2 KO neurons.

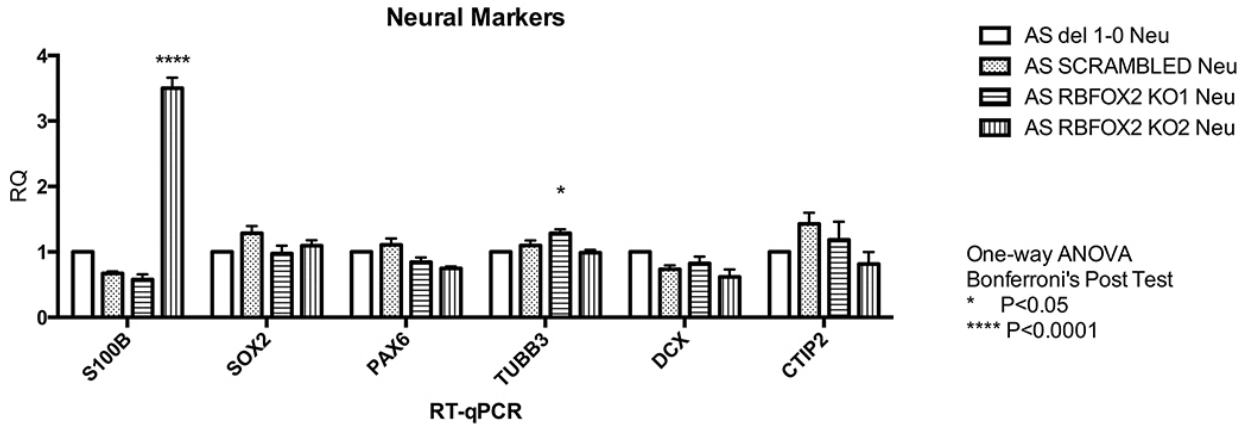

Supplementary Figure 5. RT-qPCR for neural markers in AS neurons.

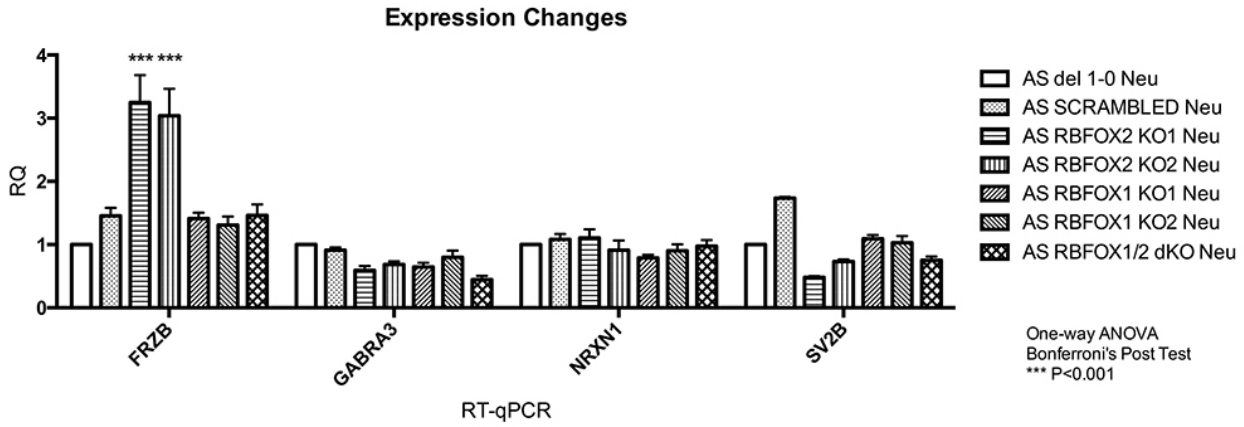

Supplementary Figure 6. RT-qPCR for genes previously shown to change in RBFOX1 knockdown human neural progenitor cells.

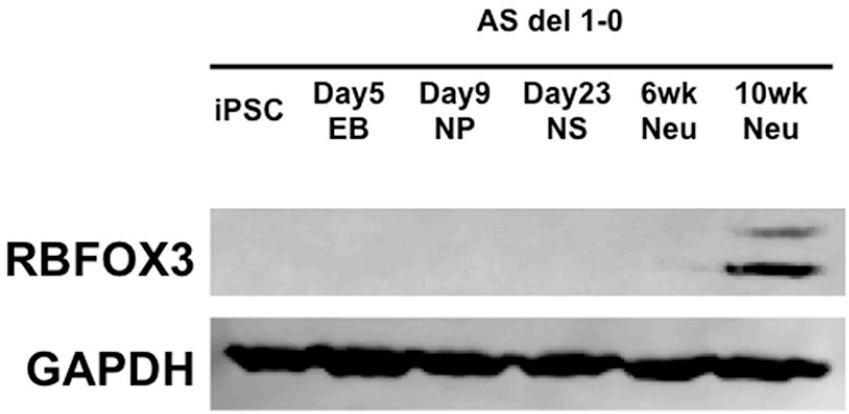

Supplementary Figure 7. Western blot showing RBFOX3 protein expression is only detectable in 10-week-old neuronal culture during neural differentiation.

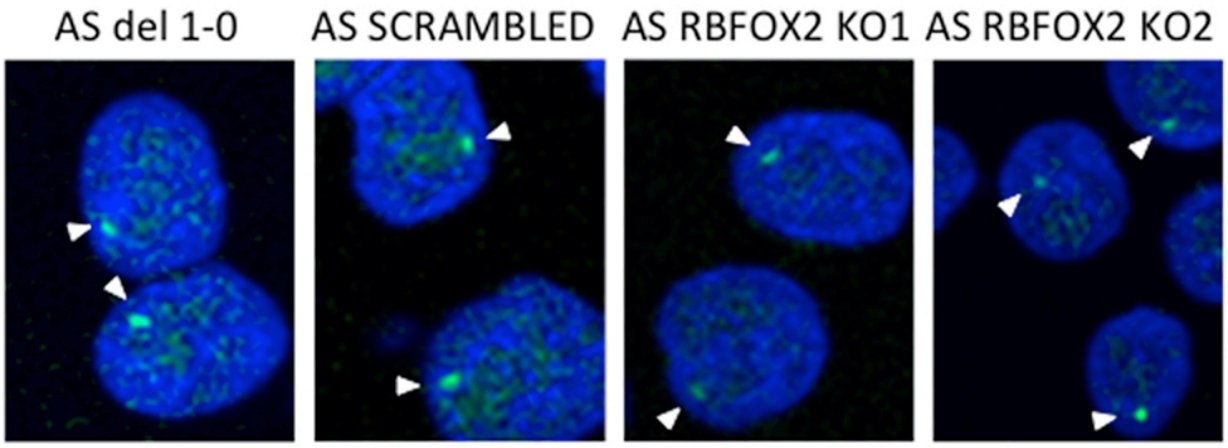

Supplementary Figure 8. RNA fluorescence in situ hybridization showing that localization of *SNORD116* transcripts (white arrow heads, labeled in green) is not altered in the absence of RBFOX2 protein.

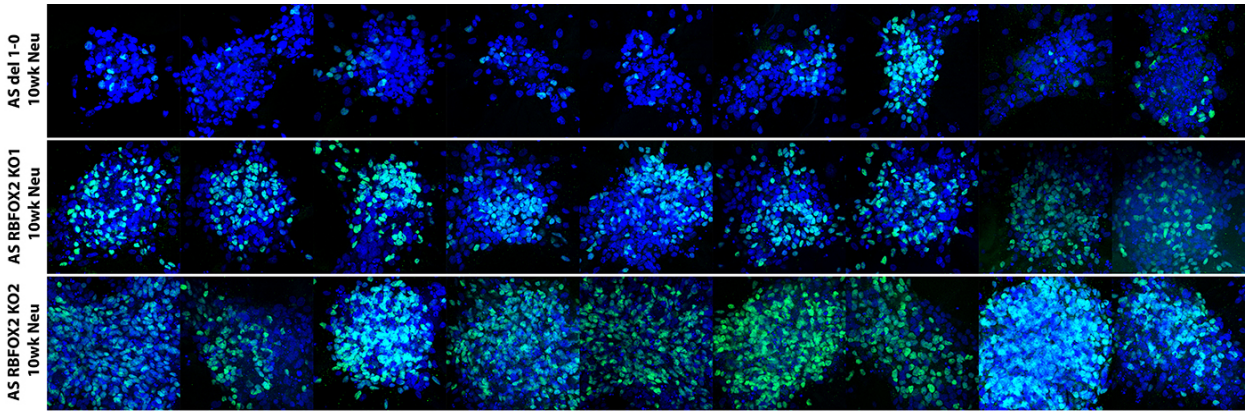

Supplementary Figure 9. Representative confocal microscopic images of TBR1^{+} cells (green) in multilayered hubs in 10-week-old neuronal culture from three independent experiments.

Supplementary Table 1. List of primers.

Primers for conventional PCR

Gene	Forward Primer	Reverse Primer	Ref.
RBFOX1	GACACAATGGCTCAGCCTTAC	CGGAACCTGAAGGGGATATT	
RBFOX2	GGTGGAAAAGAAAGCTGTGG	GTGGTGGAAATGGGATGGTA	
UBE3A-ATS	AAGGCCTGGAATCTGATCCT	CCTAGATTTTAAATAGACAATCCAAAG	(Runte et al., 2001)
PICALM	ATTCCATATCCTATCATGCCTGT	AATTGGAGTCAACCAGGTGAA	(Yeo et al., 2009)
TSC2	CGGTCCAATGTCCTCTTGTC	TCCAGGTGGAGGTTTTTCAG	(Yeo et al., 2009)
***NUMB* (exon 12)**	ATCTGCTCCGATGACCAAAC	GAGAGGCAGCACCAGAAGAT	
KCND3	AAGACCACCTCACTCATCG	TTCTTGTGGATGGGTAGTTC	
ABLIM1	CTCCATCAACTCCCCTGTGT	TAGATGGGTGGCTTTCGGTA	

Taqman RT-qPCR

Gene	Assay ID
RBFOX1	Hs01125659_m1
RBFOX2	Hs00204814_m1
RBFOX3	Hs01370653_m1
SNRPN	Hs00256090_m1
PAR5	Hs03453940_s1
SNORD116	Hs03454084_m1
SNORD116-29	Hs03300097_s1
IPW	Hs03455409_s1
SNORD115	Hs03454279_m1
UBE3A	Hs00166580_m1
SOX2	Hs01053049_s1
PAX6	Hs00240871_m1
DCX	Hs00167057_m1
TUBB3	Hs00964962_g1
CTIP2 (BCL11B)	Hs01102259_m1
S100B	Hs00902901_m1
MAP2	Hs00258900_m1
VGLUT2 (SLC17A6)	Hs00220439_m1
GAD1	Hs01065893_m1
TBR1	Hs00232429_m1
TBR2 (EOMES)	Hs00172872_m1
SV2B	Hs00208178_m1
NRXN1	Hs00985123_m1
GABRA3	Hs00968132_m1
FRZB	Hs00173503_m1
AXIN2	Hs00610344_m1

(Continued from previous page)

CLIP primers

Gene	Forward Primer	Reverse Primer
SNRPN	CCAACCTCTGGCATAAATGG	GACCTTCAGCCATCCAAAGA
PAR5	AGGTGCTTTTGCTTTGCCTA	TCTCTGAACCCCAACAGCTT
SNORD108	TGAGGTCCAGCCTTGCTAAT	CCACAATTCAAACCATGCAA
***SNRPN* (RBFOX2 cluster)**	TAATTGGCCTCTTGGGACTG	TGACCATTCCCTTCTCCTGT
SNORD116	TCATAGTGCAGCCAGGACAG	TTTTCCTTGCATTGGACACA
IPW	TCTTCTGCCTCCTGTCTCGT	TCCCATCACCACAGTGAAAA
PAR1	AGCTGCCCACACCCATATAC	GTGGGGGCTCACACATAACT
SNORD115	TGGACACATGTCCTCCTCCT	TGGGATCTCAGCATCCTCTT
UBE3A-ATS(9)	GCCTTTGGAGACAACTTCCA	AGCCCTGAATTCTCACAGAAA
UBE3A-ATS(3)	AGTCTTGGGCTTCCTTTGGT	GAGGAACCATTGCAGCTGAT
UBE3A-ATS(1)	ACTTGGGCTCTACTCGCAAA	TGGCAAGTGAGTGTGCCTAA

SYBR Green RT-qPCR

Gene	Forward Primer	Reverse Primer	Ref.
GAPDH	TACTAGCGGTTTTACGGGCG	TCGAACAGGAGGAGCAGAGAGCGA	(Cruvinel et al., 2014)
sno-lncRNA 1	CTTGGCGTATTCATGGAGGT	ACCGGCTAAGTGAGCTGAAA	(Yin et al., 2012)
sno-lncRNA 2	TGTCCTTGACTCCTGGCTCT	ATGCCAGGTGATTGGAACTC	(Yin et al., 2012)
sno-lncRNA 3	CGTGCATCCCTATGTACGTG	CAATGCTACCTGGGAGGTGT	(Yin et al., 2012)
sno-lncRNA 4	GGCCAGAGACAGGCAGATAG	GTATCTCCGCAGCTCACACA	(Yin et al., 2012)
sno-lncRNA 5	GGAACCAGGGCATAGTGAGA	TTGGATTTGGATGTTGACCA	(Yin et al., 2012)

Chapter 5

General Discussion and Future Direction

5.1 General Discussion

For rare “orphan” diseases, such as AS, PWS, and Dup 15q syndrome, current treatments are often limited to symptom management and behavioral therapies. To develop effective disease-specific treatments, it is necessary to understand the genetic causes and molecular mechanisms that lead to disease manifestation. With advances in sequencing and cytogenetic technologies, scientists have gained significant insights on disease genetic causes from patient samples, especially those carrying rare mutations. About two decades ago, scientists identified AS as a monogenic disorder caused by loss of the maternal *UBE3A* (Kishino et al., 1997). Recently, using patient samples with rare microdeletions, the PWS critical region was narrowed down to a 91 kb stretch of DNA that encodes for *SNORD116* and *IPW* (Bieth et al., 2015). Because of heterogeneity in Dup 15q disease presentation and difficulties in accurate clinical assessment, the genetic cause for Dup 15q syndrome is not as well understood. The general consensus is that maternally inherited duplication of chromosome 15q11-q13.1 leads to Dup 15q syndrome, and that additional genetic or environmental factors may contribute to variations in disease phenotype (Battaglia, 2008). Molecular mechanisms for disease manifestation can be hard to determine even for diseases with a single or few genetic cause(s), such as AS and PWS, respectively. This results from our limited knowledge on the function and/or targets of the gene products of *UBE3A*, *SNORD116*, and *IPW*. With improved molecular tools and advancement in the biology of protein and non-coding RNA, it is hopeful that we will be able to decipher the precise molecular pathway for these disorders in the foreseeable future.

AS, PWS, and Dup 15q syndrome iPSCs were useful in understanding gene regulation at chromosome 15q11-q13.1, as demonstrated in Chapter 2. Due to the fact that chromosome 15q11-q13.1 gene regulation diverges between human and mice, this was the first time we were able to study the underlying gene contributions in the most relevant tissue—human neurons. This new model system also allowed us to study chromosome 15q11-q13.1 gene expression at various developmental time points. We found that different parts of *SNURF/SNRPN* lncRNA exhibit different tissue-specificity—the more distal, the more neuron-specific (Chamberlain et al., 2010). Our observation in PWS SD iPSCs suggests the presence of a boundary element near *IPW* in non-neuronal cells that suppresses downstream *SNURF/SNRPN* lncRNA expression (Martins-Taylor et al., 2014). Moreover, chromatin structure and arrangement in neurons may play a important role in controlling gene expression at this locus, evidenced by gene expression changes in int dup(15) iPSC-derived neurons (Germain et al., 2014). In Chapter 4, we disproved our hypothesis and showed that RBFOX1 and RBFOX2 are not required for expressing or processing *SNURF/SNRPN* lncRNA by creating knockouts using CRISPR/Cas9. While this result was disappointing, we found other changes during neural differentiation in RBFOX2 knockout neurons, indicating that it may be involved in division versus proliferation decisions, glutamatergic neocortical development, and Wnt-Frizzled signaling. Finally, using gene expression as a readout, our iPSC models for AS, PWS and Dup 15q syndrome are useful tools for drug development, such as topotecan and mithramycin (Germain et al., 2014; King et al., 2013; Martins-Taylor et al., 2014).

CRISPR/Cas9 technology largely improved the efficiency and ease in human genome editing. We demonstrated the versatility of CRISPR/Cas9 as a genome-editing tool for human iPSCs. Discovery of iPSC technology to reprogram somatic cells back to a pluripotent stage revolutionized the field of disease modelling. Together, our expertise in CRISPR/Cas9 genome editing and iPSC technology holds great promise to elucidate disease mechanisms and develop therapeutic treatments for AS, PWS, and Dup 15q syndrome.

5.2 Future Direction

We would like to identify disease-relevant cellular phenotypes in AS, PWS, and Dup 15q iPSC-derived neurons. We will employ techniques like electrophysiology and microscopy to find quantifiable phenotypical changes, such as neuron excitability and neurite elaboration, respectively. To distinguish disease phenotypes from potential contributions from genetic background, it will be ideal to obtain isogenic controls for each cell line. The isogenic controls will also be useful for transcriptome analysis to identify downstream gene expression changes that may contribute to disease manifestation. Quality control for iPSC-derived neurons may be required to minimize batch-to-batch differences that cannot be attributed to disease genotype. Our current drug screening relies on gene expression changes that cannot be assessed quickly and easily and, therefore, is limited in terms of scope. With reliable and quantifiable cellular phenotypes, we will be able to adapt our iPSC-derived neurons for high throughput drug screening at a much larger scale.

Our current neural differentiation protocols produce cortical neurons. Since clinical features in PWS patients suggest a dysfunction in the hypothalamic system (Swaab, 1997), it may be important to establish a neural differentiation protocol that generates hypothalamic neurons in our lab. Recently, two separate groups published hypothalamic neural differentiation protocols (Merkle et al., 2015; Wang et al., 2015), which would be helpful in this endeavor. It will be interesting to see if PWS-relevant phenotypes, such as perturbation in the oxytocin pathway, can be observed in PWS iPSC-derived hypothalamic neurons (Grinevich et al., 2014).

As discussed previously in Chapter 3, we would like to re-design the targeting construct and sgRNA to generate a new UBE3A-GFP reporter cell line using AS iPSCs. Addition to changes proposed previously, we can utilize a split GFP-tagging system to improve protein stability by attaching a 15 aa GFP subunit 11 to UBE3A protein and expressing subunit 1-10 separately from the *AAVS1* safe harbor locus (Cabantous and Waldo, 2006). When expressed, GFP subunit 11 and subunit 1-10 associate spontaneously to form fluorescent GFP. Moreover, to improve signal detection, fluorescence intensity can be amplified by tagging UBE3A protein with up to 7 copies of GFP subunit 11. This UBE3A-GFP reporter cell line will be useful for determining the developmental time point of paternal *UBE3A* silencing as well as UBE3A protein localization during human neurodevelopment. It can also be used for fluorescence-based high throughput drug screening to identify chemicals or small molecules that re-activate paternal *UBE3A* in mature neurons. Last but not least, a remaining task in the AS field is to understand UBE3A protein function. Robust assay development assessing

disease-relevant UBE3A targets, such as Ephexin5 and GAT1, could be instrumental for drug development.

Appendix A. Primers used in Chapter 3 for UBE3A-GFP reporter. Primer sets indicate in the brackets correspond to Figure 3.1B.

Screening Purpose	Forward Primer	Reverse Primer	Product Size (bp)
HotSHOT DNA			
GFP$^+$	tSNRP GFP 1F ACGTAAACGGCCACAAGTTC	tSNRP GFP 1R GTCCTCCTTGAAGTCGATGC	338
Neo$^+$	Neo F TGAATGAACTGCAGGACGAG	Neo R ATACTTTCTCGGCAGGAGCA	171
HotSHOT DNA (Cre-Lox Recombination)			
WT [A; B]	Ube3aGFP_Cre_Fa2 TATGGGGCTCACATTGGTTT	Ube3aGFP_Cre_Rb2 GAAACACTGCTGGCAATATGA	194
Targeted Neo$^-$ [A; B] [A; D]	Ube3aGFP_Cre_Fa2 TATGGGGCTCACATTGGTTT	Ube3aGFP_Cre_Rb2 GAAACACTGCTGGCAATATGA Ube3aGFP_Cre_Rd TCGAGGGACCTAATAACTTCG	285 198
Targeted Neo$^+$ [A; C]	Ube3aGFP_Cre_Fa CCTTGCATTCCTCGTCACAT	Ube3aGFP_Cre_Rc TAAAGCGCATGCTCCAGACT	472
gDNA			
5' Homologous Recombination [5' F; 5' R]	UBE3A_GFP_5 F2 (1° PCR) CTGCCTCTACTTAAACGTACAGAAAA UBE3A_GFP_5 F1 (2° PCR) AGAACTCAAACTAACATAAGTGTCATTAAAA	UBE3A_GFP_5 R AAGTTATATTAAGGGTTATTGAATATGATCG	1552 1266
3' Homologous Recombination [3' F; 3' R]	UBE3A_GFP_3 F AACTACAACAGCCACAACGTCTATATC	UBE3A_GFP_3 R1 (1° PCR) GATCTACAGTAATCAGTTAAAACAATCAGTC UBE3A_GFP_3 R2 (2° PCR) TCTCACCTTAGTTAAAAATACATAATCCTTT	1785 1681
WT *UBE3A* [WT F; WT R]	UBE3A_intron12_F1 (1° PCR) GGCAACTTGGTAGTTACACAACA UBE3A_intron12_F2 (2° PCR) CCCATGACTTACAGTTTTCCTG	CRISPR_cut R TTTGGCATACGTGATGGCCT	269 150
UBE3A-GFP Sequencing	UBE3A_intron12_F1 (PCR) GGCAACTTGGTAGTTACACAACA UBE3A_intron12_F2 (Seq primer) CCCATGACTTACAGTTTTCCTG	tSNRP GFP 1R GTCCTCCTTGAAGTCGATGC	650
cDNA			
WT *UBE3A* expression	UBE3A ex12 F ACCTGTGGGAGGACTAGGAA	UBE3A ex13 R GGCATACGTGATGGCCTTCA	163
UBE3A-GFP expression	UBE3A ex12 F ACCTGTGGGAGGACTAGGAA	UBE3A_GFP cDNA R CTGAACTTGTGGCCGTTTAC	231

References

Amos-Landgraf, J.M., Ji, Y., Gottlieb, W., Depinet, T., Wandstrat, A.E., Cassidy, S.B., Driscoll, D.J., Rogan, P.K., Schwartz, S., and Nicholls, R.D. (1999). Chromosome breakage in the Prader-Willi and Angelman syndromes involves recombination between large, transcribed repeats at proximal and distal breakpoints. Am J Hum Genet *65*, 370-386.

Anderlid, B.M., Lundin, J., Malmgren, H., Lehtihet, M., and Nordgren, A. (2014). Small mosaic deletion encompassing the snoRNAs and SNURF-SNRPN results in an atypical Prader-Willi syndrome phenotype. Am J Med Genet A *164A*, 425-431.

Battaglia, A. (2005). The inv dup(15) or idic(15) syndrome: a clinically recognisable neurogenetic disorder. Brain Dev *27*, 365-369.

Battaglia, A. (2008). The inv dup (15) or idic (15) syndrome (Tetrasomy 15q). Orphanet J Rare Dis *3*, 30.

Bieth, E., Eddiry, S., Gaston, V., Lorenzini, F., Buffet, A., Conte Auriol, F., Molinas, C., Cailley, D., Rooryck, C., Arveiler, B.*, et al.* (2015). Highly restricted deletion of the SNORD116 region is implicated in Prader-Willi Syndrome. Eur J Hum Genet *23*, 252-255.

Bill, B.R., Lowe, J.K., Dybuncio, C.T., and Fogel, B.L. (2013). Orchestration of neurodevelopmental programs by RBFOX1: implications for autism spectrum disorder. International review of neurobiology *113*, 251-267.

Bischof, J.M., Stewart, C.L., and Wevrick, R. (2007). Inactivation of the mouse Magel2 gene results in growth abnormalities similar to Prader-Willi syndrome. Hum Mol Genet *16*, 2713-2719.

Brinkman, E.K., Chen, T., Amendola, M., and van Steensel, B. (2014). Easy quantitative assessment of genome editing by sequence trace decomposition. Nucleic Acids Res *42*, e168.

Bruce, S., Hannula-Jouppi, K., Lindgren, C.M., Lipsanen-Nyman, M., and Kere, J. (2008). Restriction site-specific methylation studies of imprinted genes with quantitative real-time PCR. Clin Chem *54*, 491-499.

Buiting, K., Gross, S., Lich, C., Gillessen-Kaesbach, G., el-Maarri, O., and Horsthemke, B. (2003). Epimutations in Prader-Willi and Angelman syndromes: a molecular study of 136 patients with an imprinting defect. Am J Hum Genet *72*, 571-577.

Buiting, K., Lich, C., Cottrell, S., Barnicoat, A., and Horsthemke, B. (1999). A 5-kb imprinting center deletion in a family with Angelman syndrome reduces the shortest region of deletion overlap to 880 bp. Hum Genet *105*, 665-666.

Buiting, K., Saitoh, S., Gross, S., Dittrich, B., Schwartz, S., Nicholls, R.D., and Horsthemke, B. (1995). Inherited microdeletions in the Angelman and Prader-Willi syndromes define an imprinting centre on human chromosome 15. Nat Genet *9*, 395-400.

Cabantous, S., and Waldo, G.S. (2006). In vivo and in vitro protein solubility assays using split GFP. Nature methods *3*, 845-854.

Cadigan, K.M., and Liu, Y.I. (2006). Wnt signaling: complexity at the surface. Journal of cell science *119*, 395-402.

Cassidy, S.B., and Driscoll, D.J. (2009). Prader-Willi syndrome. Eur J Hum Genet *17*, 3-13.

Chamberlain, S.J., and Brannan, C.I. (2001). The Prader-Willi syndrome imprinting center activates the paternally expressed murine Ube3a antisense transcript but represses paternal Ube3a. Genomics *73*, 316-322.

Chamberlain, S.J., Chen, P.F., Ng, K.Y., Bourgois-Rocha, F., Lemtiri-Chlieh, F., Levine, E.S., and Lalande, M. (2010). Induced pluripotent stem cell models of the genomic imprinting disorders Angelman and Prader-Willi syndromes. Proc Natl Acad Sci U S A *107*, 17668-17673.

Chamberlain, S.J., Germain, N.D., Chen, P.F., Hsiao, J.S., and Glatt-Deeley, H. (2016). Modeling Genomic Imprinting Disorders Using Induced Pluripotent Stem Cells. Methods Mol Biol *1353*, 45-64.

Chamberlain, S.J., and Lalande, M. (2010). Neurodevelopmental disorders involving genomic imprinting at human chromosome 15q11-q13. Neurobiol Dis *39*, 13-20.

Chamberlain, S.J., Li, X.J., and Lalande, M. (2008). Induced pluripotent stem (iPS) cells as in vitro models of human neurogenetic disorders. Neurogenetics *9*, 227-235.

Chomczynski, P., and Sacchi, N. (1987). Single-step method of RNA isolation by acid guanidinium thiocyanate-phenol-chloroform extraction. Anal Biochem *162*, 156-159.

Chotalia, M., Smallwood, S.A., Ruf, N., Dawson, C., Lucifero, D., Frontera, M., James, K., Dean, W., and Kelsey, G. (2009). Transcription is required for establishment of germline methylation marks at imprinted genes. Genes Dev *23*, 105-117.

Christian, S.L., Brune, C.W., Sudi, J., Kumar, R.A., Liu, S., Karamohamed, S., Badner, J.A., Matsui, S., Conroy, J., McQuaid, D.*, et al.* (2008). Novel submicroscopic chromosomal abnormalities detected in autism spectrum disorder. Biol Psychiatry *63*, 1111-1117.

Colman, A., and Dreesen, O. (2009). Pluripotent stem cells and disease modeling. Cell Stem Cell *5*, 244-247.

Cong, L., Ran, F.A., Cox, D., Lin, S., Barretto, R., Habib, N., Hsu, P.D., Wu, X., Jiang, W., Marraffini, L.A.*, et al.* (2013). Multiplex genome engineering using CRISPR/Cas systems. Science *339*, 819-823.

Cook, E.H., Jr., Courchesne, R.Y., Cox, N.J., Lord, C., Gonen, D., Guter, S.J., Lincoln, A., Nix, K., Haas, R., Leventhal, B.L.*, et al.* (1998). Linkage-disequilibrium mapping of autistic disorder, with 15q11-13 markers. Am J Hum Genet *62*, 1077-1083.

Cook, E.H., Jr., Lindgren, V., Leventhal, B.L., Courchesne, R., Lincoln, A., Shulman, C., Lord, C., and Courchesne, E. (1997). Autism or atypical autism in maternally but not paternally derived proximal 15q duplication. Am J Hum Genet *60*, 928-934.

Cooper, E.M., Hudson, A.W., Amos, J., Wagstaff, J., and Howley, P.M. (2004). Biochemical analysis of Angelman syndrome-associated mutations in the E3 ubiquitin ligase E6-associated protein. J Biol Chem *279*, 41208-41217.

Cruvinel, E., Budinetz, T., Germain, N., Chamberlain, S., Lalande, M., and Martins-Taylor, K. (2014). Reactivation of maternal SNORD116 cluster via SETDB1 knockdown in Prader-Willi syndrome iPSCs. Hum Mol Genet *23*, 4674-4685.

Davies, S.J., and Hughes, H.E. (1993). Imprinting in Albright Hereditary Osteodystrophy. Journal of Medical Genetics *30*, 101-103.

Derti, A., Garrett-Engele, P., Macisaac, K.D., Stevens, R.C., Sriram, S., Chen, R., Rohl, C.A., Johnson, J.M., and Babak, T. (2012). A quantitative atlas of polyadenylation in five mammals. Genome Res *22*, 1173-1183.

Dindot, S.V., Antalffy, B.A., Bhattacharjee, M.B., and Beaudet, A.L. (2008). The Angelman syndrome ubiquitin ligase localizes to the synapse and nucleus, and maternal deficiency results in abnormal dendritic spine morphology. Hum Mol Genet *17*, 111-118.

Dittrich, B., Buiting, K., Korn, B., Rickard, S., Buxton, J., Saitoh, S., Nicholls, R.D., Poustka, A., Winterpacht, A., Zabel, B.*, et al.* (1996). Imprint switching on human chromosome 15 may involve alternative transcripts of the SNRPN gene. Nat Genet *14*, 163-170.

Egawa, K., Kitagawa, K., Inoue, K., Takayama, M., Takayama, C., Saitoh, S., Kishino, T., Kitagawa, M., and Fukuda, A. (2012). Decreased tonic inhibition in cerebellar granule cells causes motor dysfunction in a mouse model of Angelman syndrome. Sci Transl Med *4*, 163ra157.

El-Maarri, O., Buiting, K., Peery, E.G., Kroisel, P.M., Balaban, B., Wagner, K., Urman, B., Heyd, J., Lich, C., Brannan, C.I.*, et al.* (2001). Maternal methylation imprints on

human chromosome 15 are established during or after fertilization. Nat Genet *27*, 341-344.

Englund, C., Fink, A., Lau, C., Pham, D., Daza, R.A., Bulfone, A., Kowalczyk, T., and Hevner, R.F. (2005). Pax6, Tbr2, and Tbr1 are expressed sequentially by radial glia, intermediate progenitor cells, and postmitotic neurons in developing neocortex. J Neurosci *25*, 247-251.

Ferguson-Smith, A.C. (1996). Imprinting moves to the centre. Nat Genet *14*, 119-121.

Ferrandiz, C., and Sessions, A. (2008). Preparation and hydrolysis of digoxygenin-labeled probes for in situ hybridization of plant tissues. CSH Protoc *2008*, pdb prot4942.

Filonova, I., Trotter, J.H., Banko, J.L., and Weeber, E.J. (2014). Activity-dependent changes in MAPK activation in the Angelman Syndrome mouse model. Learning & memory *21*, 98-104.

Fogel, B.L., Wexler, E., Wahnich, A., Friedrich, T., Vijayendran, C., Gao, F., Parikshak, N., Konopka, G., and Geschwind, D.H. (2012). RBFOX1 regulates both splicing and transcriptional networks in human neuronal development. Hum Mol Genet *21*, 4171-4186.

Gehman, L.T., Meera, P., Stoilov, P., Shiue, L., O'Brien, J.E., Meisler, M.H., Ares, M., Jr., Otis, T.S., and Black, D.L. (2012). The splicing regulator Rbfox2 is required for both cerebellar development and mature motor function. Genes Dev *26*, 445-460.

Gehman, L.T., Stoilov, P., Maguire, J., Damianov, A., Lin, C.H., Shiue, L., Ares, M., Jr., Mody, I., and Black, D.L. (2011). The splicing regulator Rbfox1 (A2BP1) controls neuronal excitation in the mammalian brain. Nat Genet *43*, 706-711.

Germain, N.D., Banda, E.C., Becker, S., Naegele, J.R., and Grabel, L.B. (2013). Derivation and isolation of NKX2.1-positive basal forebrain progenitors from human embryonic stem cells. Stem Cells Dev *22*, 1477-1489.

Germain, N.D., Chen, P.F., Plocik, A.M., Glatt-Deeley, H., Brown, J., Fink, J.J., Bolduc, K.A., Robinson, T.M., Levine, E.S., Reiter, L.T.*, et al.* (2014). Gene expression analysis of human induced pluripotent stem cell-derived neurons carrying copy number variants of chromosome 15q11-q13.1. Molecular autism *5*, 44.

Greer, P.L., Hanayama, R., Bloodgood, B.L., Mardinly, A.R., Lipton, D.M., Flavell, S.W., Kim, T.K., Griffith, E.C., Waldon, Z., Maehr, R.*, et al.* (2010). The Angelman Syndrome protein Ube3A regulates synapse development by ubiquitinating arc. Cell *140*, 704-716.

Gregg, C., Zhang, J., Weissbourd, B., Luo, S., Schroth, G.P., Haig, D., and Dulac, C. (2010). High-resolution analysis of parent-of-origin allelic expression in the mouse brain. Science *329*, 643-648.

Grinevich, V., Desarmenien, M.G., Chini, B., Tauber, M., and Muscatelli, F. (2014). Ontogenesis of oxytocin pathways in the mammalian brain: late maturation and psychosocial disorders. Frontiers in neuroanatomy *8*, 164.

Harterink, M., Kim, D.H., Middelkoop, T.C., Doan, T.D., van Oudenaarden, A., and Korswagen, H.C. (2011). Neuroblast migration along the anteroposterior axis of C. elegans is controlled by opposing gradients of Wnts and a secreted Frizzled-related protein. Development *138*, 2915-2924.

Henckel, A., and Arnaud, P. (2010). Genome-wide identification of new imprinted genes. Briefings in functional genomics *9*, 304-314.

Hilliard, M.A., and Bargmann, C.I. (2006). Wnt signals and frizzled activity orient anterior-posterior axon outgrowth in C. elegans. Developmental cell *10*, 379-390.

Hogart, A., Patzel, K.A., and LaSalle, J.M. (2008). Gender influences monoallelic expression of ATP10A in human brain. Hum Genet *124*, 235-242.

Huang, H.S., Allen, J.A., Mabb, A.M., King, I.F., Miriyala, J., Taylor-Blake, B., Sciaky, N., Dutton, J.W., Jr., Lee, H.M., Chen, X.*, et al.* (2012). Topoisomerase inhibitors unsilence the dormant allele of Ube3a in neurons. Nature *481*, 185-189.

Huang, L., Kinnucan, E., Wang, G., Beaudenon, S., Howley, P.M., Huibregtse, J.M., and Pavletich, N.P. (1999). Structure of an E6AP-UbcH7 complex: insights into ubiquitination by the E2-E3 enzyme cascade. Science *286*, 1321-1326.

Jacob, K.J., Robinson, W.P., and Lefebvre, L. (2013). Beckwith-Wiedemann and Silver-Russell syndromes: opposite developmental imbalances in imprinted regulators of placental function and embryonic growth. Clinical genetics *84*, 326-334.

Jiang, Y.H., Armstrong, D., Albrecht, U., Atkins, C.M., Noebels, J.L., Eichele, G., Sweatt, J.D., and Beaudet, A.L. (1998). Mutation of the Angelman ubiquitin ligase in mice causes increased cytoplasmic p53 and deficits of contextual learning and long-term potentiation. Neuron *21*, 799-811.

Johnstone, K.A., DuBose, A.J., Futtner, C.R., Elmore, M.D., Brannan, C.I., and Resnick, J.L. (2006). A human imprinting centre demonstrates conserved acquisition but diverged maintenance of imprinting in a mouse model for Angelman syndrome imprinting defects. Hum Mol Genet *15*, 393-404.

Judson, M.C., Sosa-Pagan, J.O., Del Cid, W.A., Han, J.E., and Philpot, B.D. (2014). Allelic specificity of Ube3a expression in the mouse brain during postnatal development. J Comp Neurol *522*, 1874-1896.

Kaphzan, H., Buffington, S.A., Ramaraj, A.B., Lingrel, J.B., Rasband, M.N., Santini, E., and Klann, E. (2013). Genetic reduction of the alpha1 subunit of Na/K-ATPase corrects multiple hippocampal phenotypes in Angelman syndrome. Cell reports *4*, 405-412.

Kelsey, G., and Bartolomei, M.S. (2012). Imprinted genes ... and the number is? PLoS genetics *8*, e1002601.

Khosla, S., Mendiratta, G., and Brahmachari, V. (2006). Genomic imprinting in the mealybugs. Cytogenet Genome Res *113*, 41-52.

Kim, K.K., Adelstein, R.S., and Kawamoto, S. (2009). Identification of neuronal nuclei (NeuN) as Fox-3, a new member of the Fox-1 gene family of splicing factors. J Biol Chem *284*, 31052-31061.

Kim, K.K., Kim, Y.C., Adelstein, R.S., and Kawamoto, S. (2010). Fox-3 and PSF interact to activate neural cell-specific alternative splicing. Nucleic Acids Res.

King, I.F., Yandava, C.N., Mabb, A.M., Hsiao, J.S., Huang, H.S., Pearson, B.L., Calabrese, J.M., Starmer, J., Parker, J.S., Magnuson, T.*, et al.* (2013). Topoisomerases facilitate transcription of long genes linked to autism. Nature *501*, 58-62.

Kishino, T. (2006). Imprinting in neurons. Cytogenet Genome Res *113*, 209-214.

Kishino, T., Lalande, M., and Wagstaff, J. (1997). UBE3A/E6-AP mutations cause Angelman syndrome. Nat Genet *15*, 70-73.

Kishino, T., and Wagstaff, J. (1998). Genomic organization of the UBE3A/E6-AP gene and related pseudogenes. Genomics *47*, 101-107.

Koressaar, T., and Remm, M. (2007). Enhancements and modifications of primer design program Primer3. Bioinformatics *23*, 1289-1291.

Kuhnle, S., Mothes, B., Matentzoglu, K., and Scheffner, M. (2013). Role of the ubiquitin ligase E6AP/UBE3A in controlling levels of the synaptic protein Arc. Proc Natl Acad Sci U S A *110*, 8888-8893.

Kuroyanagi, H. (2009). Fox-1 family of RNA-binding proteins. Cell Mol Life Sci *66*, 3895-3907.

Lalande, M., and Calciano, M.A. (2007). Molecular epigenetics of Angelman syndrome. Cell Mol Life Sci *64*, 947-960.

Landers, M., Bancescu, D.L., Le Meur, E., Rougeulle, C., Glatt-Deeley, H., Brannan, C., Muscatelli, F., and Lalande, M. (2004). Regulation of the large (approximately 1000 kb) imprinted murine Ube3a antisense transcript by alternative exons upstream of Snurf/Snrpn. Nucleic Acids Res *32*, 3480-3492.

Leyns, L., Bouwmeester, T., Kim, S.H., Piccolo, S., and De Robertis, E.M. (1997). Frzb-1 is a secreted antagonist of Wnt signaling expressed in the Spemann organizer. Cell *88*, 747-756.

Li, X.J., Hu, B.Y., Jones, S.A., Zhang, Y.S., Lavaute, T., Du, Z.W., and Zhang, S.C. (2008). Directed differentiation of ventral spinal progenitors and motor neurons from human embryonic stem cells by small molecules. Stem Cells *26*, 886-893.

Lossie, A.C., Whitney, M.M., Amidon, D., Dong, H.J., Chen, P., Theriaque, D., Hutson, A., Nicholls, R.D., Zori, R.T., Williams, C.A.*, et al.* (2001). Distinct phenotypes distinguish the molecular classes of Angelman syndrome. J Med Genet *38*, 834-845.

Lu, W., Yamamoto, V., Ortega, B., and Baltimore, D. (2004). Mammalian Ryk is a Wnt coreceptor required for stimulation of neurite outgrowth. Cell *119*, 97-108.

Lu, Y., Xu, W., Ji, J., Feng, D., Sourbier, C., Yang, Y., Qu, J., Zeng, Z., Wang, C., Chang, X.*, et al.* (2015). Alternative splicing of the cell fate determinant Numb in hepatocellular carcinoma. Hepatology *62*, 1122-1131.

Lustig, B., Jerchow, B., Sachs, M., Weiler, S., Pietsch, T., Karsten, U., van de Wetering, M., Clevers, H., Schlag, P.M., Birchmeier, W.*, et al.* (2002). Negative feedback loop of Wnt signaling through upregulation of conductin/axin2 in colorectal and liver tumors. Mol Cell Biol *22*, 1184-1193.

Mabb, A.M., Je, H.S., Wall, M.J., Robinson, C.G., Larsen, R.S., Qiang, Y., Correa, S.A., and Ehlers, M.D. (2014). Triad3A regulates synaptic strength by ubiquitination of Arc. Neuron *82*, 1299-1316.

Mack, A.A., Kroboth, S., Rajesh, D., and Wang, W.B. (2011). Generation of induced pluripotent stem cells from CD34+ cells across blood drawn from multiple donors with non-integrating episomal vectors. PLoS One *6*, e27956.

Makedonski, K., Abuhatzira, L., Kaufman, Y., Razin, A., and Shemer, R. (2005). MeCP2 deficiency in Rett syndrome causes epigenetic aberrations at the PWS/AS imprinting center that affects UBE3A expression. Hum Mol Genet *14*, 1049-1058.

Mandel-Brehm, C., Salogiannis, J., Dhamne, S.C., Rotenberg, A., and Greenberg, M.E. (2015). Seizure-like activity in a juvenile Angelman syndrome mouse model is attenuated by reducing Arc expression. Proc Natl Acad Sci U S A *112*, 5129-5134.

Margolis, S.S., Salogiannis, J., Lipton, D.M., Mandel-Brehm, C., Wills, Z.P., Mardinly, A.R., Hu, L., Greer, P.L., Bikoff, J.B., Ho, H.Y.*, et al.* (2010). EphB-mediated degradation of the RhoA GEF Ephexin5 relieves a developmental brake on excitatory synapse formation. Cell *143*, 442-455.

Martins-Taylor, K., Hsiao, J.S., Chen, P.F., Glatt-Deeley, H., De Smith, A.J., Blakemore, A.I., Lalande, M., and Chamberlain, S.J. (2014). Imprinted expression of UBE3A in non-neuronal cells from a Prader-Willi syndrome patient with an atypical deletion. Hum Mol Genet *23*, 2364-2373.

Meng, L., Ward, A.J., Chun, S., Bennett, C.F., Beaudet, A.L., and Rigo, F. (2015). Towards a therapy for Angelman syndrome by targeting a long non-coding RNA. Nature *518*, 409-412.

Mercer, R.E., and Wevrick, R. (2009). Loss of magel2, a candidate gene for features of Prader-Willi syndrome, impairs reproductive function in mice. PLoS One *4*, e4291.

Merkle, F.T., Maroof, A., Wataya, T., Sasai, Y., Studer, L., Eggan, K., and Schier, A.F. (2015). Generation of neuropeptidergic hypothalamic neurons from human pluripotent stem cells. Development *142*, 633-643.

Miao, S., Chen, R., Ye, J., Tan, G.H., Li, S., Zhang, J., Jiang, Y.H., and Xiong, Z.Q. (2013). The Angelman syndrome protein Ube3a is required for polarized dendrite morphogenesis in pyramidal neurons. J Neurosci *33*, 327-333.

Nakabayashi, K., Bentley, L., Hitchins, M.P., Mitsuya, K., Meguro, M., Minagawa, S., Bamforth, J.S., Stanier, P., Preece, M., Weksberg, R.*, et al.* (2002). Identification and characterization of an imprinted antisense RNA (MESTIT1) in the human MEST locus on chromosome 7q32. Hum Mol Genet *11*, 1743-1756.

Nakahata, S., and Kawamoto, S. (2005). Tissue-dependent isoforms of mammalian Fox-1 homologs are associated with tissue-specific splicing activities. Nucleic Acids Res *33*, 2078-2089.

Nawaz, Z., Lonard, D.M., Smith, C.L., Lev-Lehman, E., Tsai, S.Y., Tsai, M.J., and O'Malley, B.W. (1999). The Angelman syndrome-associated protein, E6-AP, is a coactivator for the nuclear hormone receptor superfamily. Mol Cell Biol *19*, 1182-1189.

Oakes, C.C., La Salle, S., Robaire, B., and Trasler, J.M. (2006). Evaluation of a quantitative DNA methylation analysis technique using methylation-sensitive/dependent restriction enzymes and real-time PCR. Epigenetics *1*, 146-152.

Pan, C.L., Howell, J.E., Clark, S.G., Hilliard, M., Cordes, S., Bargmann, C.I., and Garriga, G. (2006). Multiple Wnts and frizzled receptors regulate anteriorly directed cell and growth cone migrations in Caenorhabditis elegans. Developmental cell *10*, 367-377.

Pankratz, M.T., Li, X.J., Lavaute, T.M., Lyons, E.A., Chen, X., and Zhang, S.C. (2007). Directed neural differentiation of human embryonic stem cells via an obligated primitive anterior stage. Stem Cells *25*, 1511-1520.

Perrier, A.L., Tabar, V., Barberi, T., Rubio, M.E., Bruses, J., Topf, N., Harrison, N.L., and Studer, L. (2004). Derivation of midbrain dopamine neurons from human embryonic stem cells. Proc Natl Acad Sci U S A *101*, 12543-12548.

Pick, M., Stelzer, Y., Bar-Nur, O., Mayshar, Y., Eden, A., and Benvenisty, N. (2009). Clone- and gene-specific aberrations of parental imprinting in human induced pluripotent stem cells. Stem Cells *27*, 2686-2690.

Reis, A., Dittrich, B., Greger, V., Buiting, K., Lalande, M., Gillessen-Kaesbach, G., Anvret, M., and Horsthemke, B. (1994). Imprinting mutations suggested by abnormal DNA methylation patterns in familial Angelman and Prader-Willi syndromes. Am J Hum Genet *54*, 741-747.

Reiter, L.T., Seagroves, T.N., Bowers, M., and Bier, E. (2006). Expression of the Rho-GEF Pbl/ECT2 is regulated by the UBE3A E3 ubiquitin ligase. Hum Mol Genet *15*, 2825-2835.

Rodriguez-Jato, S., Nicholls, R.D., Driscoll, D.J., and Yang, T.P. (2005). Characterization of cis- and trans-acting elements in the imprinted human SNURF-SNRPN locus. Nucleic Acids Res *33*, 4740-4753.

Ronchi, V.P., Klein, J.M., Edwards, D.J., and Haas, A.L. (2014). The active form of E6-associated protein (E6AP)/UBE3A ubiquitin ligase is an oligomer. J Biol Chem *289*, 1033-1048.

Rougeulle, C., Cardoso, C., Fontes, M., Colleaux, L., and Lalande, M. (1998). An imprinted antisense RNA overlaps UBE3A and a second maternally expressed transcript. Nat Genet *19*, 15-16.

Rugg-Gunn, P.J., Ferguson-Smith, A.C., and Pedersen, R.A. (2007). Status of genomic imprinting in human embryonic stem cells as revealed by a large cohort of independently derived and maintained lines. Hum Mol Genet *16 Spec No. 2*, R243-251.

Runte, M., Huttenhofer, A., Gross, S., Kiefmann, M., Horsthemke, B., and Buiting, K. (2001). The IC-SNURF-SNRPN transcript serves as a host for multiple small nucleolar RNA species and as an antisense RNA for UBE3A. Hum Mol Genet *10*, 2687-2700.

Saitoh, S., Buiting, K., Rogan, P.K., Buxton, J.L., Driscoll, D.J., Arnemann, J., Konig, R., Malcolm, S., Horsthemke, B., and Nicholls, R.D. (1996). Minimal definition of the imprinting center and fixation of chromosome 15q11-q13 epigenotype by imprinting mutations. Proc Natl Acad Sci U S A *93*, 7811-7815.

Sanjana, N.E., Shalem, O., and Zhang, F. (2014). Improved vectors and genome-wide libraries for CRISPR screening. Nature methods *11*, 783-784.

Scheffner, M., Huibregtse, J.M., Vierstra, R.D., and Howley, P.M. (1993). The HPV-16 E6 and E6-AP complex functions as a ubiquitin-protein ligase in the ubiquitination of p53. Cell *75*, 495-505.

Schinzel, A.A., Brecevic, L., Bernasconi, F., Binkert, F., Berthet, F., Wuilloud, A., and Robinson, W.P. (1994). Intrachromosomal triplication of 15q11-q13. J Med Genet *31*, 798-803.

Schroer, R.J., Phelan, M.C., Michaelis, R.C., Crawford, E.C., Skinner, S.A., Cuccaro, M., Simensen, R.J., Bishop, J., Skinner, C., Fender, D.*, et al.* (1998). Autism and maternally derived aberrations of chromosome 15q. Am J Med Genet *76*, 327-336.

Schumacher, A., and Doerfler, W. (2004). Influence of in vitro manipulation on the stability of methylation patterns in the Snurf/Snrpn-imprinting region in mouse embryonic stem cells. Nucleic Acids Res *32*, 1566-1576.

Sell, G.L., and Margolis, S.S. (2015). From UBE3A to Angelman syndrome: a substrate perspective. Frontiers in neuroscience *9*, 322.

Shalem, O., Sanjana, N.E., Hartenian, E., Shi, X., Scott, D.A., Mikkelsen, T.S., Heckl, D., Ebert, B.L., Root, D.E., Doench, J.G.*, et al.* (2014). Genome-scale CRISPR-Cas9 knockout screening in human cells. Science *343*, 84-87.

Shi, Y., Di Giammartino, D.C., Taylor, D., Sarkeshik, A., Rice, W.J., Yates, J.R., 3rd, Frank, J., and Manley, J.L. (2009). Molecular architecture of the human pre-mRNA 3' processing complex. Mol Cell *33*, 365-376.

Shibata, S., and Lee, J.T. (2003). Characterization and quantitation of differential Tsix transcripts: implications for Tsix function. Hum Mol Genet *12*, 125-136.

Shirk, R.Y., Glenn, T.C., Chang, S.-M., and Hamrick, J. (2013). Development and characterization of microsatellite primers in Geranium carolinianum (Geraniaceae) with 454 sequencing. Applications in Plant Sciences *1*.

Silva-Santos, S., van Woerden, G.M., Bruinsma, C.F., Mientjes, E., Jolfaei, M.A., Distel, B., Kushner, S.A., and Elgersma, Y. (2015). Ube3a reinstatement identifies distinct developmental windows in a murine Angelman syndrome model. J Clin Invest *125*, 2069-2076.

Singh, P., Wu, X., Lee, D.H., Li, A.X., Rauch, T.A., Pfeifer, G.P., Mann, J.R., and Szabo, P.E. (2011). Chromosome-wide analysis of parental allele-specific chromatin and DNA methylation. Molecular and cellular biology *31*, 1757-1770.

Smith, C.L., DeVera, D.G., Lamb, D.J., Nawaz, Z., Jiang, Y.H., Beaudet, A.L., and O'Malley, B.W. (2002). Genetic ablation of the steroid receptor coactivator-ubiquitin

ligase, E6-AP, results in tissue-selective steroid hormone resistance and defects in reproduction. Mol Cell Biol *22*, 525-535.

Somers, A., Jean, J.C., Sommer, C.A., Omari, A., Ford, C.C., Mills, J.A., Ying, L., Sommer, A.G., Jean, J.M., Smith, B.W.*, et al.* (2010). Generation of transgene-free lung disease-specific human induced pluripotent stem cells using a single excisable lentiviral stem cell cassette. Stem Cells *28*, 1728-1740.

Swaab, D.F. (1997). Prader-Willi syndrome and the hypothalamus. Acta paediatrica *423*, 50-54.

Takahashi, K., Tanabe, K., Ohnuki, M., Narita, M., Ichisaka, T., Tomoda, K., and Yamanaka, S. (2007). Induction of pluripotent stem cells from adult human fibroblasts by defined factors. Cell *131*, 861-872.

Truett, G.E., Heeger, P., Mynatt, R.L., Truett, A.A., Walker, J.A., and Warman, M.L. (2000). Preparation of PCR-quality mouse genomic DNA with hot sodium hydroxide and tris (HotSHOT). Biotechniques *29*, 52, 54.

Tsai, T.F., Armstrong, D., and Beaudet, A.L. (1999a). Necdin-deficient mice do not show lethality or the obesity and infertility of Prader-Willi syndrome. Nat Genet *22*, 15-16.

Tsai, T.F., Jiang, Y.H., Bressler, J., Armstrong, D., and Beaudet, A.L. (1999b). Paternal deletion from Snrpn to Ube3a in the mouse causes hypotonia, growth retardation and partial lethality and provides evidence for a gene contributing to Prader-Willi syndrome. Hum Mol Genet *8*, 1357-1364.

Ule, J., Jensen, K., Mele, A., and Darnell, R.B. (2005). CLIP: a method for identifying protein-RNA interaction sites in living cells. Methods *37*, 376-386.

Underwood, J.G., Boutz, P.L., Dougherty, J.D., Stoilov, P., and Black, D.L. (2005). Homologues of the Caenorhabditis elegans Fox-1 protein are neuronal splicing regulators in mammals. Mol Cell Biol *25*, 10005-10016.

Untergasser, A., Cutcutache, I., Koressaar, T., Ye, J., Faircloth, B.C., Remm, M., and Rozen, S.G. (2012). Primer3--new capabilities and interfaces. Nucleic Acids Res *40*, e115.

Valluy, J., Bicker, S., Aksoy-Aksel, A., Lackinger, M., Sumer, S., Fiore, R., Wust, T., Seffer, D., Metge, F., Dieterich, C.*, et al.* (2015). A coding-independent function of an alternative Ube3a transcript during neuronal development. Nat Neurosci *18*, 666-673.

van Woerden, G.M., Harris, K.D., Hojjati, M.R., Gustin, R.M., Qiu, S., de Avila Freire, R., Jiang, Y.H., Elgersma, Y., and Weeber, E.J. (2007). Rescue of neurological deficits in a mouse model for Angelman syndrome by reduction of alphaCaMKII inhibitory phosphorylation. Nat Neurosci *10*, 280-282.

Verdi, J.M., Bashirullah, A., Goldhawk, D.E., Kubu, C.J., Jamali, M., Meakin, S.O., and Lipshitz, H.D. (1999). Distinct human NUMB isoforms regulate differentiation vs. proliferation in the neuronal lineage. Proc Natl Acad Sci U S A *96*, 10472-10476.

Vu, T.H., Li, T., and Hoffman, A.R. (2004). Promoter-restricted histone code, not the differentially methylated DNA regions or antisense transcripts, marks the imprinting status of IGF2R in human and mouse. Hum Mol Genet *13*, 2233-2245.

Wang, E.T., Sandberg, R., Luo, S., Khrebtukova, I., Zhang, L., Mayr, C., Kingsmore, S.F., Schroth, G.P., and Burge, C.B. (2008). Alternative isoform regulation in human tissue transcriptomes. Nature *456*, 470-476.

Wang, L., Meece, K., Williams, D.J., Lo, K.A., Zimmer, M., Heinrich, G., Martin Carli, J., Leduc, C.A., Sun, L., Zeltser, L.M.*, et al.* (2015). Differentiation of hypothalamic-like neurons from human pluripotent stem cells. J Clin Invest *125*, 796-808.

Wang, N.J., Liu, D., Parokonny, A.S., and Schanen, N.C. (2004). High-resolution molecular characterization of 15q11-q13 rearrangements by array comparative genomic hybridization (array CGH) with detection of gene dosage. Am J Hum Genet *75*, 267-281.

Weeber, E.J., Jiang, Y.H., Elgersma, Y., Varga, A.W., Carrasquillo, Y., Brown, S.E., Christian, J.M., Mirnikjoo, B., Silva, A., Beaudet, A.L.*, et al.* (2003). Derangements of hippocampal calcium/calmodulin-dependent protein kinase II in a mouse model for Angelman mental retardation syndrome. J Neurosci *23*, 2634-2644.

Williams, C.A., Driscoll, D.J., and Dagli, A.I. (2010a). Clinical and genetic aspects of Angelman syndrome. Genet Med *12*, 385-395.

Williams, K., Irwin, D.A., Jones, D.G., and Murphy, K.M. (2010b). Dramatic Loss of Ube3A Expression during Aging of the Mammalian Cortex. Frontiers in aging neuroscience *2*, 18.

Wolf, A.M., Lyuksyutova, A.I., Fenstermaker, A.G., Shafer, B., Lo, C.G., and Zou, Y. (2008). Phosphatidylinositol-3-kinase-atypical protein kinase C signaling is required for Wnt attraction and anterior-posterior axon guidance. J Neurosci *28*, 3456-3467.

Yamada, Y., Watanabe, H., Miura, F., Soejima, H., Uchiyama, M., Iwasaka, T., Mukai, T., Sakaki, Y., and Ito, T. (2004). A comprehensive analysis of allelic methylation status of CpG islands on human chromosome 21q. Genome Res *14*, 247-266.

Yamamoto, Y., Huibregtse, J.M., and Howley, P.M. (1997). The human E6-AP gene (UBE3A) encodes three potential protein isoforms generated by differential splicing. Genomics *41*, 263-266.

Yamasaki, K., Joh, K., Ohta, T., Masuzaki, H., Ishimaru, T., Mukai, T., Niikawa, N., Ogawa, M., Wagstaff, J., and Kishino, T. (2003). Neurons but not glial cells show

reciprocal imprinting of sense and antisense transcripts of Ube3a. Hum Mol Genet *12*, 837-847.

Yamasaki, Y., Kayashima, T., Soejima, H., Kinoshita, A., Yoshiura, K., Matsumoto, N., Ohta, T., Urano, T., Masuzaki, H., Ishimaru, T.*, et al.* (2005). Neuron-specific relaxation of Igf2r imprinting is associated with neuron-specific histone modifications and lack of its antisense transcript Air. Hum Mol Genet *14*, 2511-2520.

Yang, T., Adamson, T.E., Resnick, J.L., Leff, S., Wevrick, R., Francke, U., Jenkins, N.A., Copeland, N.G., and Brannan, C.I. (1998). A mouse model for Prader-Willi syndrome imprinting-centre mutations. Nature Genetics *19*, 25-31.

Yeo, G.W., Coufal, N.G., Liang, T.Y., Peng, G.E., Fu, X.D., and Gage, F.H. (2009). An RNA code for the FOX2 splicing regulator revealed by mapping RNA-protein interactions in stem cells. Nat Struct Mol Biol *16*, 130-137.

Yin, Q.F., Yang, L., Zhang, Y., Xiang, J.F., Wu, Y.W., Carmichael, G.G., and Chen, L.L. (2012). Long noncoding RNAs with snoRNA ends. Mol Cell *48*, 219-230.

Zhang, S.C., Wernig, M., Duncan, I.D., Brustle, O., and Thomson, J.A. (2001). In vitro differentiation of transplantable neural precursors from human embryonic stem cells. Nat Biotechnol *19*, 1129-1133.